Application of Oxy-fuel combustion on South African Coals using Thermogravimetric Analyses (TGA)

MSc (50/50) RESEARCH REPORT

Prepared by

Dorcas Molise (386174)

A dissertation submitted to the Faculty of Engineering and the Built Environment, University of the Witwatersrand, Johannesburg, in fulfillment of the requirements for the degree of Master of Science in Engineering.

Johannesburg, 2016

DECLARATION

I declare that this report is my own unaided work, unless otherwise stated. It is being submitted to the Degree of Master of Science to the University of the Witwatersrand, Johannesburg. It has not been submitted before for any degree or examination to any other University.

_____

Dorcas Molise

_____day of _____year_____

Abstract

The quality and grade of South African coal is declining simultaneously with depleting seams. This has a negative impact on power generation and the economics of coal mining and power production. The reason is that good quality coal is more difficult to mine and hence costly, thus affecting coal prices and the ability of mines to supply coal quality of the required specifications. There is a global environmental awareness around the CO_2 greenhouse gas and its effect on global warming. Legislations are becoming more stringent in limiting the amount of greenhouse gases and air pollutants we produce. In power generation, the most prominent greenhouse gas is carbon dioxide (CO_2) and the most prominent air pollutants are oxides of Nitrogen and Sulphur (NOx and SOx). Oxy-fuel combustion (OFC) is a process change that can reduce the production of CO_2 by increasing the concentration of oxygen in combusting air. A study is presented here, that focuses on the application of this process (OFC) to South African coals. Three different coal types were studied and characterized by conventional proximate and ultimate analyses and further characterized and graded by more specialized analyses; petrographic analyses and the quantitative evaluation of minerals b scanning electron microscopy (QEMSCAN). The gasification of the coals was then modeled to determine, qualitatively, its magnitude in comparison to combustion (oxidation) in oxy-fuel combustion. However, when modeling and conducting experiments to determine this, it was found that existing empirical formulae used to quantify char burnout are not suitable for all South African types of coal. The formulae found in literature (for both oxidation and gasification) could only be applied to two of the three samples. For the two samples that were successfully modeled, it was found that reactivity in gasification was probable but not to a significant level. For the third sample that couldn't be modeled successfully, a recommendation was made that a new model be developed to take into account the nature of low grade, high inertinite South African coal. This is required in order to successfully formulate the char burnout of South African coals and thus depict with certainty, the applicability of Oxy-fuel combustion on South African

coals. Such a step would benefit the forthcoming studies on modeling the char burnout of South African coal and therefore contribute to addressing the challenge of declining coal quality in South Africa.

Acknowledgements

I would like to acknowledge God and thank my family for their encouragement and support.

I also express gratitude to Eskom's Research and Testing Centre and their staff for provision of equipment and training me on how to conduct analyses for this work.

I thank Dr Chris van Alphen and his staff for their support in conducting QEMSCAN analyses teaching me on how to determine mineralogical constituents of my coal samples.

I'd like to thank Professor Nikki Wagner and her research staff for assisting me with conducting petrographic analyses and showing me how to interpret the results.

Finally, I thank my supervisors, Prof Falcon and Dr. Bilainu for their input and guidance through this work.

Table of Contents

LIST OF FIGURES

LIST OF TABLES

LIST OF SYMBOLS

Symbol	Units	Meaning
A	$Kg/m^2.s.Pa$	Pre-exponential factor
A_g	m^2/kg	Total surface area of the solid
D_A	m^2/s	Molecular diffusion coefficient
D_e	m^2/s	Effective diffusivity
D_{kn}	m^2/s	Knudsen diffusion coefficient
d_p	m	Particle diameter
E	J/mol	Intrinsic activation energy
φ	Dimensionless	Thiele modulus
F_{mac}	Dimensionless	Maceral correction factor
Mg	g/mol	Molecular weight of diffusing gas
η	Dimensionless	Effectiveness factor
n	Dimensionless	Reaction order
Pg	Pa	Partial pressure of the gas
ρ_g	kg/m^3	Density of the gas
ρ_s	kg/m^3	Density of the char solid
R	$kg/(m^2.s)$	Overall rate of char consumption
R	J/mol.K	Ideal gas constant
R_{ac}	$kg/(m^2.s.Pa)$	Reaction rate per unit area of the solid
R_d	$kg/(m^2.s.Pa)$	Rate of gas diffusion
R_s	$kg/(m^2.s.Pa)$	Intrinsic reactivity
r_p	m	Mean particle pore radius
S_b	Dimensionless	Stoichiometry factor
τ	Dimensionless	Tortuosity factor of the pores
θ	Dimensionless	Total porosity of the solid
T	K	Temperature
T_g	K	Temperature of the gas
T_p	K	Temperature of the solid particle

NOMENCLATURE

AD: Air Dried Basis

AFT: Ash Fusion Temperature

AR: As Received Basis

ASU: Air Separation Unit

BTX: mixtures of benzene, toluene, and the three xylene isomers all of which are aromatic hydrocarbons

CFD: Computational Fluid Dynamics

CCS: Carbon Capture and Storage

CCT: Clean Coal Technology

CFD: Computational Fluid Dynamics

CO: Carbon monoxide

CO_2: Carbon Dioxide

Cp: Specific Heat

CV: Calorific Value

DB: Dry Basis

DTF: Drop Tube Furnace

EFR: Entrained Flow Reactor

EIA: Energy Information Administration

ESP: Electrostatic Precipitator

FC: Fixed Carbon

FGD: Flue Gas Desulphurization

FG-DVC: The FG-DVC general model for coal devolatilization. which combines a functional group (FG) model for gas evolution and a statistical depolymerization, vaporization, and crosslinking (DVC) model for tar formation

GCV: Gross Calorific Value

GHG: Greenhouse gas

HGI: Hard grove Index

ICCP: International Committee for Coal Petrology

IEA: International Energy Agency

IEAGHG:IEA Greenhouse Gas

ITM: Ionic-Transport Membrane

ISO: International Organization for Standardization

MC: Moisture Content

MW: Mega-watts

NCV: Net Calorific Value

NOx: all oxides of nitrogen except nitrous oxide (N_2O). These are: NO, NO_2, N_2O_4 and N_2O_5.

NO: Nitric Oxide

NO_2: Nitrogen Dioxide

N_2O_4: dinitrogen tetroxide

N_2O_5: nitric pentoxide

OFC: Oxy-fuel Combustion

O_2: Oxygen

OF: Oxy-fuel

PA: Primary Air

PF: Pulverized Fuel

QEMSCAN: Quantitative Evaluation of Minerals by Scanning Electron Microscopy

RT&D: Research, Testing and Development

SA: Secondary Air

SABS: South African Bureau of Standards

SAPP: South African Power Pool

SCR: Selective catalytic reduction

SOC: State Owned Company

SOx: Oxides of Sulphur

TFR: Transnet Freight Rail

TGA: Thermo-gravimetric Analyzer

TS: Total Sulphur

UBC: Un-burnt Carbon (in ash)

USA: United States of America

VSP: VattenfallSchwarzePumpe

XRF: X-Ray Fluorescence

AD: Air Dried Basis

AFT: Ash Fusion Temperature

AR: As Received Basis

ASU: Air Separation Unit

CFD: Computational Fluid Dynamics

CCS: Carbon Capture and Storage

CO: Carbon monoxide

DB: Dry Basis

DTF: Drop Tube Furnace

EFR: Entrained Flow Reactor

GHG: Greenhouse gas

HGI: Hard grove Index

IEA: International Energy Agency

IEAGHG: IEA Greenhouse Gas

ITM: Ion-Transport Membrane

MC: Moisture Content

NOx: all oxides of nitrogen except nitrous oxide (N_2O). These are: NO, NO_2, N_2O_4 and N_2O_5.

OFC: Oxy-fuel Combustion

PA: Primary Air

PF: Pulverized Fuel

QEMSCAN: Quantitative Evaluation of Minerals by Scanning Electron Microscopy

SA: Secondary Air

SAPP: South African Power Pool

SOC: State Owned Company

Sox: Oxides of Sulphur

TFR: Transnet Freight Rail

TGA: Thermo-gravimetric Analyzer

TS: Total Sulphur

UBC: Un-burnt Carbon (in ash)

CHAPTER 1

1. INTRODUCTION

South Africa currently is critically in short supply of energy. This is due to the low electricity generation from coal fired generation plants, partially as a result of dwindling coal quality among other contributory factors. Another challenge brought about by conventional pulverized fuel combustion for power generation is the subsequent GHG emission levels, particularly carbon dioxide**.** One possible solution to the challenge of reducing GHG emissions is the use of pure oxygen or enriched oxygen air for combustion and the simultaneous recycle of flue gas to the boiler. This configuration is called oxy-fuel combustion. Oxy- fuel combustion (OFC) is important for its increased CO_2 capture efficiency and is one of the key technologies that are presently under development in the process of carbon capture and storage (CCS). CCS technologies are key clean coal initiatives that are proposed in the use of coal for power generation for CO_2 emissions reduction. Impending environmental legislations are the introduction of the carbon (CO_2) tax which lend weight to the absorption of such CO_2 reduction technologies as oxy-fuel combustion sooner rather than later.

The aim of this study is to characterize coal using several methods and to evaluate the oxy-combustion carbon burnout properties for certain coals presently in use for power generation in South Africa.

1.1 Background

1.1.1 Electric power generation in a conventional pulverised fuel (PF) boiler

Eskom, established in 1923, is public utility that supplies approximately 93% of electric power demands in South Africa. Eskom has been actively involved in the development and sustainability of the Southern Africa Power Pool (SAPP) since

1995. As such, it has provided reliable supply to multiple trading partners in the Southern region of Africa, including Zimbabwe, Zaire, Namibia, Tanzania, Swaziland, and Lesotho.

Eskom, a state owned company (SOC) has various means by which is produces electricity, the bulk being in coal fired power stations. Seventy seven percent of the primary energy in South Africa is derived from coal (Eskom Holdings SOC, 2014). This is produced by 13 coal-fired power stations. This excludes Medupi and Kusile coal-fired Power Stations which are still under construction and are hence considered as future projects for the purposes of this study. Furthermore, Eskom has four hydroelectric and pumped storage schemes, four gas turbines and one nuclear power station. The gas turbines, hydroelectric and nuclear power stations produce far lower capacity than the coal-fired power stations.

Due to extensive coal mining and exporting over the years, the coal in the Mpumalanga region has become unsustainable for Eskom Power Stations in the Mpumalanga Province. Many previously tied collieries to specific power stations are now unable to supply sufficient coal. This has led to multiple sourcing of feeds to these power stations. For instance, Eskom's Majuba Power Station has a railway project in operation which aims to link the coal mines from Mpumalanga with the power station, with the first train scheduled to begin operation in a 68km corridor on 31st May, 2016 (Creamer, 2013). The corridor which will be operated by Transnet Freight Rail (TFR) has been designed to transport 14 million tons of coal per annum from several mines in Mpumalanga. In addition to reducing transportation costs, one of the objectives is to improve coal turnaround times and enable Majuba to access more coal sources than is currently achieved. Waterberg coal, from the Limpopo province, is also being considered by Eskom as it has been found to be a potential coal resource for Majuba Power Station for the next 100 years (Pressly, 2013).

However, when Power Stations are constructed, the coal type and quality are taken into account and are in fact a major factor in design implementation of the boiler.

Change in fuel can affect the process in more ways than may be realized. For example, burnout times for thermal coals from a single colliery extracting several seams can range as widely as 0.8ms to 1.8ms, and in some instances South African coals burn for much longer up to 4 ms (Falcon, 2014). Thus, if that type of coal enters a PF boiler that is designed for a residence time of coal of 0.2ms, most if not all the coal particles may escape the burner without full combustion (Falcon, 2014).

The operation of a conventional air and coal-fired boiler is summarized as follows: Coal is fed from the stockpile into the mills which pulverize and dry it in primary air (PA). The coal is crushed to a target size of minus75 microns (where 65- 75% of the coal will pass the mesh on a sieve this size). The pulverised particles are then blown into the burner by the PA, where they will undergo combustion in the presence of secondary air (SA) which is introduced according to a specific stoichiometric ratio and excess air. The purpose of this combustion process is to heat the heating elements (or pipes) in the boiler, which contain demineralized water and steam. In the case of a drum –type boiler, the water in these pipes is heated to saturation point and fed to the steam drum where the phases will separate (i.e. steam and liquid). The steam is fed to a super heater and converted to high pressure steam which is then sent to the high pressure turbines for electricity generation. The liquid water, on the other hand is discharged into a down comer where it will return to the boiler for more steam generation. The steam from the high pressure turbines is returned to the re-heater pipes of the boiler before it is used to drive the intermediate and low pressure turbines respectively. Finally the steam is condensed in a surface condenser (or air cooled condenser) and sent to the chemical plant where the water is treated for demineralization before returning to the boiler where the same process is repeated.

During the combustion of pulverized coal, gases are emitted called flue gas which contains various products. Ash (which is an agglomeration of particulates) is also produced. Small agglomerations tend to rise up in the boiler as it is carried by the flue gas being emitted, termed fly ash. However larger ash particles (or coarse ash) drop downwards due to the force of gravity and exit at the bottom of the boiler. The fly ash

in the flue gas is removed in the electrostatic precipitator (or the fabric filter plant in some instances) so that the flue gas is cleaner and free from particulates before being allowed to enter the atmosphere. The particulates that are removed are mixed with the coarse ash and co-transported to the ash dump. FGD (wet or dry) may also be retrofitted onto the plant to eliminate SOx emissions produced in the flue gas (See Figure 1.1 below).

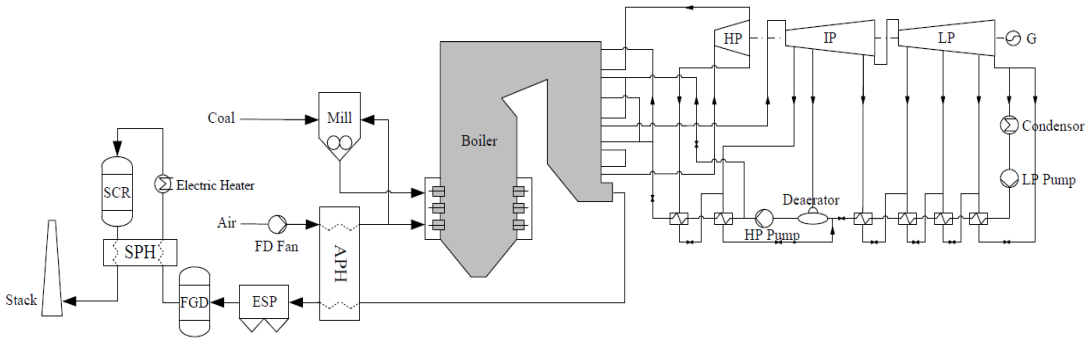

Figure 1.1: Process Flow Diagram (PFD) of an air-coal combustion power plant with SCR, FGD and ESP Flue gas conditioning technologies (Yukun, et al., 2011)

1.1.2 Oxy-fuel Combustion Retrofit Applications in a PF Boiler

There are several means by which to reduce CO_2 GHG emissions in coal fired power generation. Of those available to South Africa e.g. underground coal gasification, supercritical combustion, and coal beneficiation, carbon capture and storage (CCS) technologies offer the greatest CO_2 reduction potentials, especially when the economics are taken into account (Toporov, 2014). For this to be successful, the CO_2 concentration needs to be high, i.e. in the proximity of 90-95%.

The main difference between conventional pulverized fuel (PF) combustion in air as described above and oxy-fuel combustion is that, in the latter, the fuel (coal) is combusted in a 95-99% pure O_2 and CO_2 mixture rather than in air which typically has a composition of 78% N_2, 21% O_2 1% Argon and other gases. The benefit of oxy

fuel firing ensures that the coal is exposed to almost pure O_2 and recycled flue gas (consisting of mainly CO_2) minimizing the production of NOx[1] which leads to flue gases rich in CO_2 .

There are three types of NOx emissions: Thermal NOx, prompt NOx and Fuel NOx. These are distinguished below (Baukal, 2005)

- Thermal NOx is formed at high temperatures by the Zeldovich mechanism: $N_2+O_2 \rightarrow NO, NO_2$
- Prompt NOx is formed through a complex series of fast reactions between nitrogen, oxygen and hydrocarbon radicals. It is formed at low temperatures but is not considered to be important in PF power generation as industrial boilers typically combust in high temperatures.
- Fuel NOx is formed through the reaction of nitrogen in coal and air. $RxN+ O_2 \rightarrow NO, NO_2, CO_2, H_2O$, trace species.
- N_2O formation is minimized when excess air is avoided; excess air is typically introduced during PF firing with air to ensure completeness of the reaction. N_2O forms at low temperatures and is known to be prominent in Fluidised Bed Combustion (FBC).

The formation of thermal NOx is minimized when temperatures are reduced, hence the flue gas must be recycled, otherwise combustion in pure O_2 would result in higher flame temperatures leading to ash slagging problems and fouling, in addition to increased thermal NOx formation (Toporov, 2014).

Combustion in air, as opposed to pure O_2, results in a lower furnace temperature because dilution of the oxygen in nitrogen (during combustion in air) results in heat/energy losses. Thus combustion in pure oxygen significantly raises reaction temperatures. The ambient temperature in the furnace during oxy-fuel combustion is controlled by recycling the flue gas product which has a lower temperature (Buhre et

[1] According to the environmental protection agency, NOx refers to all oxides of nitrogen except nitrous oxide (N_2O). These are: NO, NO_2, N_2O_4 and N_2O_5.

al., 2005). Additionally, the increase in O_2 concentration during oxy-fuel combustion can off-set the heat losses that occur due to dilution of O_2 by N_2 in air. This in turn reduces the energy lost thus increasing the efficiency of the heating system. Thus oxy-fuel combustion (OFC) would seem to be the more efficient combustion process than normal air consisting of 21% O_2.

Figure 1.2 and 1.3 below are simplified schematic diagrams of Oxy-fuel combustion. From these it may be noted that retrofit applications could be easily implemented since the only major plant modifications are:

- Integrating the oxygen producing cryogenic air separation unit (ASU) with the burners in the boiler for fuel combustion and
- Recycling the stream of flue gas for cooling purposes and to make up for N_2 that is used to carry heat over
- The addition of a cooler/condenser of the flue gas before the turbine since CO_2 has a higher heat capacity than N_2

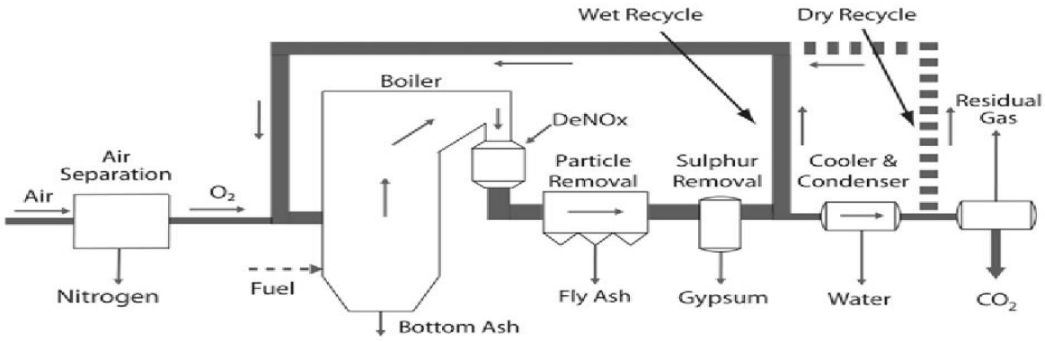

Figure 1.2: Oxy-fuel combustion scheme with both wet and dry recycle of the flue gas (Toporov, 2014)

Toporov (2014) also describes a similar configuration with ionic-transport membrane (ITM) as opposed to a cryogenic air separation unit (ASU).

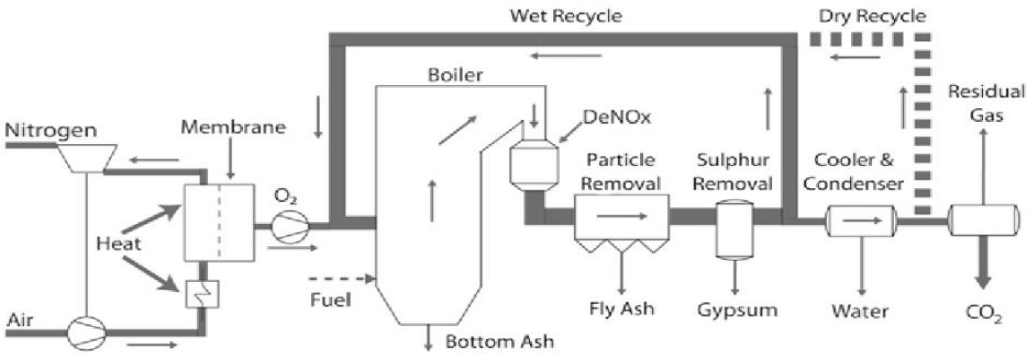

Figure 1.3: Oxy-fuel combustion scheme with ITM for oxygen supply (Toporov, 2014)

There are two main configurations for oxygen production for Oxy-fuel combustion: *traditional cryogenic air separation* and *high temperature ceramic ion-transport membrane (ITM).* The difference is shown in Figure 1.2 and 1.3.

There are other air separation technologies including adsorption and chemical methods but these methods produce high impurities and by-products in comparison to the ion-transport membrane and cryogenic separation technologies (Krugar, 2003: Smith, 2001).

The cryogenic process (by distillation) is the most mature technique for air separation but the advantage of ITM over cryogenic air separation is that it is less energy intensive and hence less costly than the cryogenic method since it consumes significantly less auxiliary power. According to Air Products and Chemicals, Inc. (2008) ITM can save up to 48% capital required for oxygen and 68% power for oxygen. Further than this, operational costs of ITM may be reduced by heat integration of the ITM with the rest of the power plant. This however is a more complicated modification to the power plant and may affect the whole power plant process, making the retrofit difficult (Toporov, 2014).

Since the flue gas product is recycled, the final product leaving the furnace will contain concentrated CO_2, at concentrations as high as 95-99%. This flue gas product

may be compressed and stored without further separation necessary. Thermodynamically, the replacement of N_2 by flue gas (consisting mainly of CO_2 and less N_2) will result in different chemical compositions of the gases present in the furnace. This will affect the chemical reactions and heat transfer evolution in the furnace.

Table 1.1: Physical properties of N_2 and CO_2 gases at 900℃ (Toporov, 2014)

Property	**Measurement Units**	**N_2**	**CO_2**	**Ratio CO_2/N_2**
Thermal conductivity	W/m K ($\times 10^{-3}$)	74.67	81.69	1.09
c_p (Molar Heat Capacity)	kJ/kmol K	33.60	56.10	1.67
ρ (Density)	Kg/m^3	0.29	0.45	1.55
O_2 Diffusion coefficient	m^2/s ($\times 10^{-4}$)	3.074	2.373	0.77
Thermal diffusivity	m^2/s ($\times 10^{-7}$)	2168	1420	0.65
MW Molecular Weight	kg/kmol	28	44	1.57
Specific heat capacity	J/m^3K	0.34	0.57	1.67

Due to the difference in molar heat capacity of nitrogen and oxygen, more O_2 will be required in the gas mixture in order to achieve similar adiabatic flame temperatures in the combustion chamber as that achieved in conventional PF combustion in air (Toporov, 2014).

Flame propagation velocity is significantly affected by gas composition. A CO_2 rich atmosphere tends to reduce the flame propagation velocity thus oxy-fuels combustion is most likely to worsen the low flame propagation velocity that is already experienced when burning South African coals. This is substantiated by observing the differences in oxygen diffusion rates in the different gas mediums in Table 1.1. It may be deduced from Table 1.1. that oxygen diffusion in nitrogen is 1.3 times faster

than the diffusion in CO_2 (1/0.77). It is this lower thermal diffusivity of CO_2 that gives rise to slower propagation speeds congruent with combustion in atmospheres with high CO_2 concentrations. The flue gas that results from OFC which must be recycled, will have a higher density because the molecular weight of CO_2 is 1.5 times greater than of N_2 (Table 1.1). When flue gas density is increased and hence gas velocities are reduced, it is expected that higher residence times will be observed in the furnace. Further than this, it is expected that flue gas temperatures will be lower for OFC gas mixtures (i.e. O_2 and CO_2) as compared to normal air (O_2 and N_2) if the O_2 concentration is kept the same in both scenarios. This would be because CO_2 has higher energy density (denoted as energy per volume in Table 1.1) and higher heat capacity than N_2 (Liu et al., 2005). It is these factors as well as gasification (char-CO_2) and oxidation (char-O_2) reactions which need to be considered and which shall be investigated in this study.

1.2 Industrial Application

A comprehensive study of the coals will be made using, apart from conventional analyses, petrographic, TGA, XRF and QEMSCAN analyses. The results of these analyses will assist to further understand the coals in question. This information may be of use in helping to decide whether or not Oxy-fuel combustion is suitable for South African coals and if there is potential to move to this space.

The Thermogravimetric analyzer (TGA) will be used for verification and validation of the proximate analyses.

The coals to be used in this investigation are currently being used in normal air-fuel combustion in three of Eskom's power stations. These are listed in Table 1.2 below. Thus, in addition to analyzing the applicability of these coals for OFC, the petrographic and QEMSCAN analyses may be used to further analyze and understand the coals for applicability in normal air-firing power stations, which have a cumulative installed capacity of 11 814MW. The coal quality requirements for each power station are obtained from Cohen B (2013).

Table 1.2: Coals under investigation

Mine	**Coal A**	**Coal B**	**Coal C**
Power Station	Matimba	Lethabo	Kendal
Installed capacity (MW)	3990	3708	4116
Coal CV Requirements (MJ/Kg)	18-20	16-18	18-20

According to Cohen (2013) and the IRP (2010) which can be found in Department of Energy (2013) all three power stations will be partly or fully decommissioned between 2030 and 2040 leaving only Majuba, Medupi and Kusile Power stations fully operational by the year 2040.

1.3 Contribution to Knowledge

Internationally, there are a limited number of oxy-combustion technologies that are currently being researched on a commercial scale. Known as the "CO_2-Free Power Plant Project", VattenfallSchwarzePumpe (VSP) made an announcement in November 2009 that it was achieving nearly 100 % CO_2 capture at SchwarzePumpe. The purpose of the VSP project is to validate the oxy-fuel combustion technology by demonstrating its usability and efficiency for future use (Power Plant CCS, 2014).

A separate project, the "Callide 'A' project" aims to demonstrate, over a period of five years, the applicability of the relatively new CCS oxy-fuels technology to an old power station built in 1962 in Germany. In addition to the above mentioned 30MWth pilot plant and 250 MW demonstration plant in Schwarze Pumpe, Germany, other demonstration plants around the world include a 30MWth retrofitted boiler in Biloela, Australia and a 30 MWth pilot plant as well as a 323 MW full scale demonstration plant in El Bierzo, Spain.

No commercial pilot or full scale OFC technology has been developed/ installed in South Africa as yet, however, in South Africa, Eskom and CSIR have collaborated to investigate OFC by laboratory scale and part of this institutional collaboration

framework falls under the National Clean Coal Technology (CCT) research portfolio. This project is titled: "Oxy-fuel Combustion (OFC) Using Various South African Coals as a Potential CO_2 Abatement Technology". The current research study forms part of this project.

This project seeks to characterize the selected coals and to evaluate their carbon conversion in the oxy-combustion process. It also seeks to theoretically model the reactivity of the coal samples in terms of oxygen-char and carbon dioxide-char reaction.

In so doing, this research hopes to prove the suitability of typical South African coals for oxy-fuel combustion and that if retrofitted in Eskom's power stations; OFC would be of relevance and importance to South Africa in reducing the CO_2 greenhouse gas emissions.

1.4 Objectives of the study

The key objectives of this research therefore are:

I. To carry out detailed characterisation of the selected coals using proximate, ultimate, petrographic, mineral (QEMSCAN) and ash analyses

II. To estimate likely combustion performance by use of the techniques in point I in a theoretical char burnout model

III. To model the char reactivities of each coal and compare them to each other under different gaseous environments

IV. To establish whether low grade coals are suitable and can be combusted as efficiently in oxy-fuel firing process as in conventional air combustion

V. To compare the gasification reaction rate versus the oxidation reaction in air and OFC

CHAPTER 2

2 LITERATURE REVIEW

2.1 Background to Coal

2.1.1. Coal Rank and its uses

Coal usage varies according to coal rank, that is, degree of coalification. The figure below (Figure 2.1) shows an inversely proportional relationship between coal's calorific value (CV) and total moisture. High rank coals (anthracite and bituminous coals) are mostly used in metallurgical applications such as iron and steel manufacture while low rank coals (lignite and sub-bituminous) are the coals typically used for steam production in power generation, particularly in South Africa and the other Gondwana regions (Zimbabwe, Australia etc.).

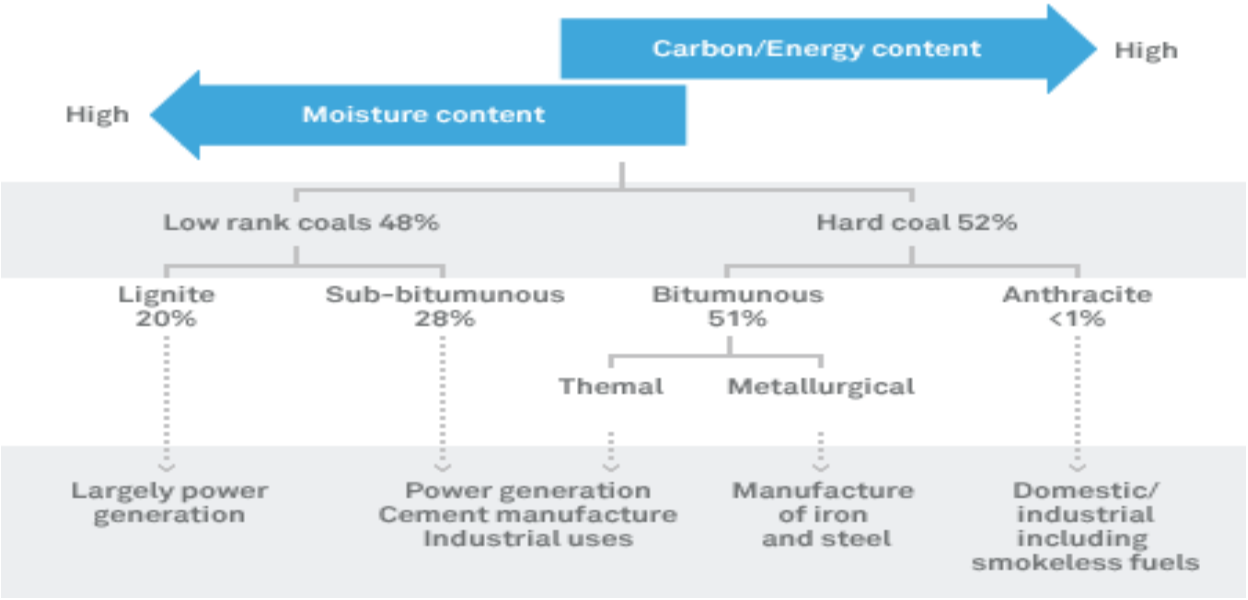

Figure 2.1: Rank of coal (Kee, 2014)

This figure below, Figure 2.2 by Bono (2012) shows the variation of other coal parameters with rank. From the graphs below, it can be seen that total moisture and volatiles generally decrease with degree of coalification, while the fixed carbon and calorific value, indicators of combustibility of coal, have a trend to generally increase with degree of coalification. This can be traced back to the formation of coal, since

we know that coal formation is enhanced by increasing heat and pressure, over time. Thus increasing heat will drive off volatile matter as observed in the graph below, increasing heat will also cause some of the inherent moisture in the coal to evaporate- this will cause a subsequent decrease in total moisture of the coal. Whilst volatile matter, fixed carbon and moisture give an indication of rank of a coal, this sequence of values is only applicable to vitrinite-rich coal such as is found in Europe and the USA. In other countries including South Africa, where vitrinite varies significantly in proportion (5 to 95%), such parameters are not reliable rank indicators. In such cases, the rank of coal is best determined by measuring the reflectance of light emitted off the surface of vitrinite as seen through immersion oil. This provides the parameter, the " reflectance of vitrinite" or RoV%, i,e, a 100 random points that are measured, from which the mean RoV% can be inferred, this indicates the true rank or level of maturity of a coal. This occurs because, as coal matures through increasing time, temperature and or pressure, the light emitted from the organic maceral vitrinite passes from dark grey in sub bituminous coal, through medium and light grey in bituminous coal and subsequently ends up white in anthracite. Statistical measurements of reflectance provide a mean which determines the final and formal rank of a coal and the ranges of rank included in that coal. Such information is extremely important in South African coalfields due to the presence of igneous intrusions in some coalfields which change the levels of rank of the coals in that area. This in turn, affects the combustibility of the coals from those areas. A range of ranks for any specific coal product is therefore important when predicting coal combustibility (Falcon, 2014; Falcon et al., 2008).

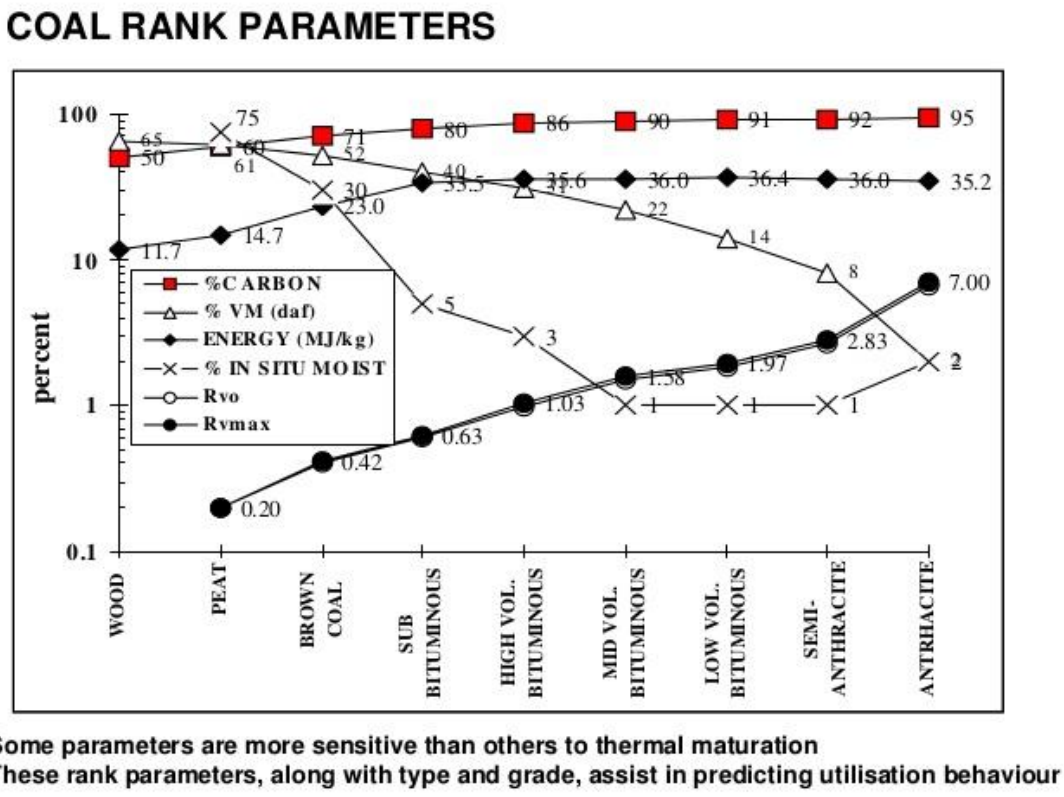

Figure 2.2: Variations of coal parameters with rank (Bono, 2012).

According to the BP Statistical review of World Energy (BP, 2013), South Africa had 30, 2 billion tons of recoverable coal reserves by the end of 2012 and according to the EIA (Energy Information Administration, 2013), about 70% of the recoverable coal reserves lay in just three of the 19 official coal fields found in South Africa. These three coalfields are, namely; Witbank, Highveld and Ermelo and are the sources for most of the total coal (288 million short tons) produced in 2012 (Energy Information Administration, 2013).

2.1.2. Effect of size on the nature of coal

Many studies have been made to determine the effect of particle size on the petrographic nature of coal. One such study was made by (Hower, 2008) who looked at the effect of particle size on the maceral/microlithotype partitioning on pulverised coals from 19 power plants. The sizes were divided into 150 micron, 75, 40 and 25 micron sizes by wet-washing on the suitable corresponding meshed screens. His

findings were that vitrite (the most common monomaceral) increased in abundance with decreasing particle size while duroclarite (the most common trimaceral) decreased while it appeared more entrenched in vitrinite (with decreasing particle size). This implies that the relative grindability of the macrolithotypes will affect combustion efficiency because vitrite, which is more brittle, is easier to grind and hence appears more in finer coal particles. Conversely, because the duroclarite is harder to grind, it is less abundant in finer particles and was found to be entrenched in vitrinite and entrenchment becomes more pronounced at finer particle sizes. All 19 coals were high volatilie bituminous coals (medium rank C) as with two of the coals analysed in this study (Coal A and B). The petrographic analyses was done on all three coals (Coal A, B and C) however at a single size fraction (-1mm) and the QEMSCAN at three different size fractions (-212um, -1mm and -106um). The literature can be taken into consideration however it must be noted that the 19 coals are all from central Appalachain and Illinois regions, which are both Laurasean.

2.1.3. Nature of Coals in South Africa

To determine the usefulness of coal, it is necessary to determine the true nature of the coal, and indeed this depends on the location of the coals original formation. Coal is formed when pressure and heat are constantly applied (over millions of years) on peat from trees, leaves and branches which accumulate in specific environments such as lakes, swamps and deltas of rivers. The concentrated heating process of peat by the sun over time drives off moisture (by evaporation) as well as molecules that contain methane and CO_2. As a result, the carbon content of the coal increases together with the energy content since energy in coal is derived from both the volatile matter and the fixed carbon (Falcon & Ham, 1988). Peat on the other hand, is formed by a complex process consisting of four general requirements: 1) Vegetation in the form of trees, leaves, branches, spores and resins. 2) Water or any other equivalent medium in which no microbial activity is possible. 3) A rising water table or a sinking floor, and. 4) suitable sedimentary environments.

The basins in which coal is found are typically associated with slow subsidence which results in the sinking of peat swamps and the floor. The coal reserves that

exist today did not form simultaneously. Rather, coal formed in the northern hemisphere first, approximately 300-350 million years ago during the Carboniferous Era whereas coal formed in the southern hemisphere during the Permian Era, approximately 50 million years later (Falcon, 2014). Continents in the northern hemisphere belonged to a supercontinent known as Laurasia where as those in the southern hemisphere belonged to a supercontinent known Gondwanaland. Thus coals are often referred to as Laurasian coals or Gondwanan coals.

The weather conditions in the northern and southern hemispheres differed substantially during these times resulting in differences in vegetation and in the levels of decomposition of the plant materials. Coal in the northern hemisphere formed mainly in warm, waterlogged equatorial climatic conditions whereas coals in the southern hemisphere formed in cool to cold and often dry climates. The warm wet conditions of the northern hemisphere gave rise to plant materials that decomposed in water which turned the organic materials into fragments (or macerals) known as vitrinite, the bright shiny highly reactive parts of coal. The warmer dry climate of the southern hemisphere gave rise to plant materials that turned mostly into organic fragments (or macerals) known as inertinite, the dull, carbon-rich, difficult to ignite and long-burning parts of coal.

After initial plant accumulation in peat swamps, and with increased burial leading to increased pressures and temperatures, plant materials go through a series of maturing stages from peat to lignite (brown coal), to bituminous (or back coal) and then to anthracite (the most mature stage of coal). The northern Laurasian coals underwent deep burial which gave rise to high pressures and temperatures which lead to high proportions anthracites, whereas the Southern Hemispheric or Gondwanan coals remained relatively shallow so they only attained the level of maturity or rank of bituminous coal, although some anthracite (high rank) coal can also be found in this region. The North Hemispheric/Carboniferous coals shows little variance in maceral and mineral content and are therefore less diverse than the Southern Hemispheric coals which are highly variable in maceral and mineral composition, This can be attributed to the regional differences highlighted above (Falcon and Ham,1988) .

Coal is conventionally analyzed in terms of moisture, volatile matter (VM), ash content fixed carbon (FC) - these factors comprising the Proximate analysis - and total sulphur (TS) content, but the way in which coal type and level of maturity (or rank) is determined is best performed under a microscope during petrographic analysis. According to Falcon et al. (1988), the fundamental composition of coal falls into three major categories namely; organic matter (which indicates the type of coal), mineral matter (which infers the grade of coal) and degree of metamorphism. These are fundamental or basic coal properties of coal which should be studied, in addition to the physical and chemical analyses which are empirical properties; Falcon and Ham (1988) .Thus, in addition to the proximate and ultimate analyses, it is the fundamental studies of coal, under a microscope (i.e. petrographic analysis) that shows the building blocks of coal which will give a more holistic appreciation of the coal in question and its associated combustion properties.

The Main Karoo Basin in Southern Africa was once open to the sea. Different suites of minerals and trace elements were brought down by rivers pouring into the inland Karoo Sea and different environments of accumulation occurred along the shoreline each varying in stability and configuration. However, the Springbok Flats, Waterberg and other smaller basins in the Limpopo regions were small, shallow, fault-bound basins with relatively similar geological histories; this is specific to the Limpopo region. Falcon and Ham (1988) have also studied the characterization of the coal resources of South Africa and briefly described the 19 major coalfields found in South Africa. In agreement with the work done by Falcon and Ham (1988) the Waterberg coalfield differs from the Springbok Flats, and Witbank coalfields differ in ways shown best in Table 2.1 below (Jeffrey, 2005).

Table 2.1: A brief summary of the characterisation of three coalfields as described by (Falcon & Ham, 1988)and (Jeffrey, 2005)

Coalfield	Springbok Flats	Witbank	Waterberg
Depth (m)	0-1000		15-400
Seams	Majority of coal found in the west of warmbad-pienaarsrivier and has been devolatilized by dolerite intrusions. There is a zone (1 meter thickness) that has been mineralized by Uranium in the top/upper part of the upper coal zone and roof strata, as well as near the pre-Karoo inliers	5 seams, No. 1 seam is patchily developed in patches and is only 0-3m thick and no. 5 seam consists of erosional remains (0-2m thick).	Vryheid has 5 seams but 4 coal zones, Grootgeluk has 7 coal zones and multiple seams
Geology	Vryheid in lower coal zone, development laterally is poor, while Volksrust is	No 2 seam (4.5-20m thickness) is most economically important for export steam coal.	Vryheid is 55m thick while Grootgeluk thickness is 60m. Lateral quality is

	in the upper coal zone is more persistent laterally and up to 12 m thick.	No. 4 seam (2.5-6.5m thickness) split by mudstone into 4 upper/4lower seams (Holland, Cadle, Pinheiro and Falcon, 1989). It is also economical but quality is not as high as no. 2 seam. no 3 seam is of high quality but uneconomic due to small thickness (0.5m),	consistent in Grootgeluk and produces greatest % of ROM coal

Coal production in the Waterberg coalfield in Limpopo, is expected to double in the next five years (Eberhard, 2011). Presently, there is only one operational coal mine in the Waterberg coalfield which is owned by Exxaro called Grootgeluk. It is a large open-cast coal mine producing multiple products and produces approximately 19 Mt of coal per annum, 77.8% of this (14.6Mt) is supplied to Matimba Power Station per annum. Grootgeluk is currently under expansion to eventually supply 14.6Mt coal to Medupi power station per annum. Furthermore, two junior Australian coal-mining companies namely; Waterberg Coal and Resource Generation (Resgen) are planning to build mines in the Waterberg region, to further exploit the coal in this region. Waterberg Coal announced that its mine plans to supply 10 Mt per annum to Eskom over a period of 30 years while Resgen plans to construct a mine, Boikarabelo , that will supply Eskom with 3Mt per annum and the same amount of coal to the Export Market (Ryan, 2014).

However, the geology in Emalahleni coalfields, Mpumalanga province differs from the geology of the Waterberg coalfields in Lephalale, Limpopo province. Due to the

large thickness and vertical variance in between seams in the Waterberg region as compared to the Witbank region, most of the coal found in the Waterberg region will be of lower quality/ purity/grade than the Witbank coal. It is advised that the mine's middle washed product (known as the middlings) from the Waterberg Upper Zone which makes up approximately 80 % of the total mine output in the Waterberg region should be supplied to Eskom in order to make-up for such misfortune in the Waterberg coalfield (Falcon, 2014). This was the model used by Exxaro at Grootgeluk, it was a success and Exxaro intends to repeat this model at the Thabazembi mine that it intends to construct (Ryan, 2014).

While the above mentioned mining strategy offers some economic benefit to the GDP, SA exports the high-grade coal and the remaining middlings and discards (lower grade coal) are being used for local industrial combustion and large scale power generation. Such low grade coal products result in the destruction of the Eskom boilers which were initially designed to burn cleaner coal. Not only does this run-down the boilers (as explained under section 1.2. above), but burning of lower-grade coal may result in higher emission levels, which contravenes the impending environmental legislations that are becoming more stringent. Oxy-fuel combustion offers an enhanced combustion process and may thus also help in addressing this problem. This will be further discussed in section 2.3 of the literature review.

Given the background of South African coal and that a model will be used to describe the combustion behavior, it is important to understand SA coal in the context of other coals from prominent international sources. Wigley et al (1997) studied the distribution of mineral matter in PF coal particles in relation to burnout behavior. 18 types of coals used in power stations worldwide were analyzed. As can be deduced from Table 2.2 produced below, South African and Australian coals possessed a significantly greater amount of minerals associated with organic matter in coal, even in the milled form, as compared to the British and American (northern hemisphere) coal. The southern hemisphere coal also possesses greater amounts of inherent forms of minerals and hence ash in the resultant chars than coal stemming from the northern

hemisphere. This can be attributed to geological formation of coal, during the Permian age in Gondwanaland (Falcon, 1986, 1989).

Table 2.2: Ash content and chemical composition (wt. %) for 12 power station coals (Wigley et al.,1997).

Coal	**Ash**	**SiO_2**	**Al_2O_3**	**Fe_2O_3**	**CaO**	**MgO**	**K_2O**	**Na_2O**	**TiO_2**
Australia 1	17.7	73.2	20.1	2.9	0.2	0.4	1.3	0.5	1.4
Australia 2	16.1	82.3	14.3	1.7	0.1	0.1	0.6	0.2	0.7
Australia 3	15.6	66.9	23.4	4.2	1.7	0.8	1.3	0.7	1.0
N. America 1	11.1	44.0	26.3	18.1	5.9	1.5	2.2	0.6	1.4
N. America 2	10.2	51.8	29.3	9.7	2.6	1.4	2.3	1.2	1.7
N. America 3	13.0	61.3	27.1	4.9	1.1	0.9	2.7	0.3	1.7
S. Africa 1	13.8	50.6	30.8	5.3	7.9	2.1	1.0	0.4	1.9
S. America 1	7.6	59.3	22.6	6.7	5.0	3.3	1.6	0.5	1.0
S. America 2	10.4	60.6	22.2	9.5	1.9	1.4	2.4	0.9	1.1
UK 1	12.3	41.6	22.7	21.5	8.4	2.6	1.8	0.5	0.9
UK 2	13.5	56.1	29.2	7.3	2.2	1.5	2.1	0.4	1.2
UK 3	17.4	54.5	25.2	11.5	1.7	1.3	3.3	1.4	1.1

2.2. Background on the Pulverised Fuel Combustion process

2.2.1. **Drying**

Drying is the first step in the combustion process which is completely separate from devolatilisation. This consists of two successive steps which are;

i. Evaporation of surface moisture

Surface moisture is the moisture in coal that is easiest to remove. It lies between the particles of coal, filling the voids. It is also removed by leaving the coal out in exposure to the sun and is conventionally excluded from coal analyses. However, measurement of the total moisture of coal typically takes into account the sum of this surface moisture and inherent moisture (the latter is explained below).

ii. Removal of inherent moisture

Inherent moisture is that moisture which is inbound the coal particle and remains after surface moisture (above) has been removed. According to some sources, complete dehydration of this form of moisture does not occur below 350 °C (Unsworth, 1988, Unsworth, 1989).

Heat is required to remove moisture in coal and in the furnace region; heat is conveyed to the particle by means of radiation and convection respectively.

Tillman (1991) states that the heat required to accomplish drying depends on the specific heat of the particle in both as-received and dry state as well as the heat required to evaporate the moisture within the particle. The particle's specific heat is a function of temperature. It is known to increase with temperature up to a maximum value of 772K and then decreases with increasing temperature. The exact value is unknown but is estimated to range between 1-2 kJ/kg K for coal particles (Williams et al., 2000).

2.2.2. **Devolatilisation**

Devolatilisation is a pyrolytic process, in which molecules in the coal particle begin to breakup and non-condensable gases and condensable volatiles are produced. This stage of the process is called primary pyrolysis (Solomon et al, 1992). A study was conducted (by Ballantyne et al., 1984) to determine the cold atmosphere pyrolysis of PF using controlled laser heating (10.6 microns). By collecting volatiles in a separate chamber and analyzing them by conventional techniques, it could be concluded that the proximate and ultimate analyses of volatiles driven off in primary pyrolysis do not differ greatly from the parent coal, suggesting that primary pyrolysis is a more

physical reaction than it is chemical (since it consists predominantly of phase change). Additionally, devolatilisation initiation temperatures largely depended on the heating rates applied, the ranks and types of coal involved. For instance, according to a study made by Sami et al 2001, devolatilisation began at 700K for bituminous coal particles heated at rates below 100℃ $(100\mathrm{K}/s)$. At 100℃$/s$, devolatilisation occurred at 1200℃ (or 1473.15K). On the other hand, devolatilisation only began at 1500K for higher heating rates (above 10 000℃$/s$). At extremely low heating rates (approx.10^{-4}℃$/s$), devolatilisation began at temperatures of about 350-400℃ (i.e. 623.15-673.15 degrees K).

Initiation of devolatilisation at constant temperatures also varies with the rank and type of coal. Bituminous coals devolatilise as lower temperatures relative to anthracites (this is a rank factor), and vitrinite macerals devolatilise earlier than semi-reactive inertinites (Tan et al., 2006), an organic maceral composition factor making up the type of coal. Rank and type of coal also determine the nature, forms and quantities of decomposition products such as light (oil and gaseous products) and heavy (tarry) hydrocarbons.

According to Glarborg et al. (2003) when sufficient heat is supplied to tar, it may be re-polymerized when in liquid form (as opposed to vaporization) whereby char and light volatiles are formed. Alternatively, if tar is released, during primary pyrolysis, as gases and temperatures exceed 1000K, it will evolve to form CH_4,C_2H_2, C_2H_4, C_2H_6, C_3H_6 and CO. However, soot is formed when tar undergoes cracking and is composed of nucleated particles as it grows in the gaseous phase (Annamalai and Ryan, 1993).

Thus, to summarize, volatile matter is derived from two sources in coal; organic matter and mineral matter. The organic matter, when the applied heat is increased, produces tars, oils, hydrocarbon gases, oxides of carbon and hydrogen. The mineral matter (inorganic materials), on the other hand, produces incombustible volatiles such as sulphur oxides from pyrites, carbon dioxide from carbonates and water (of crystallinity) from some clay (Falcon and Ham, 1988) though incombustible, these

are driven off with the volatile organic matter which if present in sufficient quantities, can quench the flame (Falcon and Ham, 1988).

The devolatilisation process varies depending on the coal rank and heating conditions and at temperatures exceeding 600℃ (i.e. 873.15K), coal pyrolysis produces light gaseous hydrocarbons, oxides of carbon, BTX and tar. The distribution of these products (and an example of this distribution is given in the table below) depends mostly on the process conditions such as temperature and heating rates, in addition to coal type (Muthu et al., n.d)

Table 2.3: Distributions of the products of primary and secondary pyrolysis from a bituminous coal sample as predicted by FLASHCHAIN (Niksa et al., 2003)

Components	**Primary pyrolysis products (wt. %)**	**Secondary pyrolysis products (wt. %)**
H_2	1.57	4.08
CH_4,	1.5	0.21
C_2H_2	0	0
C_2H_4	0.67	0
C_2H_6	0.24	0
C_3H_6	0.56	0
CO	2.5	5.2
CO_2	2.5	2.5
H_2O	5.2	5.2
HCN	1.02	1.87
H_2S	0.33	0.42
Tar	34.9	0
Soot	0	31.5
Char	49.1	

Flashchain is one of the devolatilisation network models used to analyze and predict changes in the chemical composition of coal particles. Results obtained by Niksa et al., (2003) tabulated above suggest that, contrary to the literature above by Annamalai and Ryan (1993) no acetylene C_2H_2 is formed throughout pyrolysis. However, 90%

of the tar formed in primary pyrolysis is converted into soot. Furthermore, all hydrocarbons (ethane, ethane and propene) are removed during the final stages of pyrolysis according to this source.

The fixed carbon is an organic solid carbon residue that remains after devolatilisation is complete and all the volatile matter, ash and moisture have been removed. It can thus be determined during proximate analysis by difference. The forms of carbon remaining after devolatilisation have high carbon contents and are referred to as "char" (or "coke", depending on purity). This product varies considerably in structure i.e. porosity, in texture, i.e. the nature of the matrix and in its rates of reactivity upon subsequent heating/combustion (Falcon and Ham, 1988).

2.2.3. **Char Production**

i. Char formation

As pyrolysis continues and matures beyond the secondary phase, it finally leaves behind a solid carbonaceous residue that contains up to 98% carbon. Char is thus a carbon-rich solid with small quantities of oxygen and hydrogen, as opposed to tar, which mostly comprises of hydrocarbons with a hydrogen to carbon ratio that is greater than one (Tillman, 1991). The amount of char produced during pyrolysis is significantly determined by FC (fixed carbon) and ash contents as determined during the proximate analysis on a dry basis and by maceral and rank proportions. For bituminous coal, the total char that forms has been estimated to be 40% of the coal mass when combustion commenced (Kilpinen, 2002). However, these facts may not be relevant to the South African Gondwana coal types due to the large variance in organics despite similar properties as determined by the proximate and ultimate analyses. Thus, such work remains to be verified for Southern African coals. Petrography or TGA are suitable sciences that may be considered for this.

Several studies from literature have concluded that charring of coal is similar in N_2 as it is in CO_2 the difference is only observed from combustion –which happens after devolatilisation and this difference may be attributed to the diffusion of O_2 in CO_2 versus in N_2 (Toporov, 2014 ; Toftegaard et al., 2010 and Pohlmann et al., 2010).

ii. Char combustion

While the presence of minerals in organic rich coal has been shown to influence the particle size distribution of coal exiting the mill, there seems to be no link between the levels of minerals present in coal on char combustion (Wigley et al., 1997).

In support of the above-mentioned statement, there have been instances where coal samples with similar proximate and ultimate analyses have been shown to behave differently in the furnace (Falcon and Ham, 1988) It is for this reason that theoretical modeling, petrographic, QEMSCAN analyses will be performed on the coal samples to characterize them fully and to demonstrate a deeper understanding of the oxy-fuel environment on the coal based on its inherent characteristics.

2.3. Oxy-fuel combustion: Investigations

2.3.1. OFC Retrofit applications-exploring different configurations

Oxy-fuel combustion refers to combustion in which oxidation in high concentrations of oxygen compared to nitrogen takes place. Hu et al. (2011) examined four configuration options for oxy-fuel firing for the purpose of establishing emission removal including particles, SOx and NOx in an oxy-coal combustion system for CO_2 capture. The authors observed that the concentrations of NOx and SOx in flue gas are higher in oxy-coal combustion than in air combustion; however the moles of NOx and SOx produced are lower due to the reduced volumetric flow rate of recirculating flue gas in oxy-coal combustion. This, and the fact that the fuels are more concentrated, implies greater ease in capturing the oxides of Nitrogen and Sulphur simultaneously with the carbon dioxide during the capturing phase.

In a coal-fired pulverized fuel (PF) plant consisting of a particulates removal system, FGD, SCR and a flue gas condenser (see Figure 2.3) the flue gas would reach a higher dew point temperature of 131 °C (404.15K) if recycled immediately after the ESP, before FGD and condensation, than it would if recycled after the flue gas condenser (122°C or 395.15K). However in all possible flue gas recycle configurations were to be explored (A-D in figure 2.3), the dew point temperature of the flue gas in oxy-fuels combustion would exceed that of the conventional air-

combustion systems. This is due to the increase in moisture content levels experienced in oxy-coal combustion which may have serious implications for corrosion in the heat exchange metals since the SOx may react with water to form sulphuric acid (H_2SO_4) upon condensation. Two suggestions have been made to address this problem. The first being to maintain higher cold-end temperatures (above the dew point) and secondly, to use propylene or other corrosion resistant materials such as glass reinforced plastics (Hu et al., 2011).

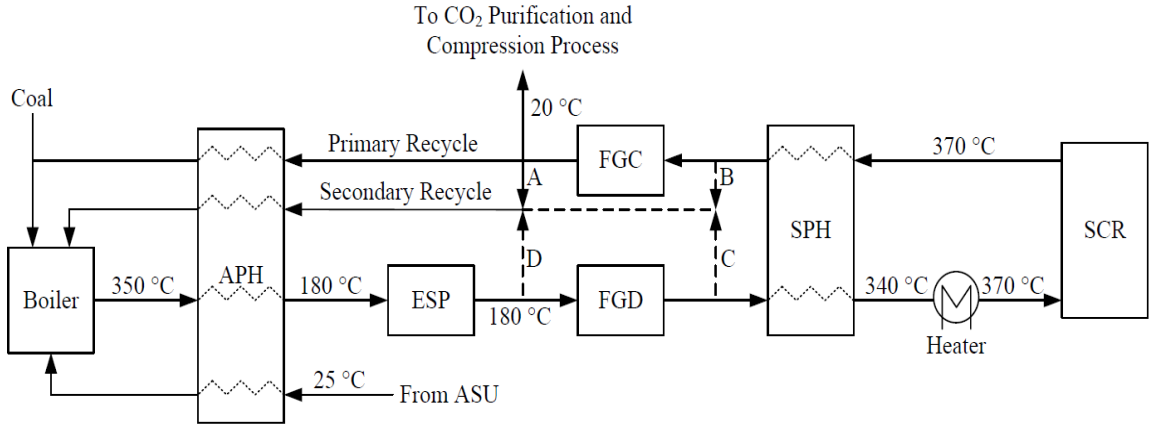

Figure 2.3: Schematic diagram showing flue gas subsystem and re-cycle options in an oxy-fuels combustion systems consisting of SCR, FGD and ESP Flue gas conditioning technologies (Hu et al., 2011).

To summarize, due to the higher preheat temperature, the boiler efficiency has been found to be higher in the oxy-fuel combustion relative to air-coal combustion. The dew point of the flue gas in oxy-fuel combustion was on average, 15 °C higher than that experienced in conventional PF combustion in air, owing to the higher moisture content in the flue gas. In addition, authors found that the change in position of the recycle flue gas stream had little effects on electrical efficiency.

2.3.2. **TGA Experiments**

In addition to performing proximate analyses in a conventional oven, coal analysis can be obtained by thermogravimetric techniques. This has been done extensively and

both methods were used to determine ash, moisture, fixed carbon and volatiles for the three coals.

Toftegaard et al. (2011) conducted two TGA experiments to evaluate the combustion of char in oxy-fuel conditions. The first was to combust char that was prepared in an entrained flow type reactor at 899.85℃ (1173K) and the second experiment was conducted with char that was prepared at 1399.85℃ (1673K). The CO_2/O_2 ratio used in the experiments was 5/95%. The heating rate was 5 ℃/min to reach 849.85 ℃ (1123K) and the sample masses ranged between 1.2-1.5mg char. The results are that chars prepared at higher temperatures in the (entrained flow reactor) EFR, had the most significant deactivation that affected only the combustion rate, as opposed to chars produced at lower EFR temperatures.

TGA can also be used to analyse the combustibility characteristics of coal. Coals with higher rank have a higher peak maximum temperature than coals of lower rank because high rank coals are generally associated with higher carbon contents and CVs. Li et al. (2010) shows the correlation of TGA experiments with proximate analysis in the Figure 2.4 below.

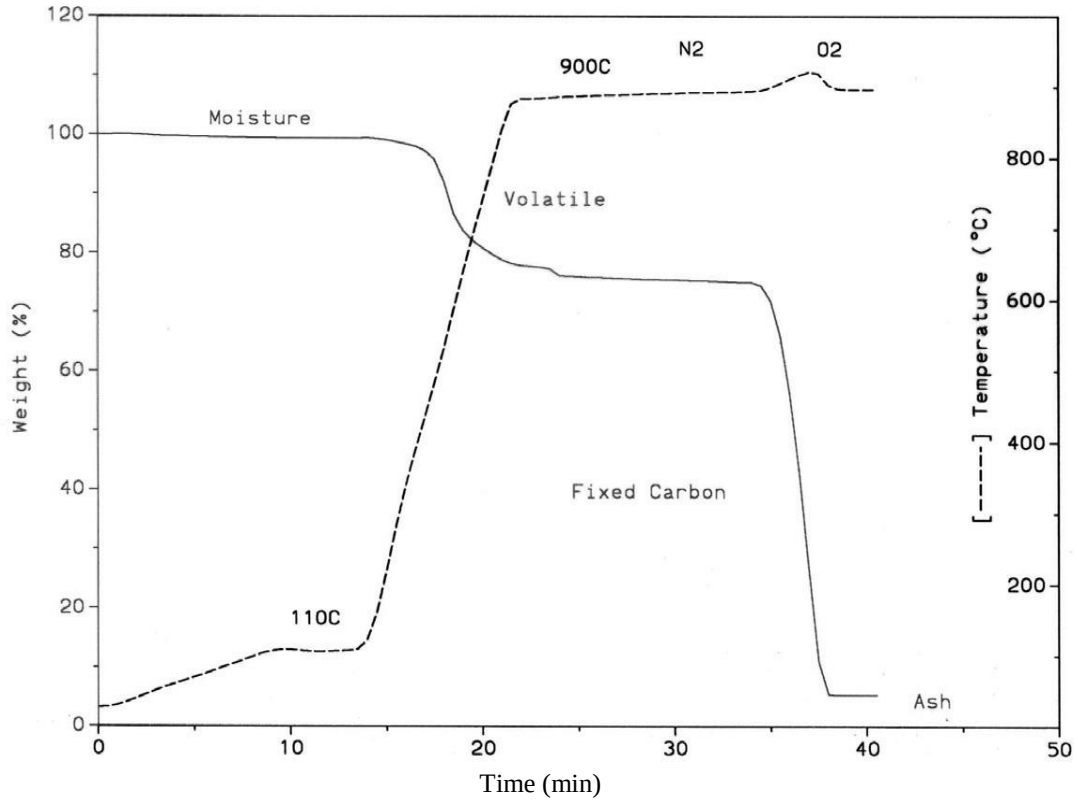

Figure 2.4: Proximate analysis using TGA (Li et al., 2010)

As part of the investigation by Toftegaard et al above, Brix et al. (n.d) also evaluated the coal char reactivity. *[NB: Char is the coal structure that remains after devolatilisation has taken place. Reactivity is the rate of consumption of the char i.e. in combustion or gasification]*. Char reactivity is the combustibility of the char i.e. the coal structure that remains after devolitatilisation has taken place. The char from the coals was prepared in different gaseous environments (O_2/CO_2 and O_2/N_2) and no differences in the char morphologies and coal devolitilisation of each process were found. In addition to this, the char was also produced in a TGA and the gasification reaction was only observed at temperatures exceeding 1100K when no oxygen was present. In the presence of oxygen, the combustion reaction depleted the char before temperatures exceeded 1000K. The coals used in the study are bituminous Laurasian low ash coal (below 10% ash).

Consistent with the study by Rathnam, et al. (2010) and Li et al. (2010), Brix et al. (n.d) found that gasification reaction only has an effect at temperatures exceeding

1100K. As with the TGA above, a similar effect was seen with chars prepared in the entrained flow reactor (EFR).

2.3.3. **Oxyfuel-Combustion Experiments in a tubular reactor**

The above-mentioned literature studies focused on coal properties, combustion mechanisms as well as an exploration of the different configurations for OFC technology. However, most studies on coal char reactivity relate modelling techniques with experiments in a mini-furnace or tubular reactor (also called a drop tube furnace). The aim of this section is to summarise results found in such research.

Naredi (2009) conducted experiments in a drop tube furnace to compare and model the combustion behaviour of high and low volatile coals in oxy-fuel environment as well as air environments. The wall temperatures ranged from 1173K to1673K. In agreement with results discussed above, combustion in oxy-fuel conditions resulted in higher carbon monoxide, lower NOx and lower UBC-(Unburnt Carbon) in ash. It may be expected that the lower NOx emissions were attributed to the fact that there is less nitrogen when air is replaced with CO_2 however this was not the case. Naredi's model showed that the lower NOx formation is attributed to the reduced flame temperatures in OFC which are a result of higher specific heat (Cp) in CO_2 (compared to N_2). This finding is in agreement with Table 1.1 (showing the specific heats of CO_2 and N_2) as well as the findings of Toporov (2014) that are discussed in section 1.1.2. However, it is interesting to note that this finding (lower NOx) is more pronounced with high-volatile bituminous coal than with the lower-volatile coals.

Dhaneswar (2011) studied the effect of coal rank during OFC with focus being on the gasification reaction. Four coals were used in this study (low-volatile bituminous coal, high volatile. bituminous coal; subbituminous coal and lignite) to produce chars in a DTF that was operated at 1873K at three residence times under air and enhanced OFC atmospheres ($30\%O_2/70\%CO_2$). Findings of this study confirmed the findings discussed above, namely that unburnt carbon content (UBC) in ash was more pronounced for low-volatile coals.

Rathnam et al (2013) performed TGA experiments on two types of coal (lignite and bituminous coal) prepared in a DTF. The lower rank lignite coal had a higher reactivity than bituminous coal in both OFC and normal air combustion environments as illustrated in Figure 2.5 below.

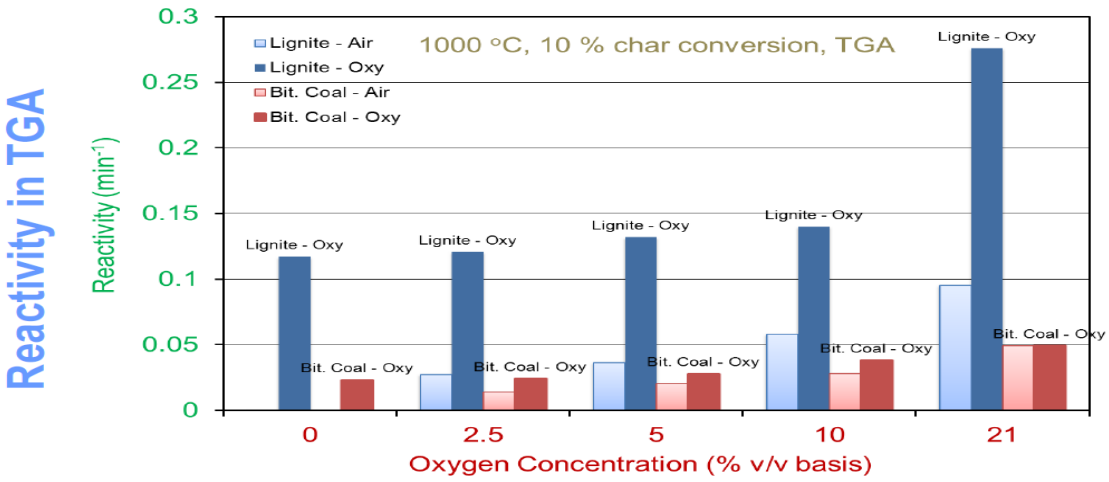

Figure 2.5: Reactivity of two ranks of coal (Lignite and Bituminous) in air versus OFC environment

Furthermore, the lower diffusivity of O_2 in CO_2 (compared to N_2) as well as high temperatures had an influence of the char gasification reaction (CO_2) for oxy-fuel combustion. The char-CO_2 gasification reaction was hence more prominent and had the greatest influence at lower oxygen levels. This was most applicable for low rank coals because there is a larger internal surface area associated with chars formed from low rank coals as compared to high rank.

Drop Tube Furnace (DTF) experiments were also conducted by Rathnam, et al. (2013) for both coals and the following observation was made: the pyrolysis rate for both coals was similar under OFC and Air combustion, and a higher reactivity was observed when pyrolysis took place under 0% O_2/100%CO_2 atmosphere rather than in the 100%N_2. This further suggests the influence of the gasification reaction at low oxygen concentrations due to the reaction of CO_2 and char.

Liu et al. (2005) also conducted and compared OFC and normal air combustion experiments for a single high volatile bituminous coal in a 20kW DTF. These authors found that OFC produces similar combustion environments and gas temperature

profiles as when combusted in air at concentrations of 30%CO_2/70%O_2. The reason for this was stated to be that CO_2 has a higher specific heat capacity than nitrogen and even has the potential to quench the combustion flame if used to replace N_2 stream. OFC of these concentrations also showed lower NOx emissions, better char burnout and reduced CO emission.

Murphy and Shaddix (2006) investigated the oxy-fuel combustion process of two coals compared to conventional air fired conditions. The operating temperatures were between 1320 and1800K and 6-36 mol%O_2. The experiments were conducted in an entrained flow reactor and the chars were collected using a rapid flame quenching sampling probe while the particle sizes were measured using an optical particle sizing pyrometry diagnosis. The findings were that OFC resulted in higher char particle temperatures and the reaction order varied between 0.1 in conventional air fired conditions and 0.5 under OFC conditions. This may suggest more rapid reactivity in OFC.

Pallares et al. (2007) investigated the integration of various CFD codes and advanced combustion models for quantitative burnout determination of three types of coal. The devolatilisation was modelled using FG-DVC as opposed to Flashchain and the char oxidation was modelled using an intrinsic reactivity approach where maceral effects were taken into account, as well as thermal annealing and ash inhibition of the coals. This work makes use of the char burnout power law model assuming the power to be 5. This law also incorporates the maceral (vitrinite and inertinite) constituents of the coal as determined from petrographic analyses (see equation 2.1 below). However, in the study by Pallares et al. (2007) no petrographic analyses were made and the vitrinite and inertinite content required for char burnout determination were estimated from literature.

$$q_{cmb} = m_p \times \eta \times f_{mac} \times R_s \times (P_g)^n \qquad \textbf{Equation 2.1}$$

The symbols are expanded in chapter 6.

As part of his research studies, Kangwanpongpan (2013) modelled the OFC of lignite coal using CFD. Although the focus of this study was on radiation properties of the OFC gas mixture, further observations were found in his study that are worth mentioning here. These are mainly that the reaction of char with oxygen and/or carbon dioxide are heterogeneous and influenced by coal pore structure, external surface area and the coal burnout rate (Kangwanpongpan, 2013). The intrinsic model for *char combustion* differs from the *overall diffusion rate* in that the former (i.e. char combustion rate) only takes into account the internal surface area of char and gas diffusion through it, while in the latter (i.e. the overall diffusion rate), the overall diffusion rate is focused on the bulk and Knudsen diffusion as explained by (Mitchell, 2013). The effectiveness factor and Thiele modulus that must be used in intrinsic rate calculations are different for char combustion in air versus in oxygen (oxy-fuel) according to sources in literature. This may be explained as follows; the Thiele modulus, from which the effectiveness factor is derived, is dependent on the partial pressure of oxygen in the gas stream (refer to chapter 6).

Murphy and Shaddix (2006) conducted combustion experiments in an entrained flow reactor to determine the combustion kinetics of two types of coal; a Highvale sub-bituminous coal and a high-volatile Eastern United states bituminous coal. The findings were consistent with what is found in literature, namely, that char particle temperatures in low oxygen concentrations are lower than in high oxygen concentrations. This observation was supported by quantifying the apparent reaction order which was found to range from 0.1 (at low O_2 concentrations) to a maximum of 0.5 at high oxygen concentrated atmospheres.

The following reaction zones are defined by rate controlled regimes (Smoot & Pratt, 1979; Naredi, 2009);

Zone I: Kinetic controlled, lower temperatures- In this phase, the chemical reaction, which is influenced by such contributory factors as activation energy, absorption of reactant or desorption of the products is the rate limiting step.

Zone II: Pore diffusion controlled regime, intermediate temperature range- in this atmosphere, the reaction rate is mostly influenced by the amount of particles able to diffuse through the pores of the surface area to react with the species involved in the reaction.

Zone III: Mass transfer controlled regime, higher temperatures- the reaction in this atmosphere is determined by the amount of particles able to physically move to the reaction zone and is also often termed the diffusion limited phase and in contrast to Zone I, the activation energy is typically low.

The apparent reaction order is the true reaction order at low temperatures, when the reaction is controlled by chemical reaction only (Zone I of the combustion regime) while in Zone II the apparent reaction order is defined as: $\frac{True\ reaction\ order+1}{2}$ Kangwanpongpan (2013). As with Kangwanpongpan (2013), Murphy et al. (2006) and have assumed reaction order to be near zero at Zone III of the combustion regime, i.e. at high temperatures and diffusion limited reaction phase.

In contrast, the authors of the IEAGHG research document on OFC (IEAGHG, 2010), in their paper on OFC of pulverised coal found that although increasing the O_2 concentration resulted in faster char burnout, the opposite effect was noticed when the gases are switched from nitrogen to carbon dioxide. As a result, this meant that in OFC (i.e. O_2-CO_2 gas mixtures), the concentration of O_2 would have to be increased above that in air to approximately 30% O_2. These findings are consistent with literature cited above (Liu et al., 2005)).

To expand on this, an experiment in a 100kW demonstration plant was conducted by Anderson et al. (2006). These authors found that combustion temperatures in OFC matched those of air at a gas concentration of 27% O_2 -slightly lower than 30% mentioned above, but still higher than oxygen concentration of normal air. This has good implications for OFC as it could imply reduced costs associated with the ASU and gas mixing (if less O_2 is needed).

In a review paper by Chen et al. (2012), these authors found that at low temperatures and low O_2 concentrations, reaction rates of OFC and air combustion are similar, while at higher O_2 concentrations and high temperatures, OFC reaction rates exceeded that of air combustion (at the same O_2 level) due to the lower O_2 diffusion rate in CO_2. This is in agreement with the observations found in literature (Toftegaard et al., 2011: Li, et al., 2009; Brix et al., n.d. ; Rathnam et al., 2009; Rathnam, et al.,2013). Chen et al., (2012) also found that the char-CO_2 reaction became more pronounced at low O_2 concentrations and high temperatures as well as at low temperatures and significantly low O_2 concentrations. This was attributed to the gasification reaction that takes place in OFC environments.

One of the reasons combustion modelling is complex is because of the interference of particle to particle interactions. This challenge has been circumvented by Bajarano and Levendis (2008) who conducted DTF experiments of single coal particles, i.e. bituminous, lignite and synthetic char samples in oxy-fuel and air combustion environments. The DTF was heated electronically to 1400 and 1600K and the particle size ranges for the bituminous and lignite coals were 45-53 microns, 150-180 microns and 43 microns for the monodisperse synthetic chars. The findings confirmed that particles had shorter burnout time and higher particle temperatures in air combustion at similar oxygen mole fractions and that this phenomenon was only reversed once O_2 mole fractions reached between 30-35%. However, an interesting observation made in this study was that there was less of a difference in O_2 mole concentrations required in the different gas mediums (N_2 and CO_2) to achieve the similar particle temperatures and particle burnout times (Bejarano & Levendis, 2008).

In another publication by Khatami et al., (2012) a comparative analysis of combustion between OFC and air combustion was made for three coal ranks on a single particle basis. The experiment was carried out for samples of four coal ranks (high-volatile bituminous coal, sub-bituminous coal and two lignites) in a DTF that was heated up to 1400K. The coals were pulverised to 75-90 microns and a three-colour optical pyrometer was used to isolate the single particles. The different ranked coals combusted uniquely in air, while the flame of all four coals was observed to be

less intense in the OF atmosphere. Furthermore, this study showed that low rank coals were the most affected by O_2 concentrations and that they reacted heterogeneously with the OF gas mixture (CO_2/O_2).

In a similar OFC study, Niu et al., (2009) conducted TGA experiments on three Chinese coals of different ranks and found that under the same conditions, higher rank coals had more combustion difficulties than their low rank counterparts.

According to literature, the O_2 purity required in OFC is 95% (Wall et al., 2009). Given this fact, Wall et al (2009) estimated the flue gas recycling requirements to be approximately 60% of the total flue gas production stream. The volume of flue gas emitted in the atmosphere is reduced by up to 80% (depending on the flue gas recycle ratio). In addition to that, 30% O_2 by volume is required in the combustion air (versus 21% in conventional air combustion), the excess air required to achieve complete combustion in OFC is 3-5% versus 20% that is typically required in normal air combustion. Wall et al., (2009) have also identified the competition of CO_2 and O_2 in heterogeneous reactions and have postulated that higher reactivities seen in OFC at high temperatures and high O_2 concentrations may be due to the char-CO_2 (gasification) reaction[2]. They speculated that the gasification reaction (char-CO_2) could contribute to char burnout (carbon loss) at higher O_2 level. Based upon their research and observations, these authors identified a gap in this area and they recommended a study for the contribution of gasification reaction to carbon loss in steam generation boilers.

In agreement with the findings above, Rathnam et al., (2009) conducted DTF and TGA experiments on four Australian coals and reached the same conclusions as Wall et al., (2009) Toftegaard et al., (2011) and Brix et al. (n.d). The coals were subject to air and oxy-fuel combustion environments at 1673k in the DTF and 1473K in the TGA and the O_2 concentrations ranged between 3-21% in N_2 (air) and 5-30% in CO_2 (by volume). As with the above-mentioned findings, char burnout was faster at high

[2] The reaction order for the overall reaction was assumed in this study is 0.2-0.5

temperatures and low O_2 concentration indicating the occurrence of the gasification reaction (char-CO_2) in this reaction zone. Rathnam et al., (2009) recommended further studies to clarify and verify the assumptions made for the differences in coal burnout under the two conditions. It is these aspects that this current study aims to explore at least in terms of modelling the initial stages, and the results obtained would still need to be verified by experimentation in a demonstration plant.

In a detailed study of the char-CO_2 gasification reaction, Liu et al. (2000) conducted a mathematical model describing this reactivity at high pressures and temperatures and found that, char type is more significant than CO_2 partial pressure in the gas stream. Temperature had the greatest influence on char reactivity over and above the pressure and char type. Another important conclusion from this study is that activation energy of 212 kJ/mol was found to be appropriate for most bituminous coal chars reacting with CO_2 in a gasification reaction. These findings were verified by conducting experimental analyses in an entrained flow reactor.

Finally, Wall et al. (2009) and several other sources in literature have observed delays in ignition even though OFC has higher carbon burnout compared to conventional air combustion. This has been attributed to aerodynamics and gas property differences. Such phenomena will not be investigated in the present study as the focus is only char burnout modelling and the effect of coal type and rank on oxy-fuel combustion. That is, burnout and delayed ignition are not included in the scope of this study.

Hitatchi have performed a study to determine the change in flue gas composition if OFC was to be retrofitted to an existing coal fired plant with minimal modifications (Tigges et al., n.d). These differences are tabulated below.

Table 2.4: Flue gas species of OFC versus air combustion (Tigges et al., n.d)

Gas species	Composition of flue gas from air-combustion after ESP	Composition of flue gas from oxy-fuel combustion after cooling
H_2O	5.9	4.8
CO_2	19.4	89.9
N_2	68.7	2.0
O_2	4.5	2.9

The configuration for the OFC retrofitted power plant used in this study is depicted in Figure 2.6 below:

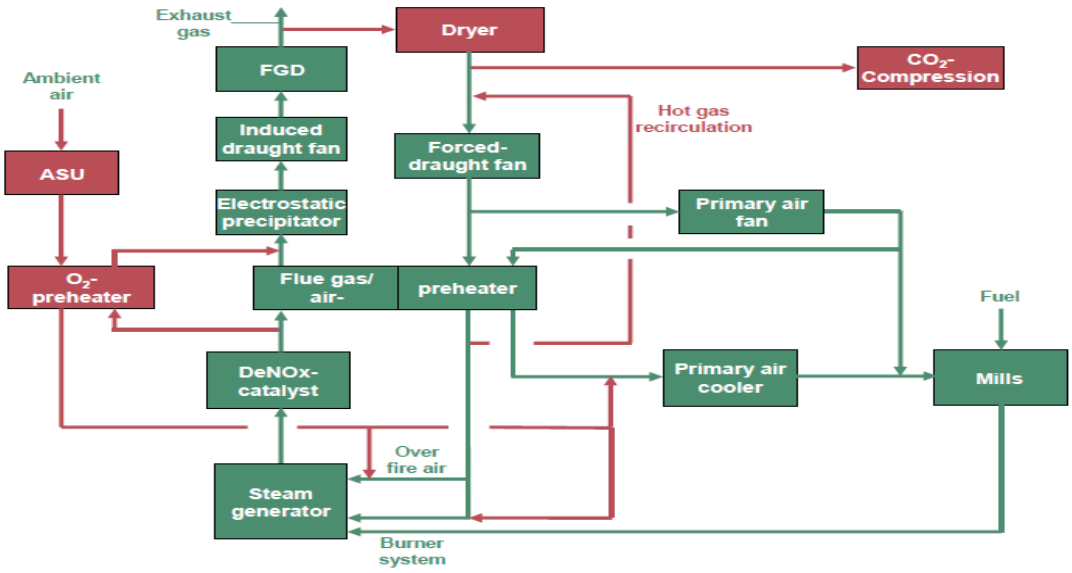

Figure 2.6: Overall process design modifications when retrofitting a power plant with OFC technology (Tigges et al., n.d)

Chapter Summary

The literature survey that was conducted can be summarised as follows;

Oxy-fuel combustion reduces coal reactivity and char burnout rates at low oxygen concentrations, for all types of coal. To achieve similar coal combustion and burnout

rate experienced in air, the oxygen concentration would have to be increased to 30% by volume in the combustion gas stream. The lower flame temperature is due to the higher specific heat of carbon dioxide compared to nitrogen.

Furthermore, the experiments conducted also show that less NOx is formed in OFC than in air and this was attributed to the lower temperatures associated with OFC explained above, this phenomenon holds true especially for higher volatile coals.

Additionally, the amount of unburnt carbon in ash is higher for low volatile coals and this phenomenon is associated for lower-volatile coal due to the char-CO_2 gasification reaction. Finally, the reduced UBC in ash was more notable for the lower-volatile coal than the high volatile. This was attributed to the gasification reaction (i.e. char and CO_2) that was predicted in the intrinsic model however only for the lower-volatile coal.

CHAPTER 3

3 METHODOLOGY

This Chapter presents the samples used in this research and the methodologies undertaken to adopt the models required to service this research.

The following methods were adopted to determine the fuel's properties:

Conventional analyses were conducted at Eskom's Research, testing and development (RT&D) centre. The proximate analyses were conducted using the conventional methods as well as using a thermogravimetric analyser (TGA) for verification and validation. The petrographic maceral contents and rank by vitrinite reflectance were determined by a qualified petrographer at the coal laboratory at the University of the Witwatersrand where the mineralogy was also estimated. The results for the coals mineralogy were confirmed using QEMSCAN at as well as by XRF experiments, both at Eskom's RT&D laboratories.

3.1 Sampling

A 3kg sample of coal from each of the three colliery sources were obtained, namely:

- Coal A
- Coal B and
- Coal C

The samples were prepared according to ISO standards (ISO 7404-2). First, the coal was crushed to -1mm, prior to splitting the coal between petrographic, QEMSCAN, ash analyses and TGA tests. For the latter three analyses, the crushed coal was used as -1mm sized particles, but for the conventional analyses (i.e. proximate and ultimate analyses) as well as the TGA tests, the coal was crushed to -212 microns. The split was as follows for each coal sample: 120g for proximate and ultimate testing, 1kg for

petrographic analysis, 100g for QEMSCAN analyses, 800g for TGA and 500g for ash analyses and AFT measurements. This totals 2520g, the remaining 480 g kept for repeat tests if necessary.

3.2 Conventional Analyses

Details of the methodologies, type of equipment used and standards and procedures for analyzing the coals under review may be found in Appendix A.2

- Proximate analyses were performed to determine; the inherent moisture, volatile matter, ash and fixed carbon contents.
- Secondly, Ultimate analyses were performed to determine the elements; Carbon, Hydrogen, Nitrogen, Oxygen as well as Total Sulphur contents.
- In addition to this, the net calorific value and petrographic analyses were also performed.
- Finally, in detailing the ash analyses found during proximate analyses, the ash elementals were determined with the use of X-Ray fluorescence (XRF) as well as the ash fusion temperature.

3.3 Petrographic analysis

Optical Petrographic analysis was performed on all three coals under investigation. Maceral, mineral and rank by vitrinite reflectance analyses were performed. A total of 100g of each coal sample was prepared (top size: -1mm). Petrographic analyses were conducted by the internationally accredited coal laboratory at the University of Witwatersrand. The methods for preparing coal samples, determining the composition of macerals, minerals as well as rank by reflectance of vitrinite were conducted according to ISO 7404. The samples were first rifled to obtain a representative sample, and formed into blocks following ISO 7404-2. The maceral analysis was performed as per ISO 7404-3 and reflectance of vitrinite was determined according to ISO 7404-5 using a Leica DM4500P petrographic microscope fitted with a J&M Spectrolytic system. The composition of macerals was determined in accordance to

the standard mentioned above using a semi-automated point counting stage and Petrog software attached to a Zeiss Universal microscope.

All petrographic analyses presented here were conducted by a certified petrographer with considerable experience and relevant ICCP accreditation. The coals are ranked using the ECE-UN in-seam classification system. Petrographic analyses distinguish between inert and reactive macerals deeming it an important indicator of reactivity. For these reasons, the vitrinite and intertinite content that were determined for each coal were used in the theoretical model developed to approximate the char burnout rate (see chapter 6 below).

3.4 QEMSCAN Analysis

3.4.1. Introduction

QEMSCAN is an instrument (microscope linked to a computer with refined software) used to identify the size, shape and chemical and optical properties of minerals and coal-mineral particles. This was done by calculating the total area as well as the area of the organic matter for each individual coal particle (van Alphen, 2007 and Liu et al, 2005).

3.4.2. Investigation into the anomalous mineral matter results between QUEMSCAN and XRF

The ash content determined using QEMSCAN was higher than that determined using proximate analyses. With the naked eye, it could be seen that all three coal samples had a high percentage of fine material and it was assumed that the fines contributed to the higher ash results seen in QEMSCAN. This was especially due to the fact that the samples that were produced for proximate analysis and QEMSCAN analyses were prepared separately. Thus it was suggested that the fines be separated from the course of each sample and both size fractions (course and fine) be re-analyzed, viz. proximate and QEMSCAN separately for each coal sample. It should be noted that the reclassification of the particle size distribution, i.e. fines vs. coarse is specific to

the samples used for the purposes of the block preparation for QEMSCAN study. The distinction between coarse and fine is thus not adopted from literature but was made solely for this study and is unique to the coal samples analyzed. This was done in order to allow for the successful use of the QEMSCAN software.

According to The South African Coal Processing Society (2011), "course coal" is classified as coal particles larger than 600 microns in diameter, while "fine coal" is coal particles having diameter less than 500 microns. However, for the purposes of this study, coarse coal was chosen as particles with diameter greater than 106 microns and fine coal less than 106 microns. The reason behind this classification was due to the nature of the three coal samples under investigation, and specific to them. The samples had been pre-crushed, all to -1mm. A particle size distribution curve was generated for the three samples and the majority of the mass of the particles were less than about 150 microns. This is true for all three coal samples and was confirmed using QEMSCAN software. It therefore appears that the fines that could have distorted the results of the ash analyses as fine particles smaller than 150 microns showed the most prevalence (see Figures 3.1 to 3.3). The procedure used in preparing and analyzing the samples using QEMSCAN is described below.

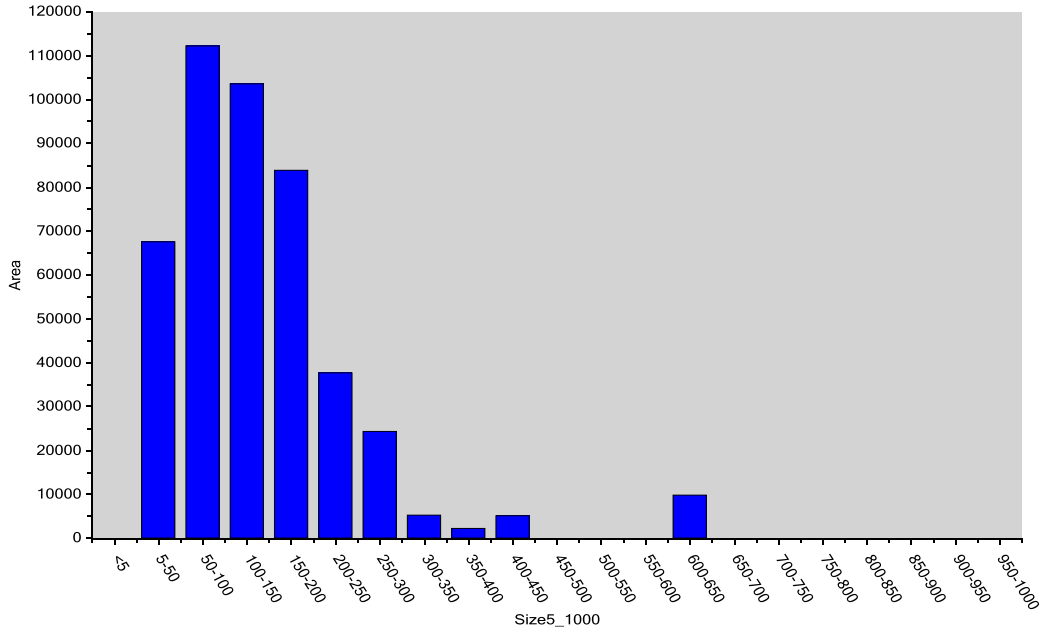

Figure 3.1: Pixel Area versus particle avg. diameter size in microns for Coal A sample

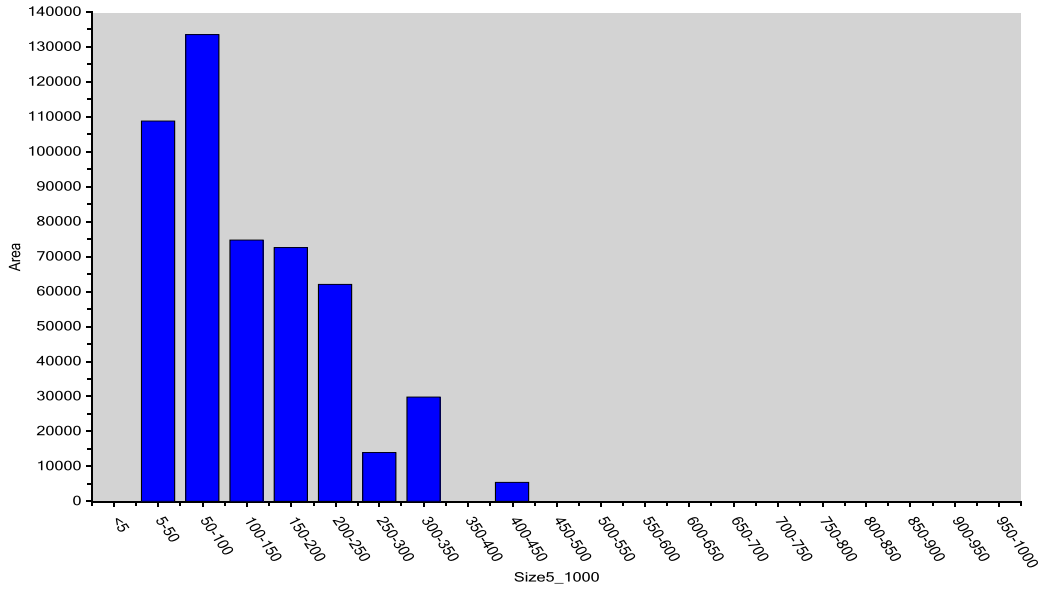

Figure 3.2: Pixel Area versus particle avg. diameter size in microns for Coal B sample

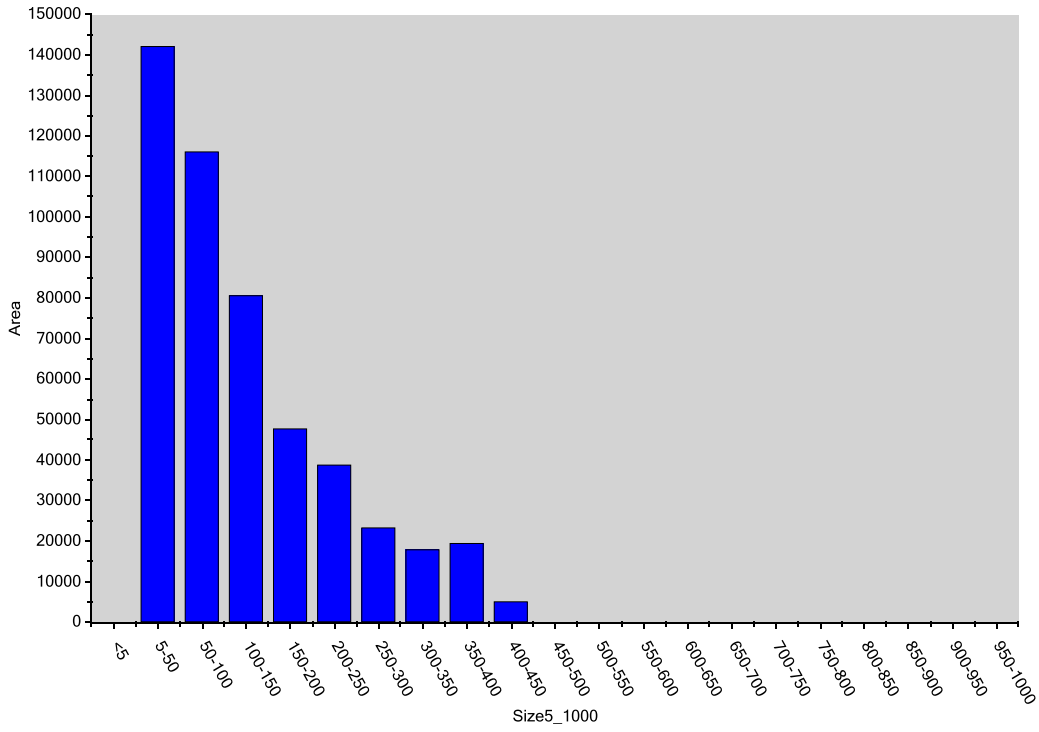

Figure 3.3: Pixel Area versus particle avg. diameter size in microns for Coal C sample

3.4.3. Screening procedure

Once the screen size was determined this way, the screening method i.e. wet or dry had to be determined. Wet screening was used to separate out the fine material (<106 micron size) from the original coal sample (-1mm).

The basis for selecting the wet screening method was due to the large amount of fines that were evident in the samples. Fine coal has higher moisture content than coarse coal, and tends to stick to course particles during dry screening, thus passing over the screen (along with the coarse material) rather than through it. Wet screening is known to generally overcome this problem and greatly increase the separation efficiency, "The South African Coal Processing Society" (2011).

The average plastic in which these coals were sampled weighed: 1.264 grams and was tarred in each measurement. Thus mass of coal was:

Table 3.1: Original mass of parent coal samples

Total Coal Sample (Before screening)	Corresponding Weight (g)
Coal A	37.98
Coal B	26.26
Coal C	19.08

The following procedure was followed for each sample:

A screen of aperture size: -106 was placed on top of a pan. 675 ml of water was slowly poured over coal particles and slightly pushed through the screen using a (clean) dry paint brush. Coal particles greater than 106 microns remained on top of the screen while those smaller than 106 microns passed through with the water and collected in the pan. The purpose of the brush was to facilitate separation by washing out the fines thus minimizing the effect of blinding and pegging of the screens.

While the fines were being washed out this way, the screen and pan were subjected to elliptical and liner vibrations and shaking motions. Water was poured until the water passing through the sieve was clean (with no fine particles to make it grey). This indicated that the separation was complete.

The two containers: i.e. the screen with course coal on top of it and the pan filled with a mixture of water and fines were left for 15 minutes to allow droplets of water with fines to continue to seep through. Thereafter, the top sieve was placed in an oven at 70 degrees Celsius for 30 minutes to allow the washing water to evaporate. The temperature was not allowed to exceed 70 degrees Celsius and the oven time was not allowed to exceed 30 minutes as either case could evaporate the coals inherent moisture, thus affecting the coals chemical makeup.

After drying, the course fraction i.e. -1mm+106mcron was slowly transferred onto a clean sheet of paper and transferred from there into a small plastic bag which was then weighed.

The following masses were recorded for the course fraction of each of the coal samples:

Table 3.2: Total mass of coals obtained after screening

Course coal Sample (After screening)	Corresponding Weight (g)
Coal A	31.10
Coal B	20.54
Coal C	13.85

A mass balance was made to calculate the (theoretical) amount of fines to be expected in the water mixture in the pan.

$$Total\ Mass = Mass\ of\ Course\ fraction + Mass\ of\ fine\ fraction$$

The following mass of fines was obtained for each of the coal samples:

Table 3.3: Mass of fine coal (less than 106 microns) obtained after screening (calculated)

Fine coal Sample (After screening)	Calculated Weight (g)
Coal A	6.88
Coal B	5.72
Coal C	5.23

The actual mass of fines for each of the coal samples are tabulated below:

Table 3.4: Mass of fine coal (less than 106 microns) obtained after screening

Course coal Sample (After screening)	Weight (g)
Coal A	6.05
Coal B	4.00
Coal C	3.08

The pan with the water/fines mixture was left overnight to allow the fine particles to settle to the bottom of the water. Thereafter, the pan was tipped over to pour out the (clear) water and then dried in the oven at 70 degrees Celsius, for 90 minutes to dry the fine particles. The mass of fines was weighed to ensure that it matched the calculated mass above. Discrepancies in total mass are tabulated below:

Table 3.5: Discrepancies in calculated and actual mass balances

Coal Sample	**Total Mass (grams Before screening)**	**Total Mass (grams After screening)**	**Mass Loss (g)**
Coal A	37.98	37.15	0.83
Coal B	26.26	24.54	1.72
Coal C	19.08	16.93	2.15

Factors that could have possibly contributed to the mass loss:

- Accumulation of coal particles to the brush during wet screening
- Accumulation of fine particles on the screen itself beneath the mash due to hydrophilic behaviour of wet (fine) coal particles that were supposed to pass through and collect with the water in the pan.
- Accumulation of coal particles in the apertures, in between the wires of the screen. i.e. particles of the size: 106 microns that would not pass through or stay afloat when brushed through as their diameter is equivalent to that of the screens aperture size. This phenomenon is known as blinding and is very common with wet screening of fine particles between 250-1000microns (The Coal Processing Society of SA, 2011:85) and (size Brantly & Thomas, 1983).
- Mass lost during transfer of dried coal from the oven to the plastic bag.

After drying, five grams were weighed out of each sample and then each crushed to -212 microns. A mill was used to pulverize the coal particles to -212 microns. In each sample, the silver tray was black with PF fixed on it. This indicated that the coal

particles were not completely dry. The PF was then transferred to a -212 micron screen that vibrated (linearly, up and down) to sieve out any particles that were >212 microns in size. Thereafter proximate analysis was done for each of the coal samples.

In preparing the sample blocks, the following masses were weighed out for each size fraction. The reason for using a slightly more sample when preparing sample blocks for the course particles is to avoid segregation often experienced when course particles separate due to the presence of air when mixing in the melted canuba wax.

Table 3.6: Recommended coal sample mass for QEMSCAN analysis according to size fraction

Size fraction description	Size fraction (μm)	Sample mass required (g)
Course particles	>212 microns	0.18-0.22
Semi-fine particles	212>Semi-fine>106	0.16-0.20
Fine particles	<106	0.15-0.18

3.5. Thermogravimetric Analyses (TGA): Combustion in Air

A Thermogravimetric Anaylser (LECO TGA701) was used to test the coals under investigation.

Each coal sample was rifled into three size fractions; -212 micron, +106 and -106 micron (fines). The TGA can test up to 18 crucibles (one for control) which were all filled as the coals were tested in duplicates. Results are tabulated in Appendix C.

- The determination of the inherent moisture content of coal (Method number 103)
- The determination of ash content of coal (Method number 101)
- The determination of the volatile matter content of coal (Method number 102)

The preparation for each coal sample was made using ISO methods and crushed to different size fractions as shown in table below. The TGA has space for 19 crucibles, allowing each size fraction to be analysed in duplicates. See below.

Table 3.7: Crucible identification and size fraction for each sample (in duplicates) analysed by TGA

Crucible Nr	Coal sample	Sample Duplicate nr.	Size fraction
1	STD CC 008 (reference coal)		-212um
2	Coal C	I	-212um
3	Coal C	II	-212um
4	Coal C	I	+106um
5	Coal C	II	+106um
6	Coal C	I	-106um
7	Coal C	II	-106um
8	Coal A	I	-212um
9	Coal A	II	-212um
10	Coal A	I	+106um
11	Coal A	II	+106um
12	Coal A	I	-106um
13	Coal A	II	-106um
14	Coal B	I	-212um
15	Coal B	II	-212um
16	Coal B	I	+106um
17	Coal B	II	+106um
18	Coal B	I	-106um
19	Coal B	II	-106um

3.6. Theoretical Modelling of Char Burnout: Development and application

The development and application of the model and key assumptions made are presented in chapter 6. The models selected for use were those of Dhaneswar (2012) and Pallares, (2007).

CHAPTER 4

4. RESULTS

This chapter presents the results of the tests and analyses conducted on the three coal samples.

4.1. Conventional Analyses

Conventional analyses in this study include: Proximate, Ultimate analyses, Calorific Values (CVs), ash fusion temperature and ash composition using ISO standards. The results are presented in Appendix A-B and summarised in Figure 4.1 and 4.2 below. The coals are all categorised as grade D with CV's ranging from 17.3 to 21.1 MJ/Kg (AD basis). Ash contents range from 32 to 37.5% (AD basis) with Coal C the highest value. Volatile matter contents range from 22.7% to 25% (AD basis) with Coal A the highest value and Coal C the lowest.

In all other respects, these coals have similar analyses, with Coal C the only coal showing marginally variable values relative to the other two i.e. lower carbon contents and higher ash fusion temperatures.

Based upon the fuel ratios (FC to VM), Coal A and C presented values of 1.65 and 1.66 respectively whereas Coal C presented 1.8 (See Figure 4.1). The latter signifies a higher FC content when compared to the other two samples, as their VM content was not too dispersed.

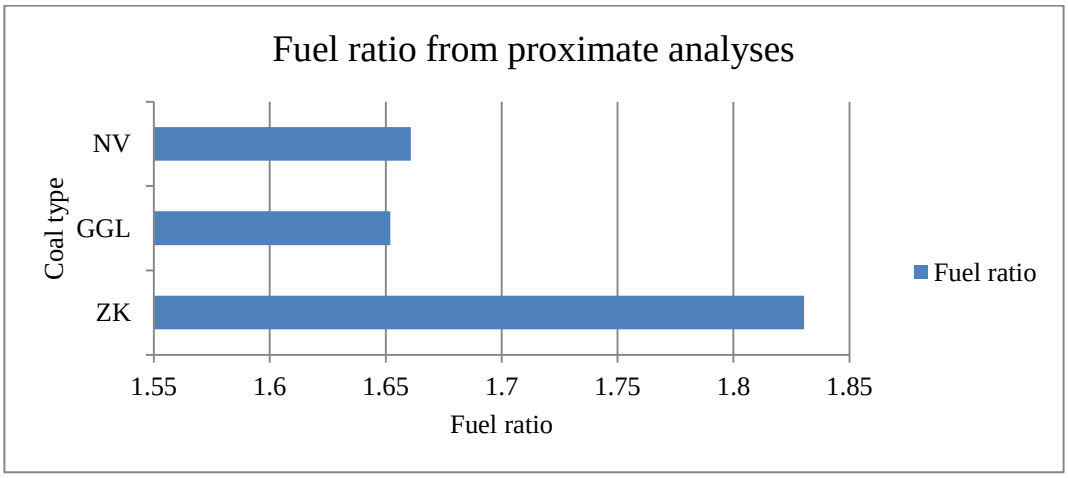

Figure 4.1: Fuel ratio for the coal types from proximate analyses

The Oxygen to Carbon as well as Hydrogen to Carbon ratios were calculated from the ultimate analyses. Coal B once again showed the lowest O/C ratio while Coal C was the highest. See Fgure 4.2 below.

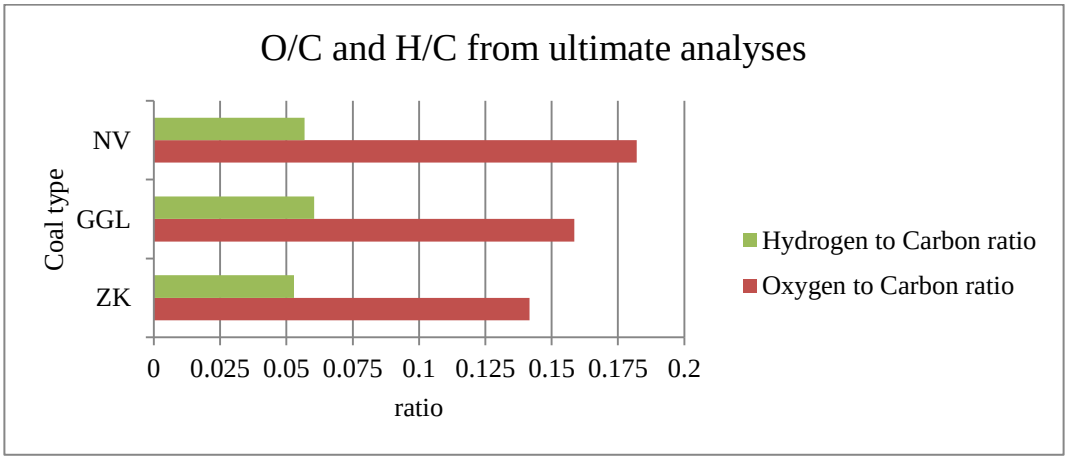

Figure 4.2: Hydrogen to Carbon and Oxygen to Carbon ratios for the coal types from ultimate analyses

The above ratios are useful for predicting char reactivity as discussed in further detail below (Chapter 5: Discussion).

4.2. Specialised Analyses

4.2.1. Thermogravimetric Tests versus Size Fractions

The proximate analyses were undertaken using conventional laboratory-based SABS methods (as reported above) and were also measured using a Thermogravimetric analyser (TGA). A summary is presented below, where proximate analyses are trended against size fractions.

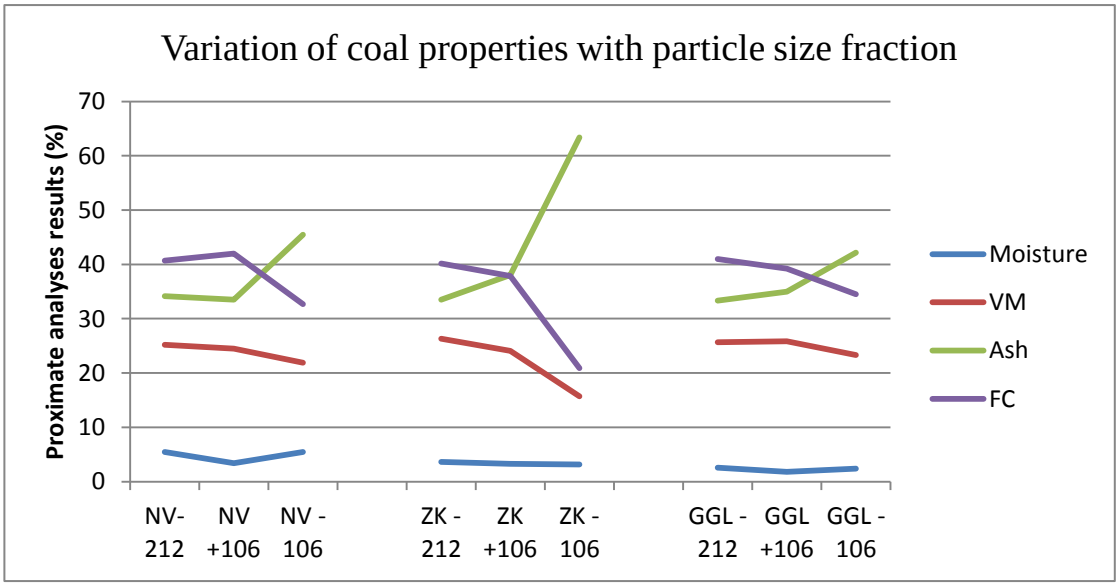

Figure 4.3: Variation of coal properties with particle size fraction

As seen in Figure 4.3, a qualitative relationship can be drawn between the proximate analyses results and particle size for each coal sample. The volatile matter and fixed carbon content decrease with decreasing size fraction, while the ash content increases with decreasing size fractions. This trend has implications on coal combustion as subsequently elaborated below (discussions).

4.2.2. Petrographic Analyses

The coals have a relatively similar rank, medium rank C/D with Coal C the lowest rank based on the vitrinite reflectance (0.54RoV %). Coal A and B have vitrinite reflectances of 0.65-0.66 RoV%. Vitrinite contents vary significantly with Coal C possessing lowest values (18.3% mmf) and Coal A and B relatively high values (57.1% and 65.8% mmf).

The results are tabulated in the Appendix C2: Optical Petrographic Analysis.

Table 4.1: Inertinite to Vitrinite ratios (volume %) from petrographic analyses on a mineral matter free (mmf) basis.

Coal	Coal A	Coal B	Coal C
Total Vitrinite	57.1	65.8	18.3
Total Inertinite	37.8	31.8	76.1
Inertinite/Vitrinite	0.66	0.48	4.16
Total Reactive Macerals	65.2	31.9	76.2
Rrandom	0.65	0.66	0.54
Rank Category	Med rank C	Med rank C	Med rank D

Total Inertinite contents vary equally with Coal C containing 76.1% mmf and the remaining two coals; A and B 37.8 to 31.8 % mmf respectively.

It is interesting to note the Inertinite to Vitrinite ratios of the coals under investigation. Coal C has the highest ratio of the three, and is the only coal classified as medium rank D, making it the lowest reactive rank and maceral coal of the three, as it has four times more inertinite than vitrinite. It is the most inert-rich coal relative to the other coals analysed.

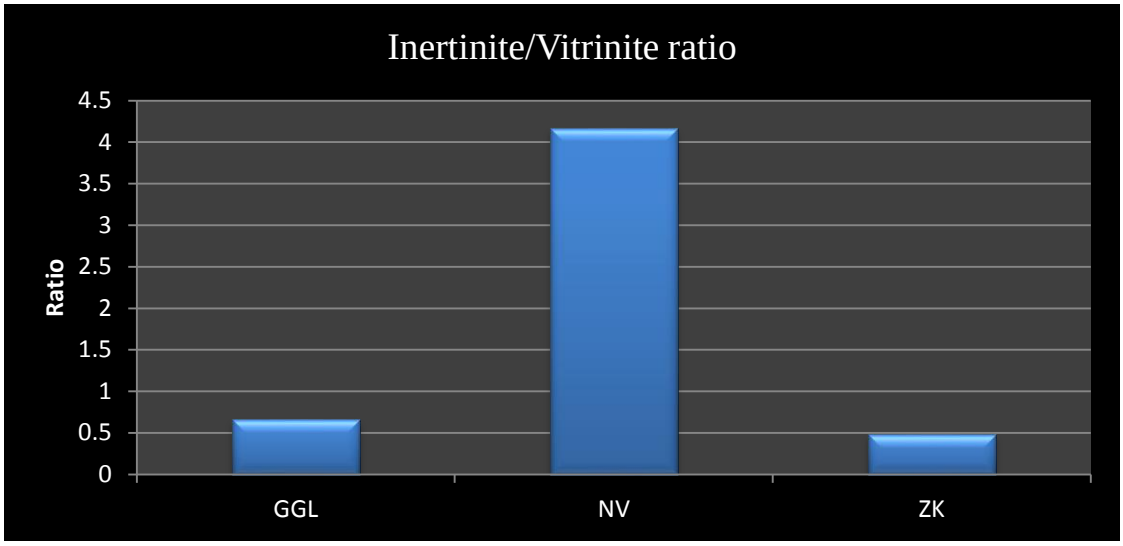

Figure 4.4: Inertinite to Vitrinite ratio of the coals under investigation

As with the proximate results by TGA, the petrographic results displayed in the figure above; i.e. reflectance and vitrinite, will have implications on the char reactivity. Further discussion can be seen in chapter 5 below and the modelling in chapter 6.

4.2.3. Ash determination using different analyses

The TGA was used to conduct proximate analyses. The results obtained are produced below in graphical format and are consistent with the conventional proximate analysis results displayed above that was conducted in 2013 and 2014. Further discussion is provided in section 5.2.

The laboratory ISO methods for proximate analyses were performed in 2013 and verified by conducting more SANS laboratory tests, as well as by TGA techniques (both conducted in 2014). QEMSCAN analyses were also conducted to quantify the mineralogy of the three coal samples. The results of both sets of analyses are fairly similar for all three coal samples, with the exception of the ash content determined by QEMSCAN. When calculating the ash content via QEMSCAN mineralogical analyses, the QEMSCAN mineralogy (ash) analyses consistantly showed much higher ash contents.

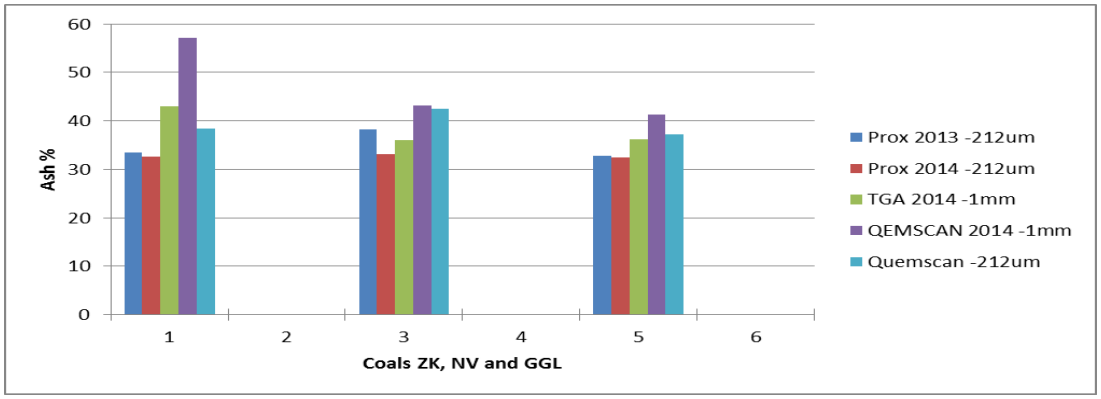

Figure 4.5: Summary of Ash results from different analyses (proximate, TGA and QEMSCAN).

Fuel characteristics of coal also form an important consideration in OFC. In this study, an in-depth analysis of the fuel properties has been conducted to assess the potential implications of retrofitting South African coal-fired power stations with OFC technology. From literature, the moisture content of coal has been shown to have an inversely proportional relationship with the flue gas recycle ratio, i.e. the flue gas recycle ratio decreases with increasing moisture content of parent coal (Hu, 2011). The (higher) oxygen content will also result in a decrease in flue gas recycle ratio as it will take part in the combustion reaction process. When looking at coal rank, the sub-bituminous coal (of same moisture content as bituminous) required less oxygen than bituminous, further emphasising the point made above of the relationship between oxygen and flue gas recycle ratio. A more comprehensive discussion on fuel properties and their relation to oxy-fuel combustion is subsequently presented in chapter 5 below.

CHAPTER 5

5. DISCUSSION ONE: CHARACTERISATION OF COALS

This Chapter will present detailed discussion on the coal qualities.

5.1. The combustion characteristics of the three coals under investigation using ISO standards method

The results of the proximate analyses presented below (Figure 5.1) indicate that the Coal A sample had the highest volatile matter content, followed by B whereas Coal C had the lowest volatile matter content.

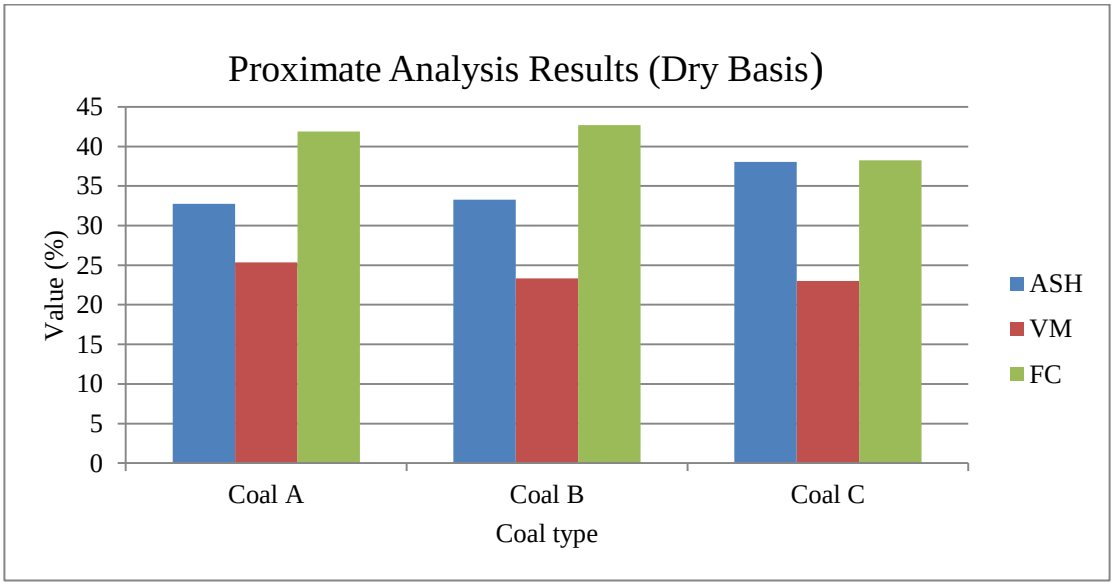

Figure 5.1: Comparison of the proximate analysis results of the three coals (Dry Basis)

Based on the results above it would appear from literature that Coal B would have the highest carbon conversion under oxy-combustion, lowest ignition temperature and lowest burn out time due to the fact that it has the highest fuel ratio (Figure 4.1) and

the highest fixed carbon content (Figure 5.1) relative to the other coals. This prediction is also verified by the results of the mathematical model that was developed and discussed in chapter 6 below. However, it must be noted that coal with a high fuel ratio also has the highest O_2 requirement (exceeding 30%) of the other two coals and on the same basis of assessment, Coal C would appear to have the least carbon conversion, highest ignition temperature and longest burnout time, whilst coal A would appear to lie in its combustion properties between B and C coals, and marginally closer to Coal B.

The oxygen-to-carbon and hydrogen-to-carbon ratios drawn from ultimate analyses are also important considerations for OFC. Coals with the lowest O/C and H/C ratios have been shown in literature to have the closest correlation between O_2 concentration, ignition and burnout temperatures. The H/C ratio has the greatest impact on the temperature at maximum char reactivity (Yi et al., 2015). Of the three coals sampled, Coal A sample has the highest H/C ratio while Coal C has the highest O/C ratio. This means that the temperature at maximum reactivity of Coal A is more affected by O_2 concentration in the combustion gas than the remaining two coal samples. The ignition and burnout temperatures of the Coal C sample on the other hand, having the highest O/C ratio, are likely to be the least sensitive to O_2 concentration compared to the ignition and burnout temperatures of the remaining two samples.

The reasoning behind these statements is because an inverse relationship exsists between characteristic combustion temperatures and H/C and O/C ratios as has been reported in literature from prior works (Yi, et al., 2015). In practice, these conclusions are likely to be true because the higher the carbon content (i.e. the lower these ratios), the more O_2 is needed to burn that fuel.

It has already been established from literature, that OFC requires more O_2 concentrations (approx. 30% by volume) in gas than air (which consists of 21% v/v O_2). Thus it may be concluded that, when considering coal properties and oxygen

diffusion only, and disregarding external factors like radiation and flame propagation velocities, all three coals analysed would have lower ignition temperature and higher carbon burnout under OFC conditions than they would when burnt in air.

In their techno-economic assessment of OFC retrofit to South African coal-fired power plants, Oboirien and North (2014) studied six power plants. The three coals that are analysed in this study (A,B and C) were included in their assessment and it was also found that the retrofit would require the installation of NOx and SOx removal technology and would thus further enhance the CO_2 capture efficiency by a factor of 10.

5.2. The determination of the proximate analyses using TGA

In terms of investigating the role of inherent moisture in OFC, the analytical results show that Coal C has the highest moisture content for all size fractions analysed compared to the other coals, while Coal A had the lowest moisture content (for all size fractions analysed) and specifically for the two smaller size fractions (see Figure 5.2).

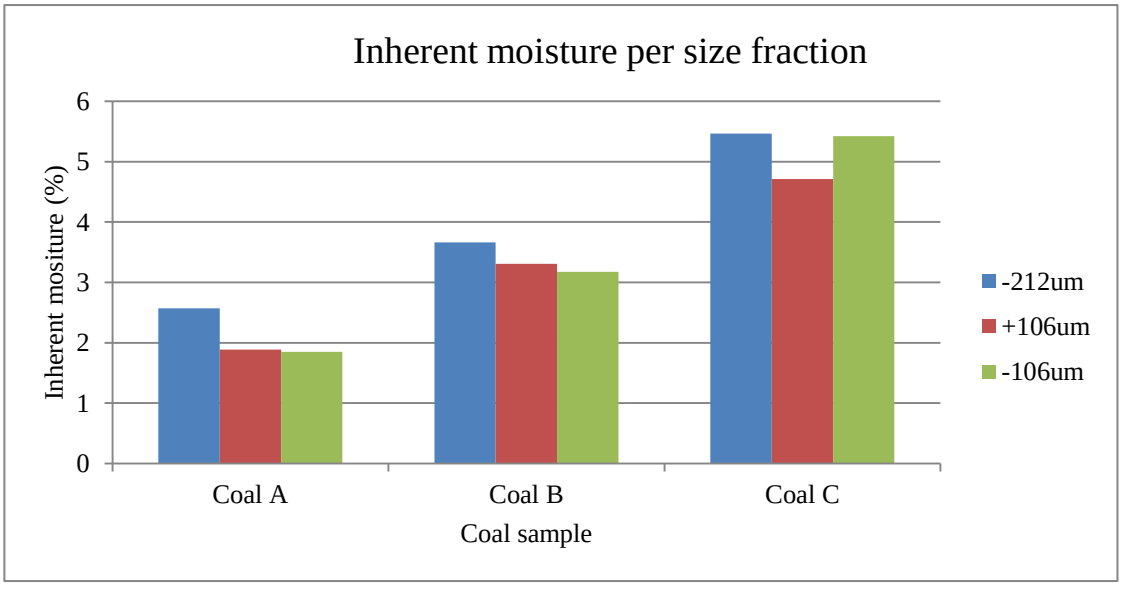

Figure 5.2: Comparison of Inherent moisture per size fraction for the three coal samples

The largest particles had the highest inherent moisture (IM) even in the case of Coal C where the IM was 5.47% and 5.42% for the -212um and -106um size fractions respectively. In the case of Coal A, the IM is almost equal between the +106 and -106 µm size fractions but was actually determined as 1.89% and 1.85% respectively.

5.2.1. TGA versus conventional methods- for Inherent moisture determination

The inherent moisture determined in the TGA is generally higher than that determined in the oven by conventional SABS methods, thus only qualitative and not quantitative comparisons are made here. Coal A has the lowest moisture content of all three coal types and this is consistent in both conventional methods and TGA analyses.

Inherent moisture also correlates with porosity, which can improve combustion. However, from literature, coals with high inherent moisture content (IM) have a considerable effect on burnout temperature and the temperature at maximum reactivity when combusted in the TGA. The reason behind this is that moisture, as explained in chapter 2 (Section 2.2) consumes heat energy before devolatilisation and char combustion commences.

Following from this reasoning, the burnout temperature of Coal C is therefore likely to be more sensitive to temperature at maximum reactivity and O_2 concentration than Coals A and B which have significantly lower moisture contents. This sensitivity becomes more pronounced with increase in O_2 concentration.

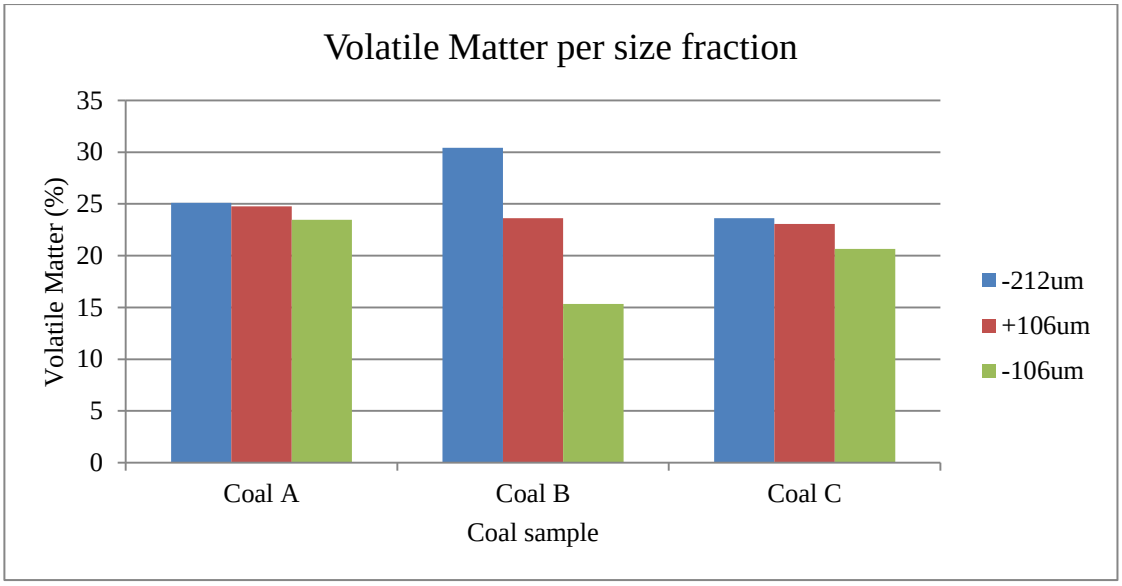

Figure 5.3: Comparison of volatile matter per size fraction for the three coals

In terms of volatile matter content, Coal B showed the highest value in the biggest size fraction (-212um) with considerable decreases in volatile matter with decreasing size. Coals A and C showed minimal differences between the size fractions with the sample C suite of sized coals marginally lower in volatile matter than sample A coal.

5.2.2. TGA versus conventional methods- for Volatile Matter content determination

According to Yi et al (2015), coals with high VM have the greatest effect on ignition and burnout temperature and not so much on Tmax (temperature at maximum reactivity), while low VM coal has the greatest influence on Tmax.

VM as determined by conventional proximate analysis methods is highest for Coal A at 25.54% while Coals B and C were determined to be 23.5% and 23.18% respectively. The results obtained using conventional methods are taken as the correct ones because they are consistent (the proximate analysis was repeated twice for VM determination, once in 2013, and in 2014).

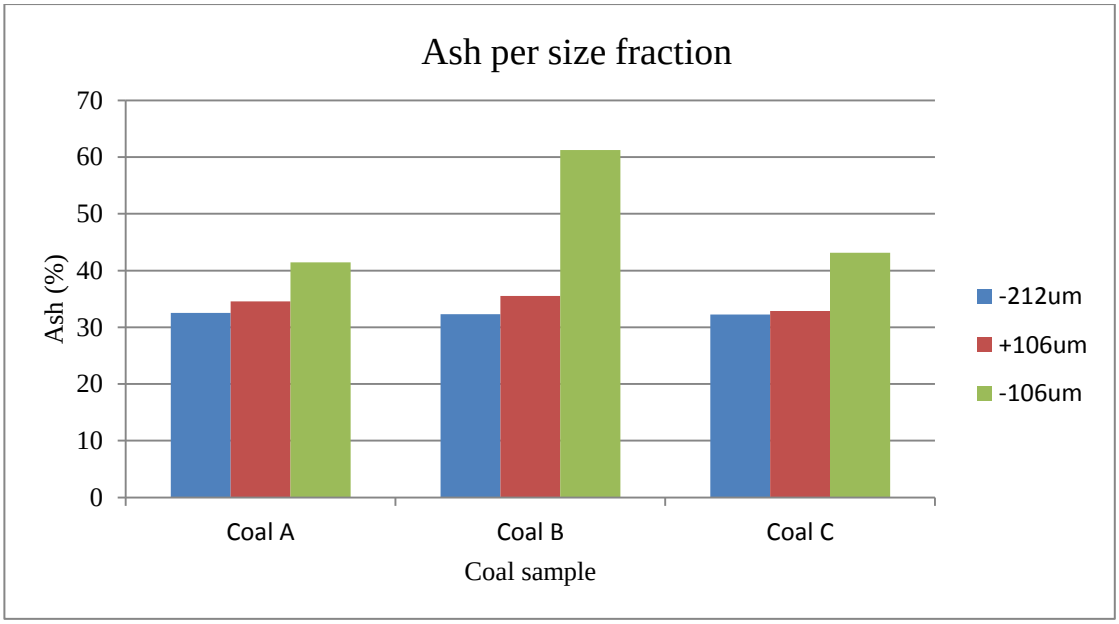

Figure 5.4: Comparison of ash per size fraction for the three coals

According to literature, high ash coal (low grade) has an effect on ignition temperature only, and little effect on burnout temperature and Tmax. Yi et al. (2015) have specified the ash content range of coal that affects ignition temperature the most to be between 5-53%. The ash content of all coals in this study falls within this range. The ash results are fairly conclusive. With the exception of the -212um size fraction, Coal B has the highest ash content across all size fractions. In the -212 µm size fraction, Coal A had the highest ash content which was found to be 32.545% compared to 32, 28% and 32.26% for Coals B and C respectively.

5.2.3. TGA versus conventional methods-for Ash determination

Coal C was found to have the highest ash content in conventional proximate analyses at 38.3% while Coal A had the lowest at 32.99% for the -212 microns size fraction. This is inconsistent with TGA which approximated 32.545% ash in Coal A and 32.36% in Coal C. The results obtained by conventional methods are still taken to be the correct ones because they were reproduced in a second run and are consistent with the VM results observed and reported above.

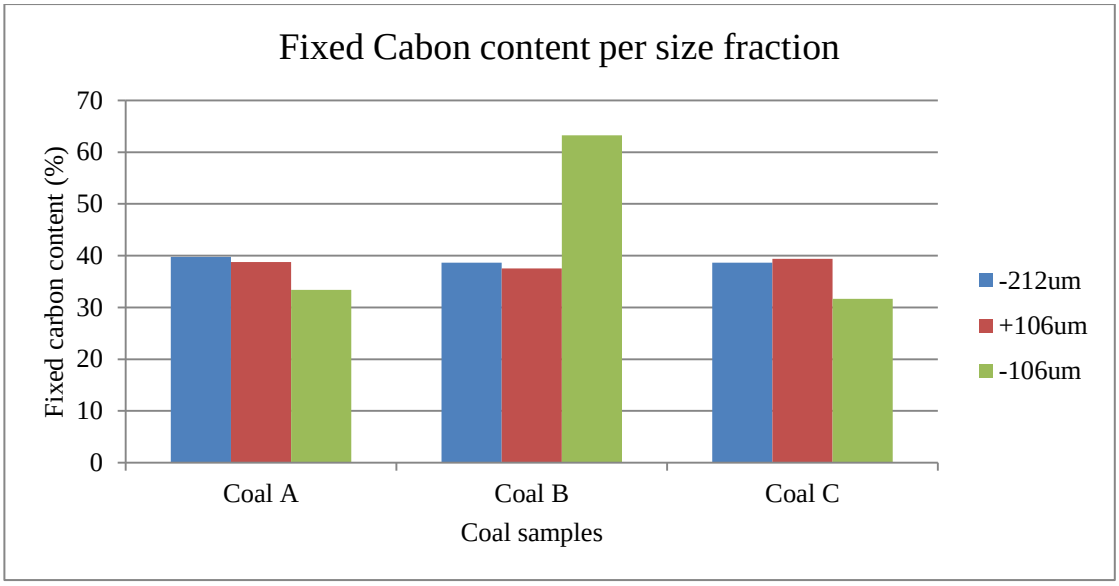

Figure 5.5: Comparison of fixed carbon content per size fraction for the three coal samples

The FC content of the coals is correspondent with the ash results for the +106 µm size fraction. Coals with the highest ash have the lowest FC content. In the +106 um size range, Coal C has the lowest ash content (32.87%) and the highest fixed carbon content (39.37%). For the -212 µm size fraction, the FC content of Coals B and C is equivalent (38.66%) while their ash content only differs by 0.02%, the exact values are reported in the appendix (under ash content results). For the -106 µm size range, the FC is proportional to the ash content as Coal B has the highest FC and ash content (61.26% and 63.27% respectively). This proportional relationship holds true for all three coal types studied.

For the smallest size fraction, Coal sample B had the highest FC content followed by A and C; it also has a lower VM content than Coal A and exceeds the VM content of Coal C by only 0.3%.

5.2.4. TGA versus conventional methods-fixed carbon content of coal (FC) determination

The FC content is comparable between the two methods but at different size fractions. TGA read 63.275% at -106 µm while the conventional method found

63.99% FC for Coal B at -212 microns. The two methods of analyses cannot be compared satisfactorily for fixed carbon. Once again, the conventional methods are chosen over the TGA results for FC content determination because the analysis were repeated and proved similar in ordinary conventional analyses (2013 versus 2014).

Of the properties discussed in proximate analyses, fixed carbon (and hence ash) is the biggest indicator of O_2 concentration on combustion reactivity. Coals with a high FC require longer burnout times, the reason being that ash is formed as combustion takes place and the O_2 gas must diffuse through the ash layer to reach the inner core of the char particle for complete combustion.

However, as seen above, VM has an opposite effect and reverses this phenomenon. Thus the fuel ratio, the ratio of FC to VM, effectively combining the two properties empirically, is taken to be the indicator of char reactivity. Coal B has the highest fuel ratio as shown above, further asserting the observation made here, of Coal sample B and burnout time in relation to O_2 content.

5.3. The chemical characteristics of the three coals using ultimate analyses

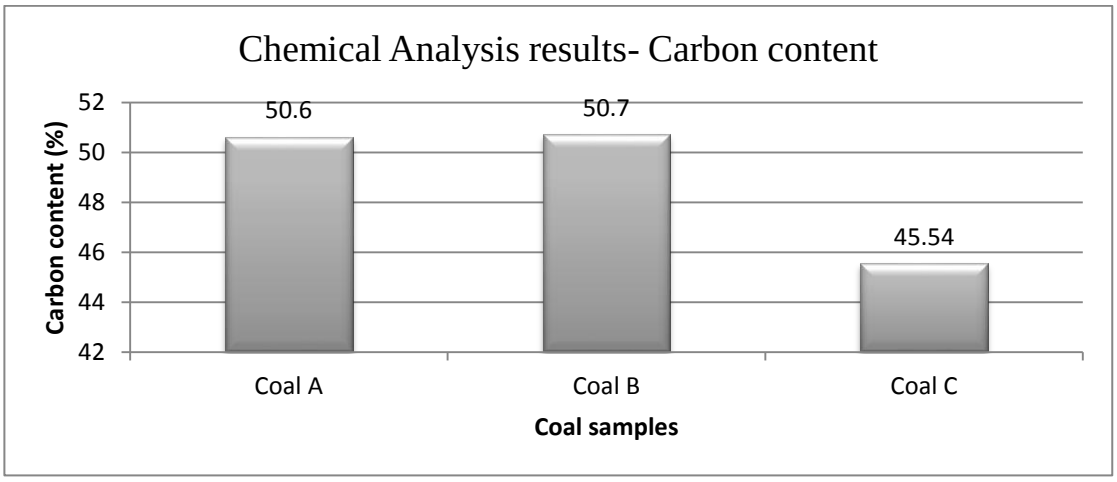

Figure 5.6: Comparison of the fixed carbon content of the three coals

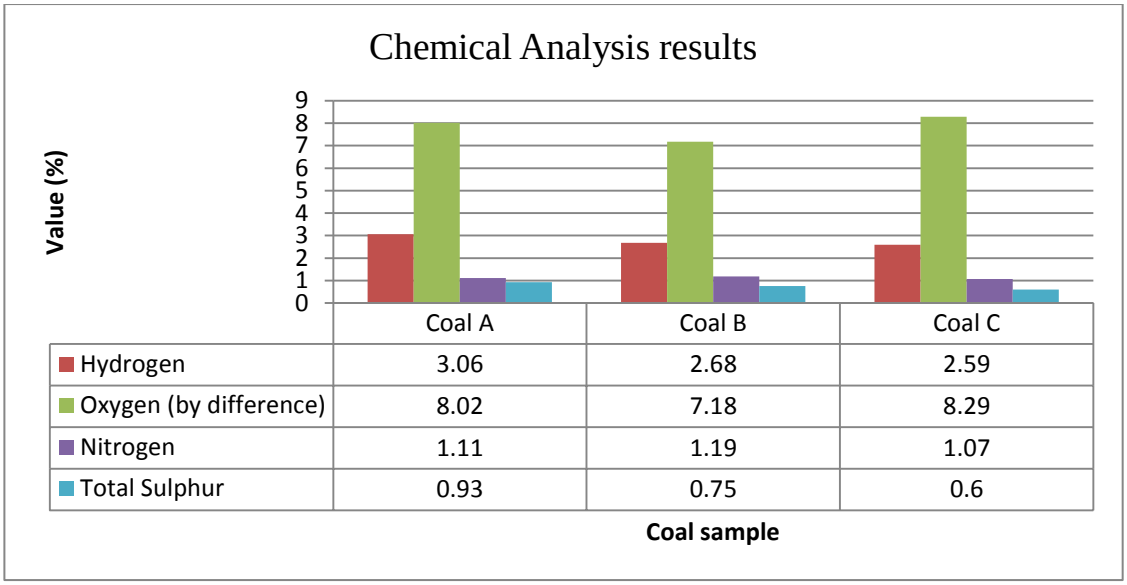

Figure 5.7: Comparison of the chemical analysis results of the three coals[3]

(Yi, et al., 2015) have provided O/C and H/C ranges in coal that have the most significant effect on combustion reactivity with O_2 concentration as 0.037-0.531 and 0.035-0.078 for the O/C and H/C ratio respectively. All coals used in this study have O/C and H/C ratios that fall within this range; however Coal A has the highest H/C ratio of the three coals (0.060). See Figure 4.2 above, as well as Table B3 in the Appendices.

This means that all coal samples' reactivity have significant sensitivity to O_2 concentration in the gas mixture in the regime that is oxygen diffusion limited only (excluding the region where diffusion must take place through products of reaction). It can be seen (Table B2 and Figure 5.9) that Coal A has the highest sulphur content and this can be a challenge when retrofitting South African power stations with OFC technology.

(Oboirien, et al., 2014) conducted a comprehensive techno-economic assessment of OFC technology for South African coal-fired power stations and found using a model developed by Carnegie Mellon University (in the USA) that the auxiliary power (i.e. between 27-29% of energy generated) was used by the stations to capture CO_2, of this

[3] The proximate and ultimate analyses results for Coals A and C are very similar to an analysis by Ham and Riet (1993) on a similar basis. This further asserts the accuracy levels of the analysis reported here, in 2015.

sulphur content increased the energy requirements for flue gas cooling before recirculation. Carbon content (Figure 5.6) is both highest and lowest for Coals B and C respectively. This suggests that if OFC technology were to be retrofitted, these stations would, accordingly, generate the largest and least amount of CO_2 to be captured respectively. This assumption is verified by the study made by (Oboirien, et al., 2014) using the IECM (Integrated Environmental Control Model, Version 8.1). If designing to capture comparable concentrations of CO_2, the station that is retrofitted with OFC technology for samples C coal supply would have the greatest reduction in efficiency as more compression would be required to capture CO_2 from its flue gas stream if the fuel source is Coal C.

Based on the properties of the coal samples analysed, the higher ratios derived from the proximate analyses, H/C and O/C, should lead to lower oxy-combustion efficiency due to the higher ignition point and burnout temperature (Yi et al, 2015). This would have an effect on the CO_2 capture potential. However, in addition to the latter work and that of Oboirien at al (2014), more experimental work would be required to draw a conclusive argument.

5.4. Ash fusion temperatures of the three coal samples

The ash fusion temperature was determined as per method described in the methodology. The findings are summarised in figure 5.8 below.

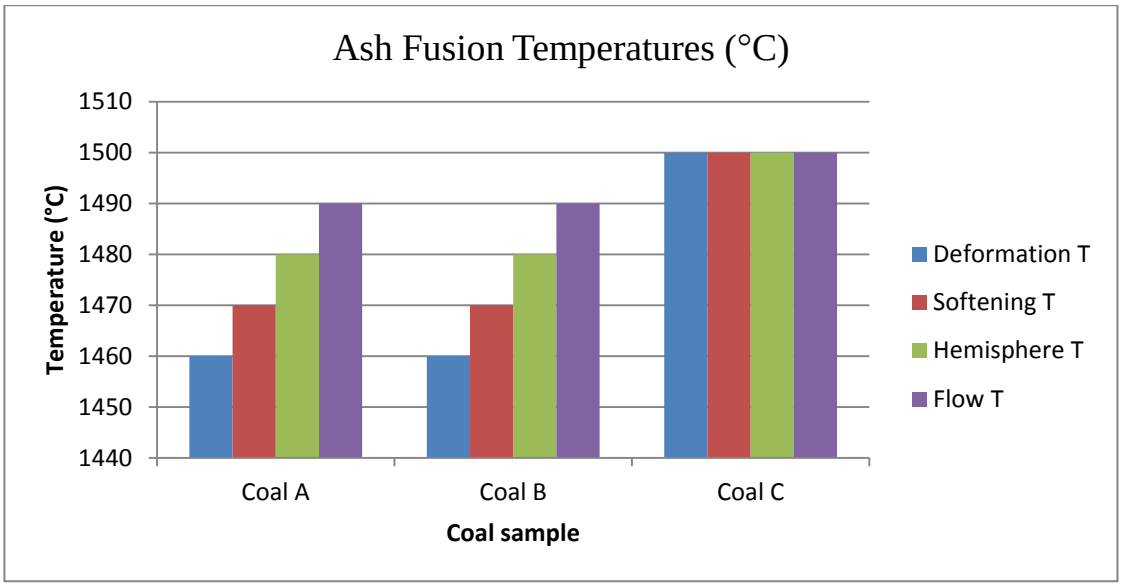

Figure 5.8: Comparison of the Ash fusion temperatures℃ of the coal samples

The Coal A and B samples had similar Deformation, Softening, Hemisphere and Flow temperatures while the coal C sample had the highest AFT's of the three samples. This has implications on combustion in the furnace as it can be inferred that Coal C, having the highest ash fusion temperature, can withstand higher temperatures before melting (deforming, softening and flowing as a liquid) in the upper regions of an industrial boiler. This also implies less chances of slagging, which is advantageous in oxy-fuel applications where temperatures are typically high.

5.5. Mineral Matter content determination using XRF

The most abundant minerals in the coal samples are Silica, Aluminium, Calcium and Iron. This is because the most abundant oxides found in the ash analyses for all three

coals are SiO_2, Al_2O_3 CaO. The analyses are also characteristic of South African coals. See Figure 5.9 for comparison.

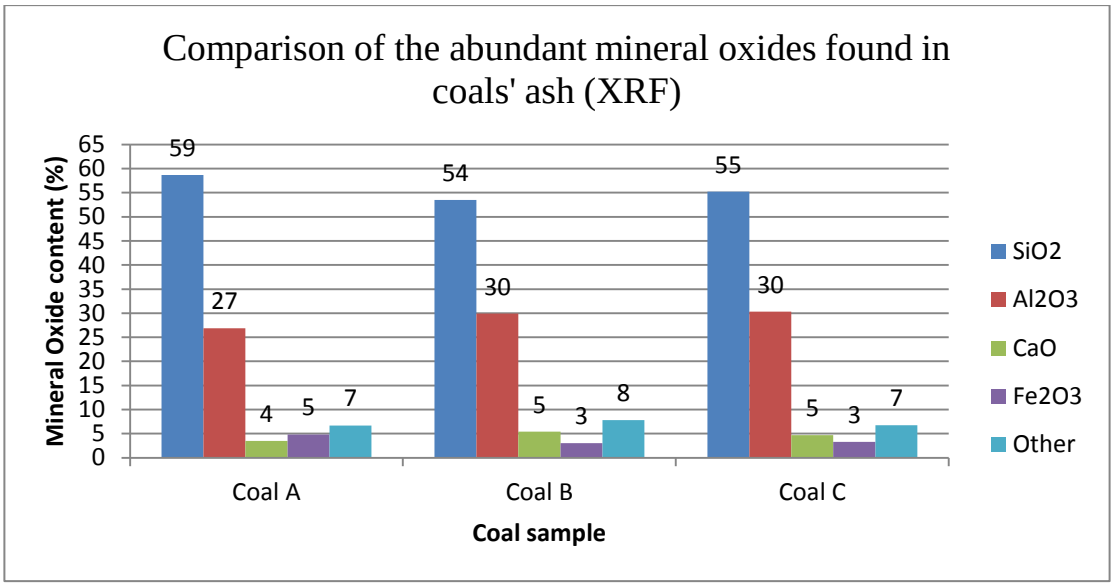

Figure 5.9: Comparison of ash elementals for the three coals as determined by XRF

Coal A has the most Silica content followed by C and B. Conversely, Coals C and B had the most Aluminium compared to Coal A (30% Al_2O_3). The overall mineral composition of the three coal samples is fairly similar as they differ only by maximum four per cent (in SiO_2).

5.6. Mineral Matter content determination using QUEMSCAN

QEMSCAN was also used to determine the mineral matter content of the three coals. The results obtained were compared to those reported for ash analyses by SABS standards as well as ash content determined by using the TGA. The comparison is demonstrated in Figure 5.10 below.

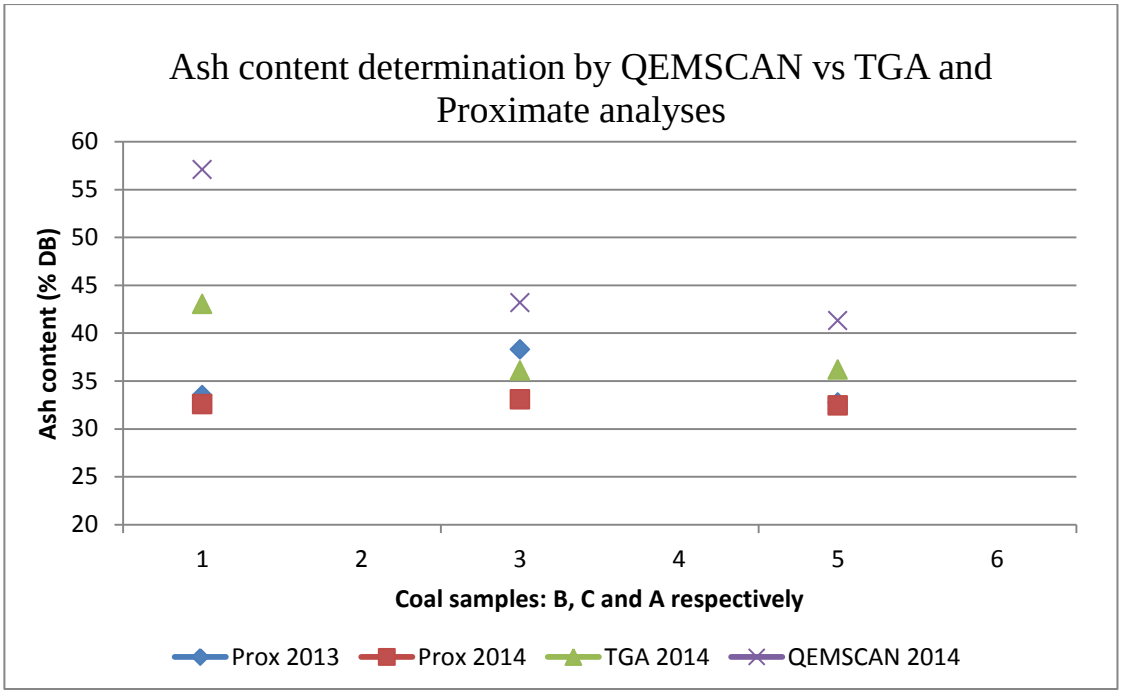

Figure 5.10: Comparison of ash content determined using different methods

The method of ash determination by the SABS standard was performed twice, and the results are fairly consistent as there is an overlap in values, i.e. between the (blue) diamond shape and the (red) squares. This is a good indicator of precision of the laboratory techniques. The ash determined using the TGA also showed fairly close results to the SABS method, especially for the C and A coal samples. However, the QEMSCAN results reflected much higher ash content of all three coals (on dry basis) than the remaining techniques, indicating that there may be settling in the preparation of the sample which may have lead the software to misread the data. Further discussion on this point has been described in above (section 5.2.3) and the anomaly diagnosed as per the procedure detailed above (section 3.4.2: Investigation into the anomalous mineral matter results between QEMSCAN and XRF).

5.7. Formation history of the coals (characterisation) by Petrographic analysis

5.7.1. Determining the rank of coal using Reflectance of Vitrinite (%RoV)

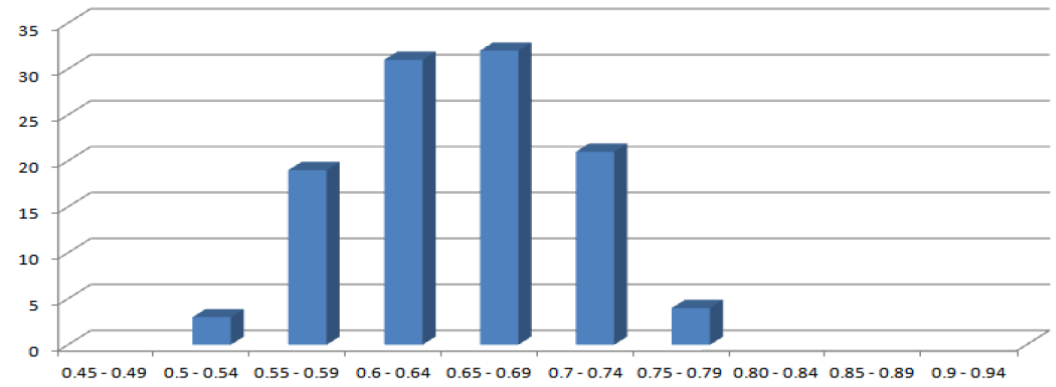

Figure 5.11: Reflectance histogram for Coal A

The Coal A sample is fresh, also vitrinite rich and has a high visible mineral matter content, though not as high as Coal C sample analysed (below). The mean reflectance of Vitrinite (%RoV) shown above for Coal A has a very broad band-width compared to the remaining two coal samples as it ranges between 0.75-0.79 and 0.5-0.54. This implies a corresponding variation in coal seams and coal quality (due to possible inter-seam contamination) in the parent coal source from the mine.

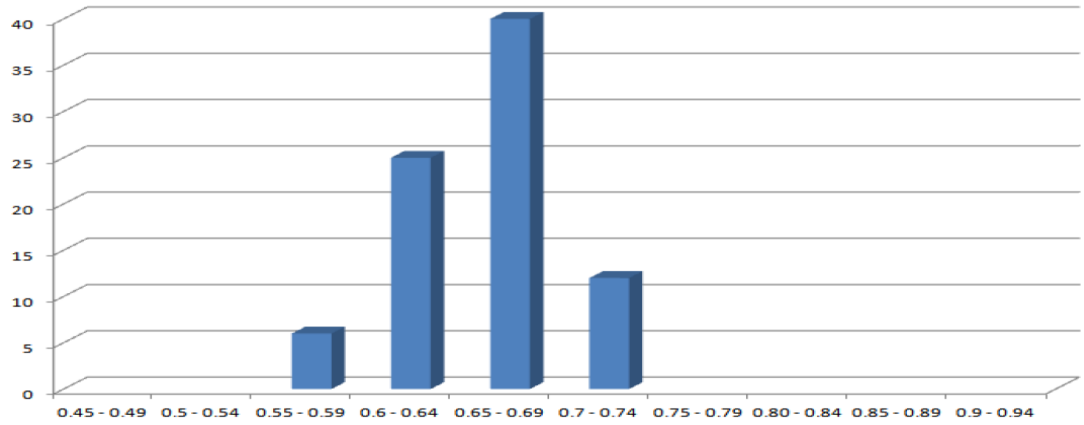

Figure 5.12: Reflectance histogram for Coal B

The Coal B sample had the highest visible mineral matter content of all three samples analysed, but is still vitrinite rich. The mean reflectance of Vitrinite (%RoV) shown above for the Coal B sample is narrow band-width as it ranges between 0.7-0.74 and 0.55-0.59.

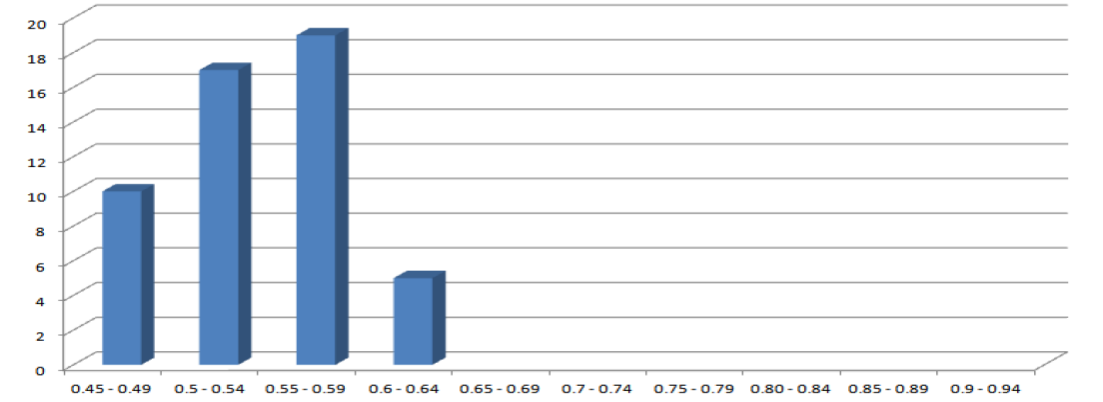

Figure 5.13: Reflectance histogram for Coal C

Coal C also had high mineral matter content but was slightly weathered in comparison to the other coal samples as it is inertinite rich (from maceral results in 4.2.4. above).

There is a narrow distribution on all histograms above, indicating that the samples are uncontaminated or minimal contamination. It also means that they originated from a single seam. The coals were classified as per the ECE-UN in-seam classification system; Coal A and B samples were classified as medium rank C bituminous coal category while the Coal C sample falls into the medium rank D category.

5.7.2. Determining the maceral-mineral associations of the coal samples

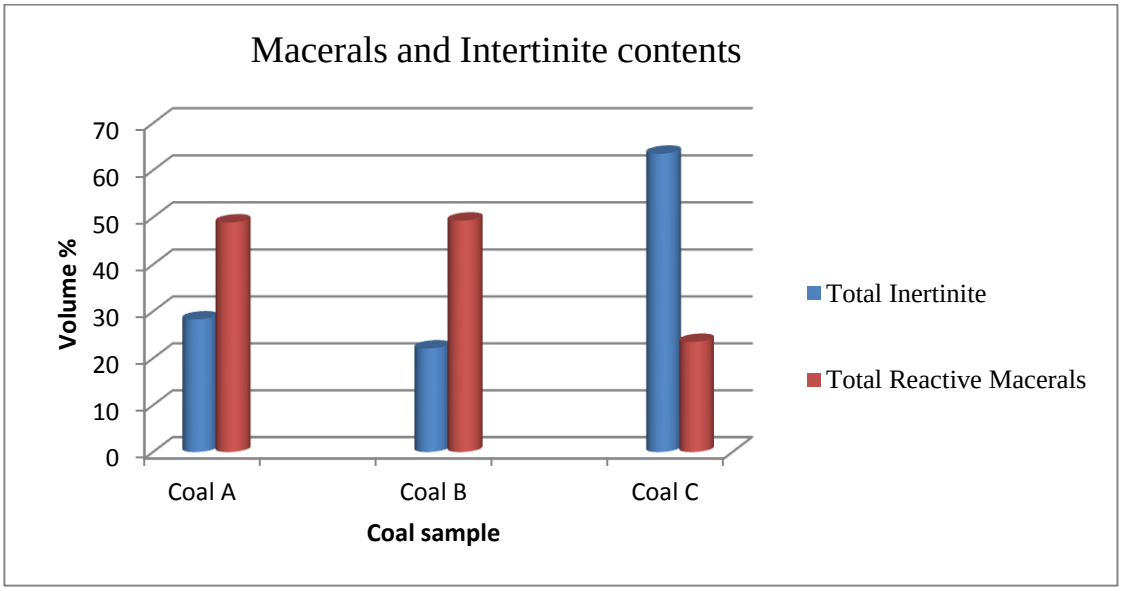

Figure 5.14: Macerals and inertinite content

Coal C has the highest amount of inertinite (63.5 vol %) followed by Coal samples A (28.3%) and B (22.1 vol. %). Coal B had the highest amount of macerals (49.3%) closely followed by Coal A (48.9%). The Coal C sample had the lowest amount of reactive macerals (23.5 vol %). These petrographic results are coherent with those obtained by proximate analysis by conventional methods above because inertinite is representative of the minerals that form ash when combusted while organic macerals represent combustible matter in coal (VM and FC).

Chapter Summary

From the results and discussion provided above, a conclusive characterisation can be made for all three coals. The proximate analyses by conventional means as well as Thermogravimetric analysis indicate that all three coals used in this study have considerably higher ash content than typical Laurasian coals. The QEMSCAN analyses, although having indicated even higher ash content (due to possible settling

of fines during the preparation of blocks) also alluded to this conclusion. Furthermore, the high ash content of the coals make it a challenge to rank the coals using European standards; as such, petrographic analyses were conducted to determine the coals' maceral and inertinite content. This information was used as input in the theoretical char burnout model developed below (chapter 6) as the laws used from literature were derived empirically, for the combustion of Laurasian coals. The vitrinite and inertinite contents of the coals were thus used in the empirical formulae to accommodate for the combustion of South African, (Gondwanaland) coal.

The fixed carbon content decreased with coal size fraction, for all coals indicating a conclusive relationship between size and ash (as there is a relation between fixed carbon content and intertinite or ash). The petrographic results (the mean reflectance histrograms) also show that the Coal A sample emanated from a contaminated seam with large seam variations as it is the broadest, while B and C Coal samples have narrow reflectance histograms. Narrow histograms on the other hand show that the coal is derived from a single seam with no variations and contaminations.

Additionally, the Coal C sample, though narrow, had the lowest mean reflectance range of the three samples analysed, indicating low organic reactive maceral matter content.

Finally, Coals A and C have been analysed historically (by Ham and Riet, 1993) and the proximate and ultimate analyses results were similar in 1993 to that found in this investigation in 2014 on a similar basis of comparison. This has provided confidence in the analytical methods employed in this research which were based upon ISO standards and verified by the TGA in addition to results in literature: Ham and van der Riet 1993).

CHAPTER 6

6. DISCUSSION TWO: THEORETICAL MODELLING OF REACTION RATE IN O_2/N_2 AND O_2/CO_2 ENVIRONMENTS

In this study, properties of three SA coals and their relation to oxy-fuel combustion were evaluated . The study also modelled the reactivity of the coal samples in terms of oxygen-char and carbon dioxide-char reaction using the models of Dhaneswar (2012) and Pallares, (2007).

This Chapter will present the methods used to select and adapt the models used in predicting OFC reactions and their applications to the three coals under review.

6.1. Introduction

In the literature survey conducted and presented above, very little was found on the contribution of char-CO_2 (gasification) reaction to the overall combustion process. The reason might be due to that other OFC applications require pure or nearly pure O_2 content in the combustion gas to facilitate high temperatures that are required. However, in power production, OFC is desired for carbon capture and thus temperatures must be reduced to accommodate existing infrastructure if a power station is to be retrofitted with OFC technology. This means reducing the oxygen purity in the feed stream to the lowest acceptable levels and recycling the flue gas stream (which would consist of approximately 79-89% CO_2). The lowest acceptable O_2 concentration that would emulate air combustion conditions would consist of approximately 30-35%O_2 as concluded from literature. The char-CO_2 gasification reaction is an important consideration as some literature alludes to it as a contributor in the increased char burnout and CO emissions observed in oxy-fuel combustion experiments. As quoted from the literature survey above, several TGA and DTF experiments have been conducted to explore the effect of the char-CO_2 reaction (Rathnam et al., 2008; Rathnam et al., 2006; Borrego et al., 2007; Alvarez et al.,

2005). Different conclusions have been drawn from these experiments about the role of the char-CO_2 gasification reaction. For example, Alvarez et al. (2005) found that high volatile bituminous coals had lower burnouts under OFC while Borrego et al. (2007) and Naredi & Pisupati (2009) found the opposite: high rank coals had higher burnout rates (i.e. shorter burnout times). Other than rank comparisons, (Naredi and Pisupati (2007a) and Rathnam et al. (2009) found the gasification reaction to have a significant impact on char burnout however; different sources in literature performed similar studies and found contradictory results. Thus the behaviour of coal combustion in oxy-fuel environment is a function of the nature of the coal itself which must be determined by mineralogical and petrographic analyses. It was recommended (IEAGHG, 2010) that more studies be made to determine the effect of coal rank on OFC. Thus although this has been done, not much was done on the modelling of char reactivity of South African coals, taking into account its unique petrography.

Char reactivity can be used to understand carbon conversion in oxy-combustion. The key reactions are; 1) Char-O_2, 2) Char-CO_2 and Char-H_2O reactions. Although influence of the lattermost (char-H_2O) reaction is negligible (Bejarano & Levendis, 2007), both Char-O_2, and Char-CO_2 and can be determined experimentally or predicted theoretically. In this study, the aim was to predict the char reactivity of the three coals under different oxy combustion conditions. The reactivity of the three coals' char particle were modelled against temperature using theory from literature (Naredi, 2009; Dhaneswar, 2011;Murphy et al, 2006 ; Rathnam et al, 2009).

All calculations were made using Microsoft Excel (2010) and the formulae used may be found in Appendix 4.

The char particle reactivity (burnout rate, kg/m^2.s) was calculated using the following equation (Dhaneswar, 2012 ; Pallares, 2007):

$$q_{cmb} = m_p \times \eta \times f_{mac} \times R_s \times (P_g)^n \qquad \textbf{Equation 6.1}$$

The two modes of reactivity were analysed using the equation above: Gasification and Oxidation (combustion reaction), both of which are dependent on the following factors,

q_{cmb} , the overall char burning rate (kg/m^2.s)

Mp, mass of coal sample,

η, effectiveness factor,

f_{mac}, maceral correction factor,

R_s, Intrinsic reactivity (1/s.atm or kg/m^{2}sPa),

P_g, Partial pressure (atm or 101.3E+03Pa) of the gas in consideration (O_2 for oxidation; CO_2 for gasification) and,

n, Order of reaction

The maceral correction factor is found from the following empirical correlation (Hurt et al, 1998):

$$\boldsymbol{F_{mac} = 1.68Vit - 0.6In} \qquad \textbf{Equation 6.2}$$

Thus the following Arrhenius equation was employed to determine the intrinsic reactivity:

$$\boldsymbol{R_s = Ae^{\left(\frac{-E}{RT}\right)}} \qquad \textbf{Equation 6.3}$$

Where:

$R_s$is the intrinsic reactivity (kg/m^{2}sPa)

A is the pre-exponential factor (kg/m^{2}sPa)

E is the activation energy (J/mol)

R is the ideal gas constant and (J/mol K) and

T is the temperature of the particle (K)

6.2. Key Assumptions:

6.2.1. Reaction mechanism

The global rate based combustion model is the most historically used for predicting char burnout behaviour and is used here however in this study; the single layer intrinsic Thiele modulus (core model) approach was taken for determination of the effectiveness factor as it is the reaction mechanism that considers the gasification reaction, which is consistent with what was found in literature (Thiele, 1939; Naredi, 2009; Dhaneswar, 2011).

6.2.2. Intrinsic Reactivity (R_i) and intrinsic rate parameters (A and E)

6.2.2.1. Intrinsic reactivity model

The Arrhenius equation was chosen here because it is the most historical formula and because in both expressions, k, the Temperature-dependant rate co-efficient, is described by the Arrhenius equation.

$$k_{s,1,2}(T_p) = Ae^{\left(-E/RT_p\right)} \qquad \textbf{Equation 6.4}$$

6.2.2.2. Intrinsic rate parameters used

An attempt therefore was made to determine the intrinsic rate parameters for the individual coal samples from literature (Naredi, 2009 ; Dhaneswar, 2011) who both performed a similar study for various coals. In order to match the coals in this study, it was necessary to classify them according to ASTM standards as this is the classification used for the coals found in literature. When classifying the coals in ASTM standards, the following procedures were followed namely; ASTM Method and Parr's method (previous equations from which the ASTM method was derived). Both methods depend on volatile matter and calorific value (CV) however, the

detailed procedures for these methods may be found in (ASTMD388) and (Parr 1928) respectively. The results are summarised in section 6.3 below. Both methods require the determination of proximate analysis and CV of coal on dry ash free basis.

In order for the evaluation of char reactivity, the activation energy and pre-exponential factors are required. These were not available for the selected coals, and were thus adopted from literature. The selection criterion was based on the rank of coals. Medium rank coal C's (i.e. Coal samples A and B) were assumed from the Pittsburgh coals in literature (Dhaneswar, 2011) because they correlated to the same rank; while the activation energy and pre-exponential factors for the medium rank D sample (i.e. Coal C in this study) were taken from Dietz coal (Dhaneswar 2011).

Thus the activation energy and pre-exponential factors were taken as 97.1 kJ/mol and 0.3 kg/m^2.s.Pa respectfully for the oxidation reaction and 306.1kJ/mol and 289.119 kg/m^2.s.Pa respectfully for the gasification reaction for these two coals (Dhaneswar, 2011). For the coal C sample, the intrinsic rate parameters were taken to be the same as that of Dietz coal, i.e. activation energy and pre-exponential factors were taken as 92.5 kJ/mol and 1.9 kg/m^2.s.Pa respectfully for the oxidation reaction and 103.1 kJ/mol and 0.005 kg/m2.s.Pa respectfully for the gasification reaction.

Further than this, because the Dietz and Pittsburgh coals are Laurasean (northern hemispheric) and the coals used in this study are Gondwana (southern hemispheric) coals, the geochemical petrographic identities were found to differ substantially (see section 2.1.2 for details). This was taken into account, however, when determining the overall reactivity of the coals (by using equation 6.1).

6.2.3. Effectiveness factor (η)

The effectiveness factor was estimated for both oxidation and gasification reactions using the Thiele modulus approach and is given for different coals in (Dhaneswar & Pisupati, 2012). The following equation was used:

$$\eta = \left(\frac{3}{\emptyset^2}\right)\left(\frac{\emptyset}{tanh\emptyset} - 1\right) \qquad \textbf{Equation 6.5}$$

Where $\emptyset$ is the Thiele modulus. The Thiele modulus is dependent on several factors as shown in equation 6.6 below. Refer to table 6.1 for the values of all parameters used with references.

6.2.4. Calculation of Thiele modulus

$$\emptyset = \left(\frac{d_p}{2}\right)\left(\sqrt{\frac{S_b \rho_p A_g R_s P_g}{D_e \rho_g}}\right) \qquad \textbf{Equation 6.6}$$

Where:

d_p is the diameter of the particle

S_b is the stoichiometry factor,

ρ_p is the density of the particle

A_g is the total surface area of the particle

R_s is the intrinsic reactivity as determined from equation 6.3

P_g is the partial pressure of O_2 in the gas stream

ρ_g is the bulk density of O_2 in the gas stream and

D_e is the effective diffusivity

$$\boldsymbol{D_e = \left(\frac{\theta}{\tau^2}\right)\left(\frac{1}{D_{kn}} + \frac{1}{D_A}\right)^{-1}} \qquad \textbf{Equation 6.7}$$

Where:

τ is the tortuosity of the pores of the char particle

D_{kn} is the Knudsen Diffusion coefficient

D_e is the molecular diffusion coefficient

$$\boldsymbol{D_{kn} = 97 r_p \sqrt{\frac{T_p}{M_g}}} \qquad \textbf{Equation 6.8}$$

$$D_A = D_{A,0} T_g^{1.75} \quad \text{Equation 6.9}$$

Where:

$D_{A,0}$ is the molecular diffusion coefficient

r_p is the pore radius

T_p is the temperature of the particle

T_g is the temperature of the gas

M_g is the molecular weight of the gas

6.2.5. Calculation of overall reactivity due to diffusion and solid surface area contributions :

$$R = \left(\frac{1}{R_{ac}} + \frac{1}{R_d}\right)^{-1} P_g \quad \text{Equation 6.10}$$

Where:

R is the overall char reactivity, per unit external area (kg/m^2.s)

R_{ac} is the reaction rate per unit area (kg/m^2.s.Pa) calculated as per equation 6.11 below

R_d is the rate of gas diffusion (kg/m^2.s.Pa) calculated as per equation 6.12 below and

P_g is the partial pressure of the diffusing gas (Pa)

$$R_{ac} = \frac{\eta d_p A_g R_s}{6} \quad \text{Equation 6.11}$$

$$R_d = \frac{C T_p^{0.75}}{d_p} \quad \text{Equation 6.12}$$

6.2.6. Reaction order (n)

The reaction order is an empirical function of char properties and combustion conditions and ranges between zero and one (Hurt & Calo, 2001). All references in literature above used a reaction order of 0.5 for the oxidation reaction and 0.8 for the gasification, however in this study; the reaction order for the oxidation reaction was estimated based on the oxygen concentrations, while the order for gasification was maintained at 0.8 since CO_2 was the reacting gas and not O_2.

The reasoning behind this was based on the findings made by (Murphy & Shaddix, 2006) of oxidation reaction orders that decreased with decreasing oxygen concentrations (which represent diffusion-limited chemical reactions). The reaction order only reached 0.5 at enriched (36%) oxygen concentrations for all types of coals analysed. Thus in this study the reaction orders of 0.1 was used at O_2 concentrations of 3%, 0.3 at 21% O_2 and 0.5 at 30% O_2 to 50%O_2, consistent with the findings by Murphy et al. (2006).

6.2.7. Theoretical char particle temperature (T)

Expanding from the determination of coal char transport properties (particle diameter, density and travelling velocity) by Wang et al. (1988), Dhaneswar & Pisupati (2012) were able to model the char particle temperature using a heat balance correlation formulated by Eisermann et al. (1980). The findings were that, in oxy-fuel conditions, the lower the oxygen concentrations and the higher the gas temperature, the more the char particle temperature asymptotes towards the gas temperature. Indeed it was found to be closest at an oxygen concentration of 3% and gas temperature of 1873K as it differed by just 83K. Thus, while studies in literature (Dhaneswar and Pisupati, 2011; Dhanswar, 2011) always took the char particle temperature to be the same as that of the gas, in this model, the char particle temperature was assumed to be equal to that of the gas $\pm$ 150K since the O_2 concentration was calculated at values up to 50% and the gas temperatures used began at 800K.

Equations 6.3-6.12 were used to formulate the char burnout according to the model by Roshan (2011). It should be noted that this excludes the contribution of the coal chars petrographic parameters; the maceral correction factors. These factors were modelled and taken into account in Equations 6.1 and 6.2 and the results are produced in figures 6.3-6.10 below.

Table 6.1: Parameters used in theoretical char burnout model.

Parameter	**Value used**	**Source**
A (kg/m^2.s.Pa)	0.3 (for Coals A&B) and 1.9 (for Coal C) Oxidation reactions 289.119 (for Coals A&B) and 0.005 (for Coal C) Gasification reactions	Taken from the corresponding pre-exponential factors from Pittsburgh and Dietz coals used in literature –Naredi (2009) and explained in 6.2.2.2. above.
A_o (m)	1E-10	Assumed from Naredi (2009)
A_g (m^2/kg)	100000	Assumed from Naredi (2009)
C (dimensionless)	5E-12	Assumed from Naredi (2009)
$D_{A,O}$ (m^2/s)	1.53E-05 m^2/s (at 273K)	Assumed to be constant with Temperature, from Naredi (2009)
d_p (m)	0.000081	Assumed from Naredi (2009)
E (J/mol)	97100 (for Coals A&B) and 92500 (for Coal C) Oxidation reactions 306100 (for Coals A&B)	Taken from the corresponding activation energy values from Pittsburgh and Dietz coals

	and 103100 (for Coal C) Gasification reactions	used in literature –Naredi (2009) and explained in 6.2.2.2. above.
M_g	32 for oxidation reaction 44 for gasification reaction	Molecular weights are derived from the periodic table of elements
P_g (Pa)	The O_2 and CO_2 partial pressure were varied as follows: 21%O_2/79%CO_2 30%O_2/70%CO_2 40%O_2/60%CO_2 and, 50%O_2/CO_2	
R (J/mol K)	8.314	Assumed oxygen and carbon dioxide behave as the ideal gas law.
r_p (m)	100 A^0	Assumed from Naredi (2009)
ρ_g (kg/m^3)	See table 6.2 and 6.3 below.	Density of the O_2/CO_2 gas was determined at different temperatures and pressures assuming the ideal gas law
ρ_p (kg/m^3)	1300	Density of the particle, assumed from Naredi (2009) to be constant with Temperature and Pressure.
S_b (dimensionless)	2.67	Assumed from Naredi (2009)

τ (dimensionless)	2	Assumed from Naredi (2009), May not exceed 10 (Smith, 1982)
θ (dimensionless)	0.5	Assumed from Naredi (2009)

Table 6.2: Density of Oxygen with Temperature and Pressure

Temperature (K)	**Density of the Oxygen Gas**			
	rho at 21000 Pa	rho at 30000 Pa	rho at 40000Pa	rho at 50000 Pa
800	0.101	0.144	0.192	0.241
1000	0.081	0.115	0.154	0.192
1100	0.073	0.105	0.140	0.175
1200	0.067	0.096	0.128	0.160
1400	0.058	0.082	0.110	0.137
1473	0.055	0.078	0.105	0.131
1600	0.051	0.072	0.096	0.120
1800	0.045	0.064	0.086	0.107
1873	0.043	0.062	0.082	0.103
2000	0.040	0.058	0.077	0.096

Table 6.3: Density of Carbon Dioxide with Temperature and Pressure

Temperature (K)	**Density of the Carbon Dioxide Gas**			
	rho at 79000 Pa	rho at 70000 Pa	rho at 60000Pa	rho at 50000 Pa
800	0.523	0.463	0.397	0.331
1000	0.418	0.370	0.318	0.265
1100	0.380	0.337	0.289	0.241
1200	0.348	0.309	0.265	0.221
1400	0.299	0.265	0.227	0.189
1473	0.284	0.251	0.216	0.180
1600	0.261	0.232	0.198	0.165
1800	0.232	0.206	0.176	0.147
1873	0.223	0.198	0.170	0.141
2000	0.209	0.185	0.159	0.132

6.3. Results: Theoretical Modelling of Reactivities in oxy-combustion conditions

6.3.1. Classification of coal by rank

Table 6.4: Classification of coals under investigation by different standards

Standards	**Rank**	**Coals**	
ASTM	High Vol C	Coal A	Coal C
	High Vol B	Coal B	
Parr	Bit D	Coal A	Coal B
	Lignite	Coal C	
ISO (or ECE-EU)	Med rank C	Coal A	Coal B
	Med rank D	Coal C	

The ASTM system of classification relies on the following proximate analysis results: Fixed Carbon (FC)-on Dry Ash Free (DAF) basis, Volatile Matter (VM)-on Dry Ash Free (DAF) basis, Gross Calorific Value (GCV)-on an Ash Free (DAF) basis and Agglomerating Character.

The ASTM Method could not be used to classify these coals due to that 1) It relies on the conversion of ultimate analyses to DAF basis which is derived from coals with typically lower ash (or mineral matter) contents. This is especially true for the Coal C sample that had ash values as high as 38.3%. 2) [4]Similarly, Parr's equations could not be used successfully either to classify the South African coals because they were derived empirically from American coals which are Laurasian and thus have a significantly lower ash content by their geochemical nature.

[4] Coal C has been mentioned here for reference as it had an ash content of 38.3% on a DAF basis. The remaining coal samples, A and B had ash contents of 32.7 and 33.5% respectfully which is in agreement with the average ash content of South African coals found in literature. Falcon (1986) is one such reference.

When Parr's equations were used in conjunction with the ASTM standard American Society for Testing and Materials (1998), this resulted in higher GCV content for all three samples on an ash free basis thus ranking Coal C as High volatile bituminous C. The Parr's formulae as well as Figure 3 and Table 14 (both found in Parr 1928) were used to classify the coals and the results are also tabulated above, in Table 6.1. While there is no "bituminous D" ranking in ASTM standards (i.e. in ASTMD388), the results obtained from Parr's equations are preferred over ASTM standards because it was observed that Parr's system classifies Coals A and B in the same rank as ISO and both (Parr and ISO) leave Coal C as an outlier from the remaining two samples.

ASTM on the other hand, classified Coals A and C as both having a lower rank (High Vol C) than Coal B (High Vol B), which is contradictory to both Parr and ISO systems of classification. Further detail regarding the applicability (or inapplicability thereof) of international systems of coal classifications for South African coals may be found in the following sources of literature: the Seyler system (which is also described in Parr, 1928) as well as in Falcon (1986).

As already mentioned, the above methods and even more previous ones are based on the use of proximate analyses (FC, VM, GCV and Agglomerating character) on an ash free basis assuming ash content of below 10% (AD Basis). The resolution to this problem therefore was to incorporate petrographic analyses to classify the coals and cross-link between the different methods of classification. This solution was adopted from Falcon (1986) and relies on only two petrographic (or inferred) coal parameters for classification of coal by rank, that is the %RoV (random and or maximum) as well and vitrinite colour (Falcon, 1986:1912).

The method of classification described above is more accurate because it considers inherent properties of coal which represent the true nature of coal (as these properties do not always correspond to proximate analyses results).

From the petrographic results reported above, the vitrinite reflectance (%RoV) for all coal samples analysed ranged between 0.54-0.66 and thus all fell in the high volatile bituminous category according to the USA system of classification (also found in Falcon, 1986:1912). The intrinsic rate parameters assumed were thus for corresponding bituminous coals (Pittsburgh) for Coals A and B, and Dietz coal's

parameters were taken for Coal sample C (which had the lowest %RoV of 0.54). Dietz was classified as sub-bituminous and this was taken here for Coal C as both Parr's equations and ISO standards classified this coal (Coal C) as being a rank below that of the remaining two.

6.3.2. Intrinsic Oxidation and Gasification Reactivities of the coal samples in OFC conditions

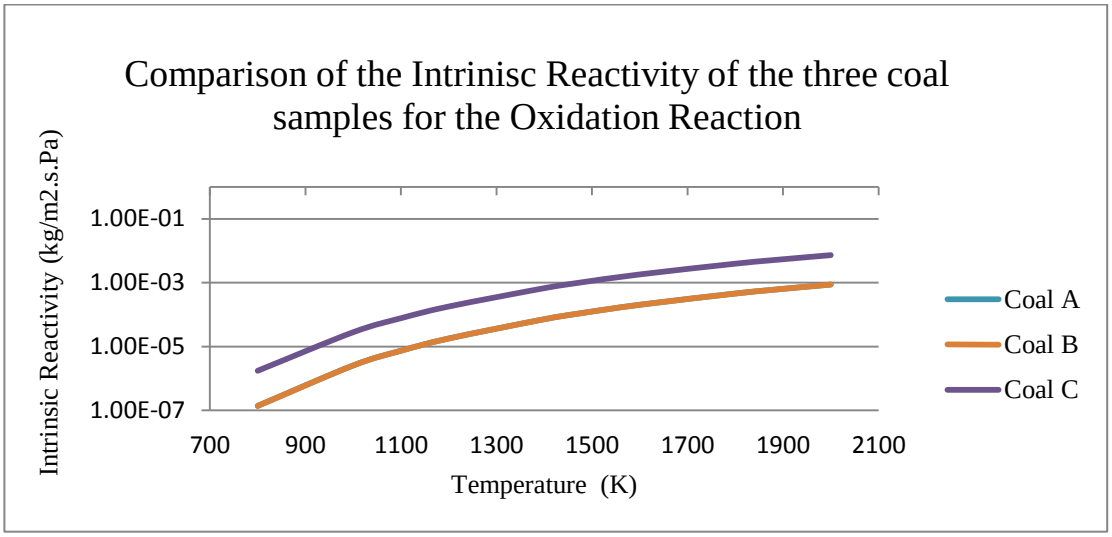

Figure 6.1: Comparison of the Intrinsic Reactivity of the three coal samples for the Oxidation Reaction

The intrinsic reactivity of the three coal samples per unit surface area ($kg/m^2.s.Pa$) under the oxy-combustion condition are presented in Figure 6.1. The results show that intrinsic reactivity of Coals A and B are similar and lower than that of Coal C sample.

This result is true for both oxidation (above) and gasification model results (below). This is mainly due to that Coal C has a higher pre-exponential factor in equation 6.3 which was in turn assumed from a coal with similar properties (proximate, ultimate and petrographic ranking) in literature. It is also in agreement with theory from literature which postulated that under oxy-fuel firing conditions, low rank coals have a higher carbon conversion than high rank coals (Dhaneswar, 2011; Naredi, 2009). The intrinsic reactivity of the gasification reaction, although small, would still be

higher for Coal C than for Coals A and B, especially at high temperatures and low oxygen concentrations.

The graph shows two graphs as opposed to three for the three coals, due to the overlap in intrinsic reactivity of Coals A and B.

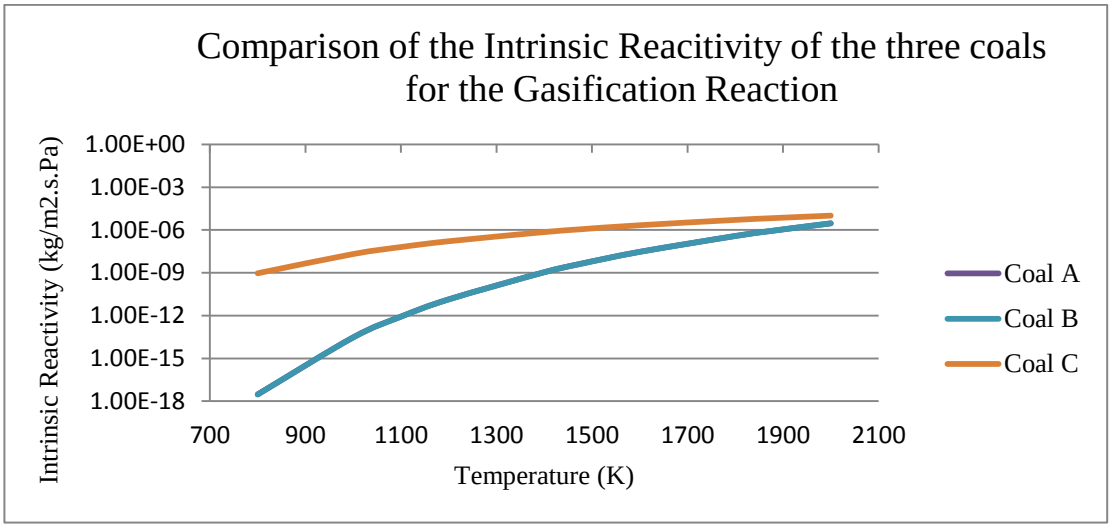

Figure 6.2: Comparison of the Intrinsic Reactivity of the three coals for the Gasification Reaction

6.3.3. Char burning rate-Oxidation and Gasification at different atmospheres

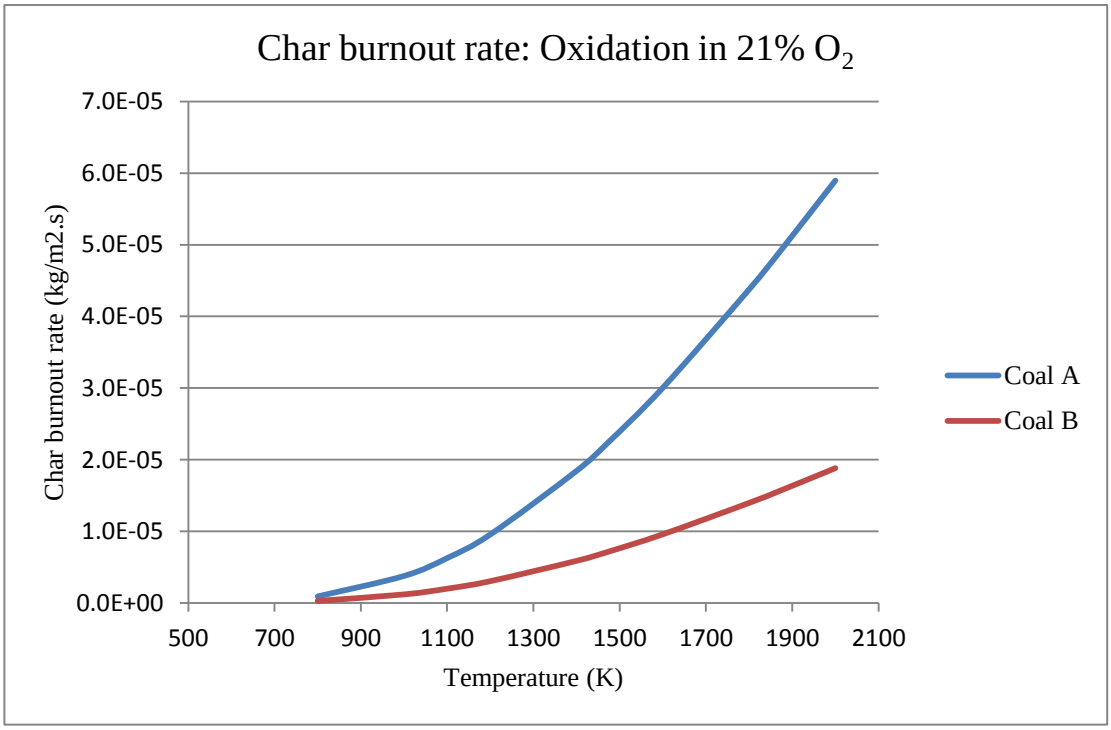

Figure 6.3: Char burning rate: Oxidation in 21%O_2

‘

i. Oxidation

This result (fig 6.3) seems to be contradicting the intrinsic reactivity results described in fig. 6.1 above whereby Coal C is predicted to have a higher intrinsic reactivity.

This can be explained as follows: in the model, the coals’ maceral constituents have been taken into account in the char burning rate model used (equation 6.1), whereas these are not taken into account when determining a coal’s intrinsic reactivity alone (i.e. equation 6.3). From the petrographic results in Section 4.2.2, the Coal C sample had the highest inertinite content (63.5 vol. %) followed by Coal A (28.3%) and B (22.1 vol. %). This correlation can be seen explicitly in the predicted char burning rate curves above.

ii. Gasification

The predicted char burning rate for Coals A and B are almost identical from 800K and then begin to diverge where Coal A's char burning rate lags behind that of Coal B from temperatures beyond 1400K onwards. The useful results are from 1400K as this temperature was found in literature to be the temperature as which the global power-law kinetics theory has been found to be most practical. (Hurt & Calo, 2001) found the global power-law kinetic expression to be of the most practical use in temperature ranges of 1500-2000K.

Again, the graph for Coal C decreases with increasing temperature because the maceral correction factor yielded a negative value. Overally, for all oxygen concentrations (and corresponding CO_2 partial pressures), the char gasification burning rate is lower than that of oxidation by a factor of ± 10 kg/m^2.s.

iii. The Coal C Sample

The reactivity increases with increasing temperatures for all coals except Coal C. This is seen for both oxidation and gasification reactions. The reactivity of the Coal C sample is predicted to decrease because the maceral correction factor (Fmac) is negative for this coal. The reason for this is that the inertinite content for Coal C is greater than the vitrinite content, yielding a negative value for the maceral correction factor (Fmac) determined from equation 6.1. When the petrographic results (Table 4.1) are used as inputs in equation 6.1, a negative value is found for Coal C. This suggests that the empirical equation for the maceral correction factor cannot be used for all South African coals as it was developed for Laurasian coals which typically have a vitrinite content that is much higher than inertinite. The development for this correction factor can be found in (Pallares, 2007). It can be concluded that the current method for determination of the maceral correction factor is not suitable for all Godwanaland coals and it is recommended that the existing formulae be modified to suit coals from the Gondwanaland region, especially the low rank, high ash coals with ash contents exceeding 30% on an air dried basis (Coal C being an example).

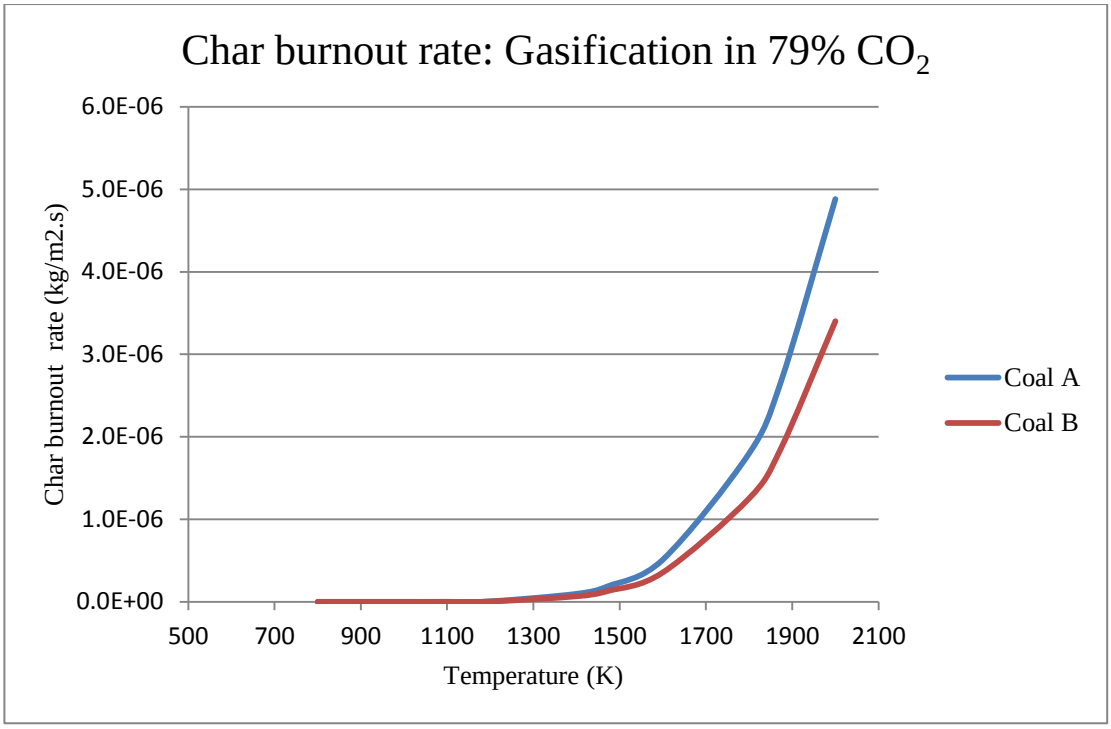

Figure 6.4: Char burning rate: Gasification in 79%CO_2

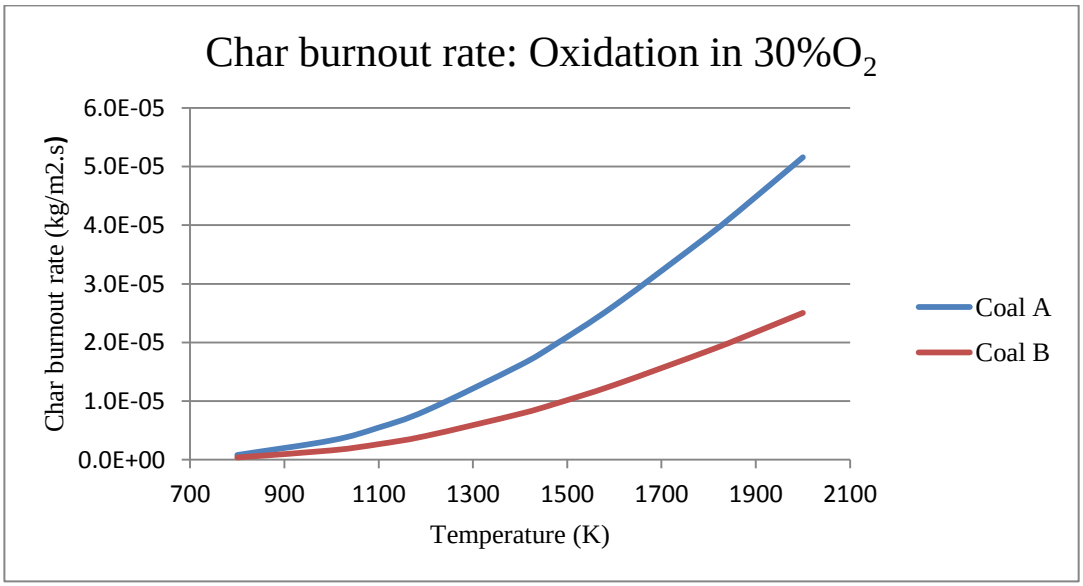

Figure 6.5: Char burning rate: Oxidation in 30%O_2

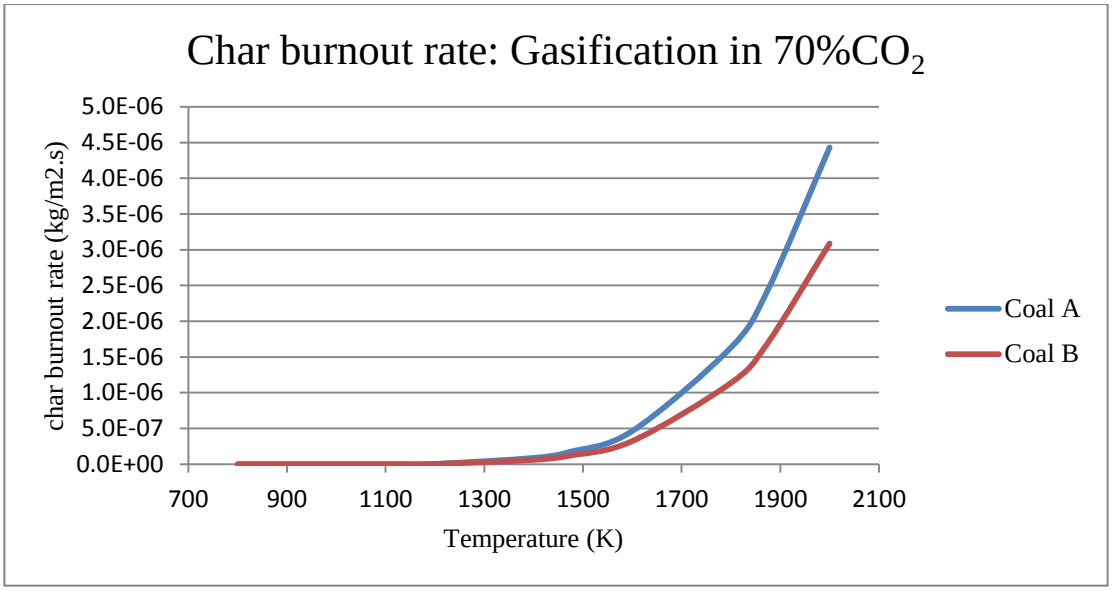

Figure 6.6: Char burning rate: Gasification in 70%CO_2

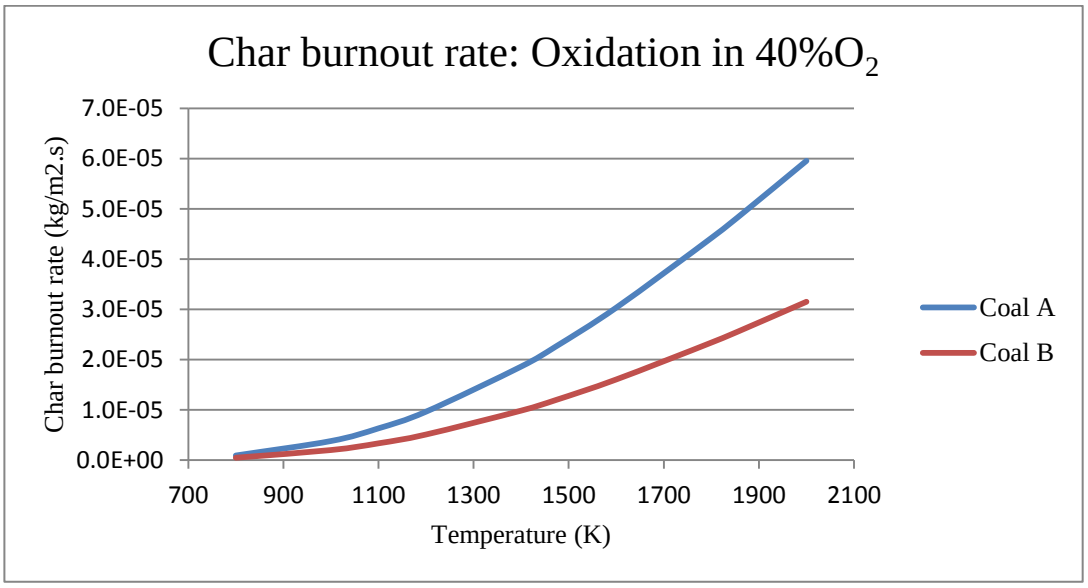

Figure 6.7: Char burning rate: Oxidation in 40%O_2

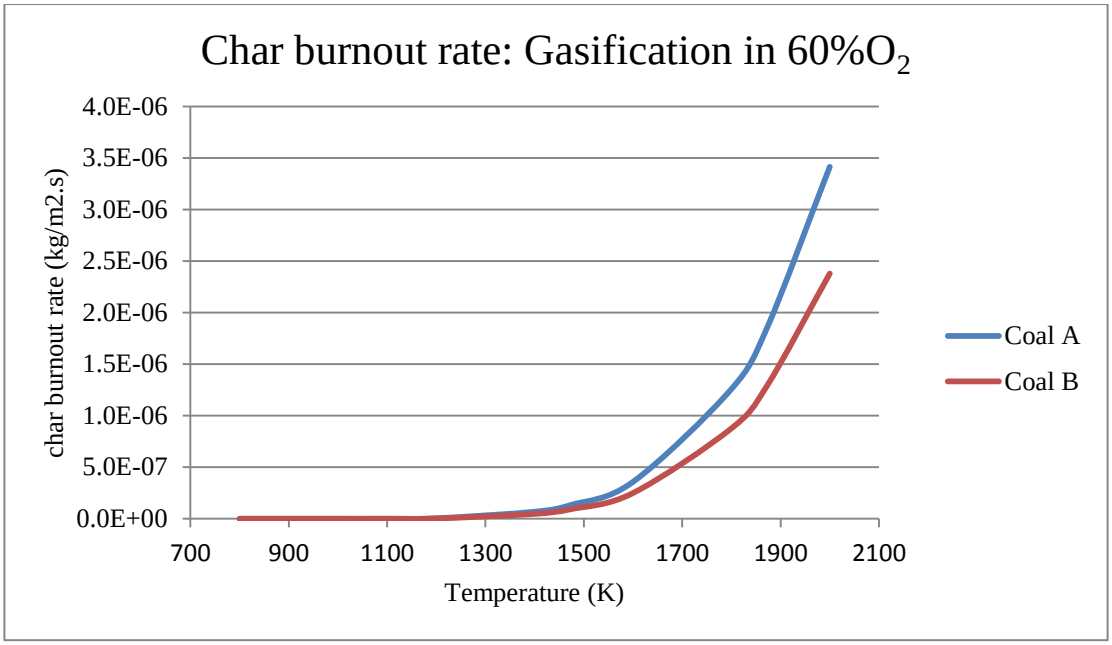

Figure 6.8: Char burning rate: Gasification in 60%O_2

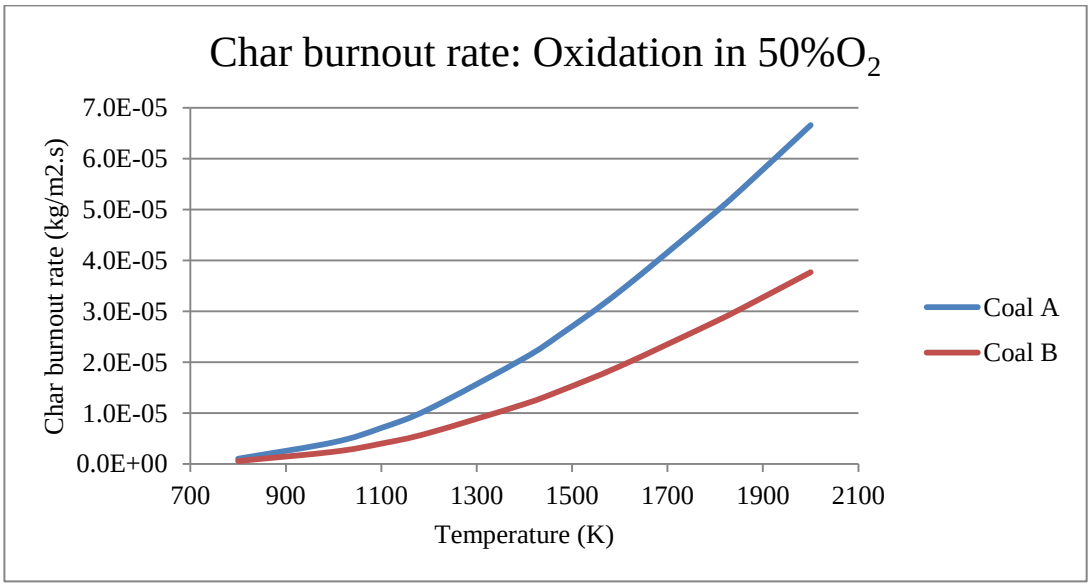

Figure 6.9: Char burning rate: Oxidation in 50%O_2

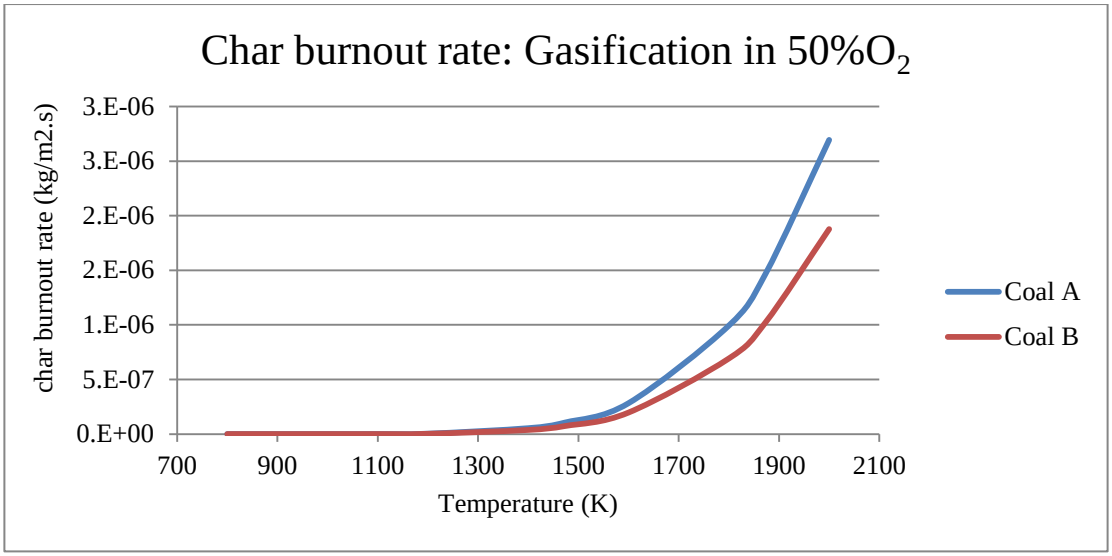

Figure 6.10: Char burning rate: Gasification in 50%O_2

The char burnout rate for coal C is not plotted in these graphs as they yield a negatively shaped curve. This is due to the negative maceral correction factor employed for Coal C that took into account the maceral and inertinite contents and yielded a negative value in Fmac (Equation 6.1- Equation 6.2).

6.3.4. Comparison of overall reactivity results with experimental data from literature

The data obtained from the theoretical model employed in this study was compared with results obtained from the experimental work performed by Roshan (2011). The comparisons are plotted in figures 6.11-6.15 below.

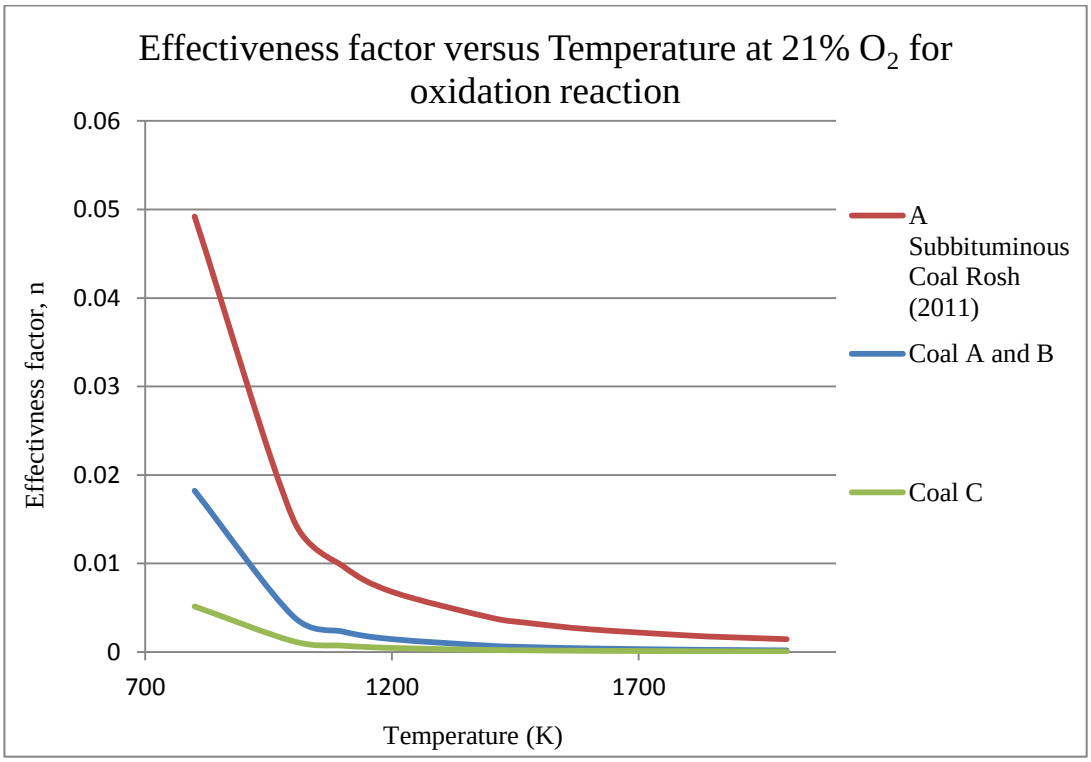

Figure 6.11: Comparisons between theoretical model and literature of the effectiveness factor for the oxidation reaction at 21% oxygen

Figure 6.11 shows the differences in effectiveness factors for the coals studied under the same conditions. The coal used in literature (Roshan, 2011) is a subbituminous coal with a lower intrinsic reactivity than the coals used in this study. The intrinsic reactivity calculated in equation 6.3 was used in determining the Thiele modulus (equation 6.6) which was then used to determine the effectiveness factor (from equation 6.5). There is an inverse relationship between the effectiveness factor and Thiele modulus. Due to the low activation energy and pre-exponential factors for this

coal, the resulting intrinsic reactivity was correspondingly lower at all temperatures and hence the lower Thiele modulus that resulted in a higher effectiveness factor.

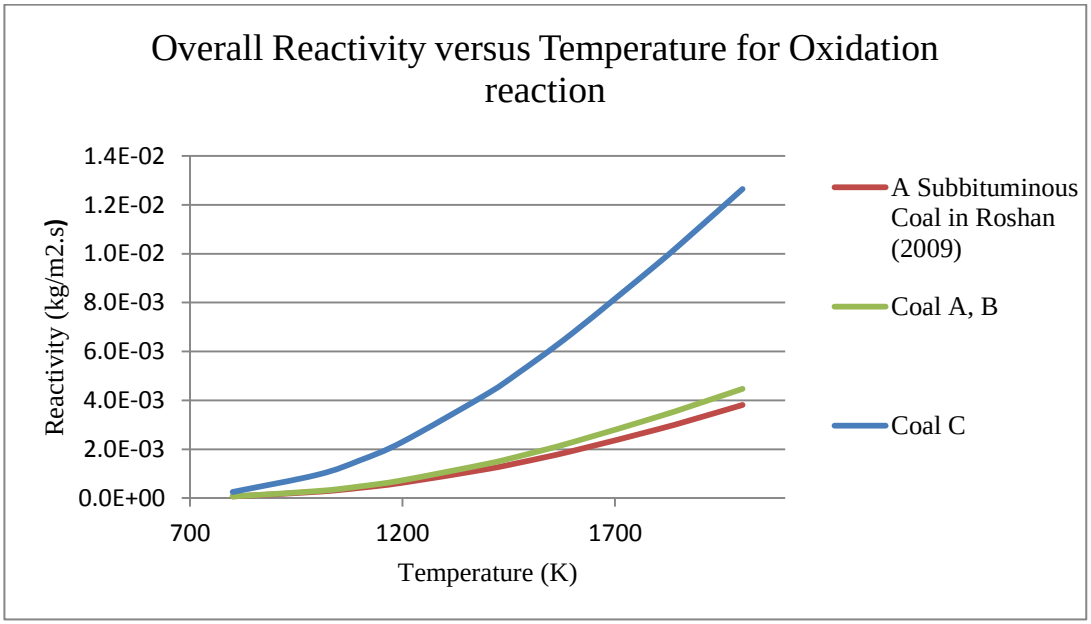

Figure 6.12: Comparisons between theoretical model and literature of the overall reactivity for the oxidation reaction at 21% oxygen

The Subbituminous coal from literature was modelled in a 21%Oxygen atmosphere and the result in figure 6.12 depicts this. A comparison is made between this and the two coals used in literature, namely, Pittsburgh and Dietz coals. It is worth noting that due to similarities in proximate, ultimate analyses and coal rank by petrographic analyses, the properties for Pittsburg coal were used to simulate Coals A and B, while the reactivity for Coal C was approximated using the properties of Dietz coal. Specivity however was made on the maceral correction factor (determined from percentage of inertinite and vitrinite as in equation 6.1) for the different coals analysed. The reason for the overlap in Coals A and B reactivity here are due to that the formulae used to model this reactivity (equations 6.3-6.12) only take into account the reaction rate per unit external area. That is, they disregard the char consumption that is influenced by the maceral correction factor.

Further than this, the reason behind the observed high reactivity by Coal C is due to the pre-exponential factor which was assumed from the Dietz Coal.

These values are summarised in the table below.

Table 6.5: Summary of Intrinsic parameters used for the overall reactivity model calculation

	Subbituminous Coal (Roshan, 2011)	Pittsburgh (Coals A & B)	Dietz (Coal C)
$A_{oxidation}$	0.0143	0.3	1.9
$E_{oxidation\ (J/mol)}$	83600	97100	92500
$A_{gasification}$	Not Applicable	289.119	0.005
$E_{gasification\ (J/mol)}$	Not Applicable	306100	103100

A comparison was not made for the gasification reaction as the literature source (Roshan, 2011) only provided the reaction kinetics, i.e. activation energy and pre-exponential factor, for the oxidation reaction.

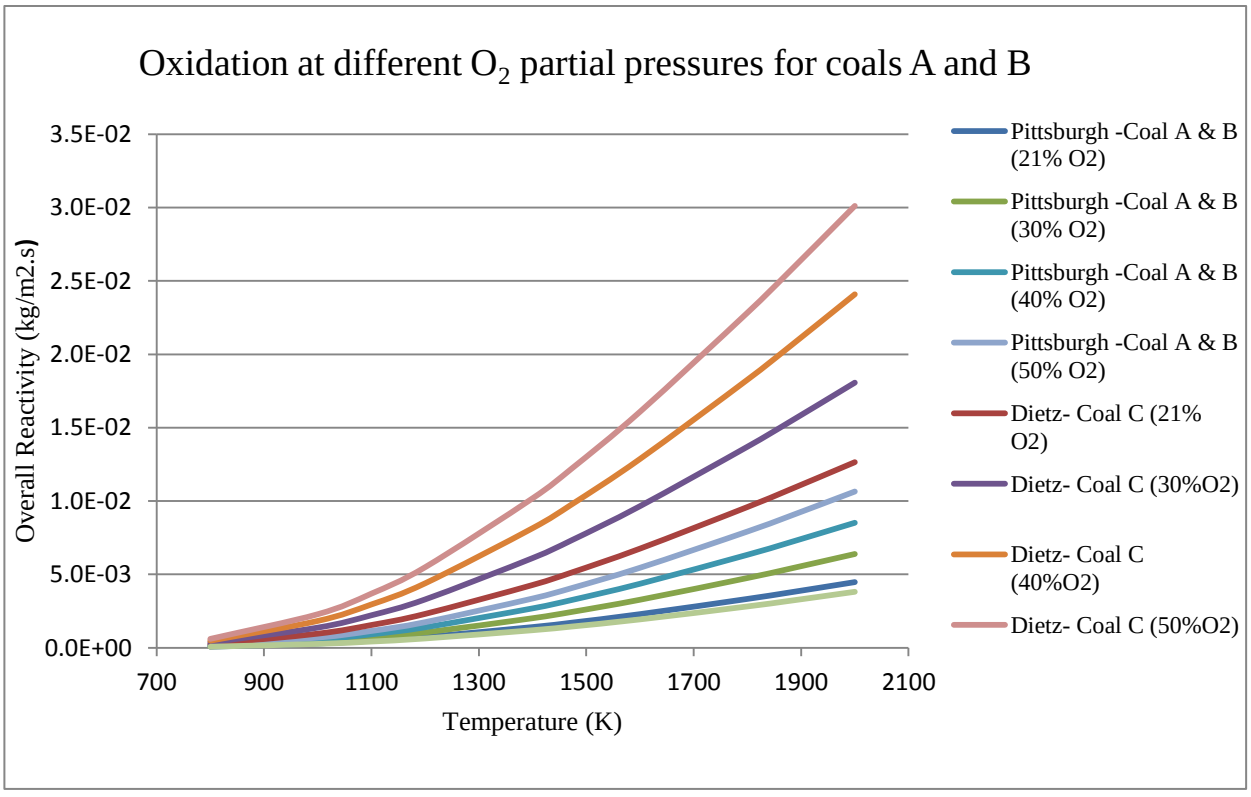

Figure 6.13: Comparison of the overall oxidation reactivity at different Oxygen partial pressures for coals A, B, C and a subbituminous coal from literature (Roshan, 2011)

A comparison was made for the three coals, using some of the data from literature. The reactivity properties for the Coals A and B were taken from literature for Pittsburgh and Coal C's parameters were assumed from Dietz coal in the same literature study (Roshan, 2011). These intrinsic rate parameters were used to model the theoretical char burnout and the results are plotted on a single chart for comparison. Based on figure 6.13 it can be deduced that combustion reactivity increases with temperature and oxygen concentration. Furthermore, it also increases with decreasing rank as the intrinsic rate parameters (assumed from literature) are different for the different coals. The subbituminous coal with intrinsic rate parameters included in table 6.5 above was also plotted as described in Roshan's work for comparison and it appears to have the lowest reactivity of all at 21%O_2/79%CO_2 environments. This further asserts that the combustion rate increases with decreasing coal rank and the finding is similar to that made in the literature review above.

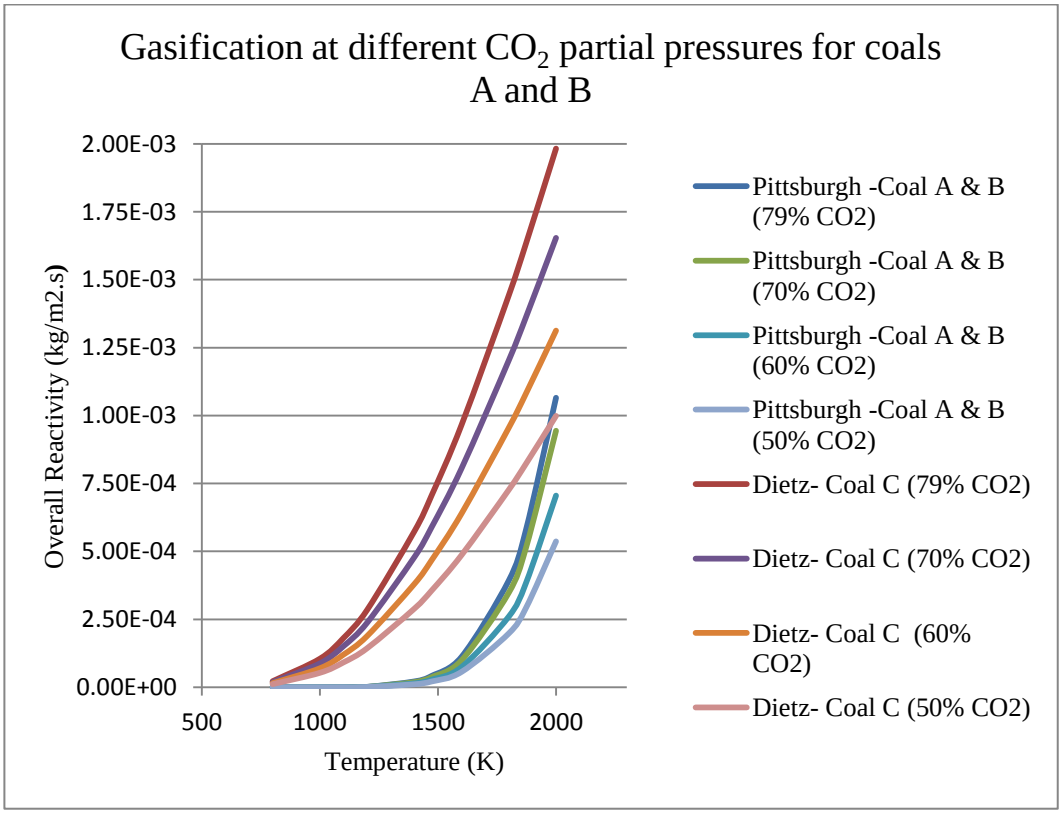

Figure 6.14: Comparison of the overall oxidation reactivity at different Oxygen partial pressures for coals A, B and C.

Finally, the gasification rate was compared and the figure 6.14 above depicts the compared results. As in oxidation, the gasification rates also increase with increasing temperature and partial pressure of the oxidising gas, in this case, carbon dioxide. The reactivity also increases with decreasing rank and the conclusion holds, i.e, the reactivity is influenced by rank even for gasification. It is worth noting that while the trends are similar, the gasification reaction rate is consistently less than that of oxidation by a magnitude of 10 $kg/m^2.s$ at all temperatures and pressures.

Chapter Summary

Given the literature survey conducted above, the ideal process for the evaluation of oxy-combustion properties for South African coals for the pulverised boilers would have been to generate the chars in a drop tube furnace and then evaluate the reactivity of the chars in a combustion test facility under different O_2-CO_2 conditions. However, the unavailability of suitable equipment lead to the use of proximate and ultimate analyses (amongst other tests) of the selected coals in evaluating the carbon conversion for oxy-combustion process and the evaluation of these key samples in terms of oxygen-char and carbon-dioxide-char reactivity using a theoretical model. The char reactivity results were then used to determine the overall burnout.

The work by Roshan (2011) and Naredi (2009) has been successfully applied to the coals in this study to determine the overall external reaction rate (R in equation 6.10) of the three coals in this study. From these results (figures 6.12-6.15) it can be concluded that oxidation and gasification of coal chars is proportional to temperature and pressure of the oxidising gas and inversely proportional to coal rank. That is, the higher the coal rank the less the reactivity. This phenomenon became more clearer at higher reaction temperatures.

Another theoretical model, Equation 6.1-6.2, was used to predict the char burnout rates of Coals A and B in O_2 (oxidation) and CO_2 (gasification) environments. However, the model could not be applied to Coal C. The reason for this was in the high inertinite content often experienced when handling Coal C that yielded a negative value in the maceral correction factor (Equation 6.2). As a result only the char burnout for Coals A and B were reported and discussed here.

For the models to be verified, it is strongly advised that the SA coal chars should be prepared in a DTF at oxy-combustions conditions and the char reactivity should then be measured by a TGA aslo at oxy-combustions conditions.

In summary, as stated above, for the models to be verified, it is strongly advised that a DTF be used over TGA for experimental determination of the coals intrinsic reactivity parameters since the DTF can simulate an industrial power generation boiler more accurately than the TGA (Ham and Riet, 1993). Also it was noted that Coals A and C were analysed historically (by Ham and Riet, 1993) and the 2014 proximate and ultimate analyses results were found to be similar to those reported in 1993. This has provided confidence in the analytic methods employed in this research here that are standard and verified by the TGA in addition to literature.

CHAPTER 7

7. CONCLUSIONS

Based on the research and investigations undertaken, the following conclusions may be drawn.

7.1. Coal Characterisation

The coal samples were characterised by means of conducting conventional proximate and ultimate analyses. In summary, the three coals are high ash (32-37% ad basis), moderate volatile (22-25% ad) grade D coals with low to moderate total sulphur contents (0.6-0.9%).

XRF (X-ray fluorescence) was also conducted to determine the oxides of the ash elementals from the ash content that was produced after heating to obtain the proximate analyses. Further analyses were performed which validated the conventional analyses results. These were petrographic (for maceral and mineral matter determination and rank determination by ECE-EU classification standards), QEMSCAN (for mineral characterisation) and thermogravimetric analyses (for proximate analyses).

The three coals have highly variable petrographic contents: 18% Vitrinite in the Coal C sample compared to 65% in Coal B and total reactives of 28% (mmf) in Coal C compared to 71% (mmf) in Coal B. Coal A is closest to Coal B in petrographic organic matter composition e.g. Vitrinite content of 57% (mmf basis) and total reactives of 65% (mmf).

In terms of rank, as determined by vitrinite reflectance (RoV random %), the coals are all classified as Bituminous Medium rank C/D.

7.1.1. Proximate analyses by conventional methods and TGA

In order to determine coal char reactivity, volatile matter as well as the fixed carbon content of the coals were each individually used in theoretical models from literature to better understand their impact on predicted char reactivity. However it was found that the two properties had opposite effects, i.e. fixed carbon requires longer burnout times while volatile matter reverses this phenomenon. Hence, as opposed to using the two properties in isolation (which yielded conflicting analyses) the fuel ratio was used as the better indicator of char reactivity. The fuel ratio, defined as the ratio of FC to VM, indicated that the Coal B sample would have the highest reactivity; this result was also verified by the theoretical model.

7.1.2. Ultimate analyses

The oxygen-to-carbon (O/C) and hydrogen-to-carbon (H/C) ratios determined from ultimate analyses indicate that when considering coal properties and oxygen diffusion only, (disregarding external factors such as radiation and flame propagation velocities) all coals analysed are likely to have lower ignition temperature and higher carbon burnout under OFC conditions than they would (individually) in air. This conclusion was drawn from comparing characteristic temperatures with O/C and H/C ratio ranges. The ratios all fall within the ranges stipulated in literature as coals that have a significant sensitivity to O_2 concentration (in turn affecting ignition and burnout temperatures). While the ratios of all coal samples analysed fall within this range, the level of sensitivity to O_2 concentration is different as Coal A had the highest H/C ratio while Coal C had the lowest.

7.1.3. Ash content & composition

The Coal C sample was found to have the highest mineral matter content of the three coals by conventional proximate analysis as well as petrographic analysis. While all three coals have similar ash compositions, XRF showed that Al_2O_3 content in the Coal C sample is highest compared to Coals A and B. Given that oxy-fuel combustion to some extent (as with combustion in air) depends on the properties of the fuel, it can be concluded that Coal C will produce the most ash of the three coals

under OFC and also more ash than it currently produces when combusted in air in comparison to the other two coals.

7.1.4. Analysis of Ash Fusion Temperatures (AFT)

The ash fusion temperature (AFT) of Coal C is highest (1500℃) indicating that the ash that is produced will accommodate higher furnace temperatures before softening and slagging. As O_2 has higher diffusion coefficient in CO_2 (compared to N_2) and CO_2 has a higher heat capacity compared to N_2, furnace temperatures are likely to be higher in oxy-fuel conditions than normal combustion in air (hence the need for recycling the flue gas stream). Thus, the higher ash fusion temperatures of Coal C suggests that it could exceed the flue exit gas temperature thus preventing the ash from melting and solidifying on the tubes at the back-end of the boiler. This conclusion was made on the assumption that the flue gas recycle in OFC will be controlled in a manner that ensures that current flue gas exit temperatures are maintained to preserve ESP and FFP performance when retrofitting the boiler with OFC.

The SOx emissions for Coal A may be slightly higher since it displayed the higher total sulphur content in the ash analyses (TS %), and the highest amount of inorganic sulphur (SO_3) in XRF analyses compared to the other two coals. Thus consideration must be made for flue gas desulphurisation technology when retrofitting oxy-fuel cpmbustion to a station that is supplied with Coal A. Based on the findings suggested here, it seems that the station that uses Coal B feed could be fitted with OFC technology with minimal changes adapted to FGD as compared to the other coal samples analysed. This conclusion is made based on the chemical ultimate characteristics of the coals studied.

It is understood that conclusions regarding OFC implications on FGD and associated plant modifications cannot be made on chemical analyses alone, thus the implications of the mathematical char model results are considered: that is the role of the gasification reaction due to the presence of CO2 in OFC. This conclusion is further discussed below (section 7.2.1). However, other considerations must be taken into

account such as burner air-swirl ratio (if low NOx burners are to be used for NOx emission reduction) as well as flame propagation and stability factors. This can be assessed using CFD modelling and alternative commercial CFD packages available on the market, as well as bigger scale experimental tests in a combustion test facility.

From the petrographic analyses, Coals A and B have high proportions of reactive macerals and may therefore be expected to devolatilise and burn out rapidly. Coal C has lower proportions of reactive macerals and a relatively high inert maceral content (intertinite) and is therefore expected to be more difficult to ignite and combust. The wide variations in petrographic compositions are not reflected in the proximate and ultimate values.

7.2. Char Reactivity: Intrinsic reactivity and overall burning rate

The results from the char burnout model in this research indicate that the intrinsic reactivity of Coals A and B are similar while Coal C seemed to have the highest intrinsic reactivity. This is contradictory to the conclusions made above (based on petrographic observation) as Coal C had the lowest rank (medium rank D), lowest reactive macerals and highest ash content. Char burnout is, to a large extent, influenced by coal composition and rank and should match the model. This was investigated further.

The model used was developed from empirical formulae which in turn required coal classification by ASTM standards. The coals were classified using petrographic analysis according to ECE-EU standards as follows; Coal A (Medium rank C bituminous), Coal C (medium rank D bituminous) and Coal B (Medium rank C bituminous). However, since the ranks were required in terms of ASTM rankings, a conversion had to be made. This was attained using the fixed carbon content, volatile matter content and GCV (gross calorific value). When this was completed, the ranking category did not match the ECE-EU standards, i.e. Coals A and B were in the same rank when ECE-EU and Parr's equations were used however when ASTM method was used, Coals A and C had the same rank.

The intrinsic reaction rate for all coals above increases with temperature with Coal C having the highest rate of the three. However, the results for the char combustion, taking into account the pressure and concentration of the combustion gas, gave dissimilar results. The Coal B sample had the highest reactivity across all temperatures and oxy-fuel combustion environments, followed by Coal A for both oxidation and gasification reactions. This is contrary to the first results on intrinsic reactivity ($kg/m^2.s.Pa$), indicating that intrinsic reactivity does not always compare qualitatively to overall char burning rate (which is given in $kg/m^2.s$).

The reason for the discrepancy between the intrinsic reactivity and char burnout is that the model used for char burnout (Equations 6.1 and 6.2) takes into account, in addition to intrinsic reactivity (Rs), the coal's chemical properties, petrographic analysis in the maceral correction factor while the formula for intrinsic reactivity; i.e. Equation 6.4 disregards all these factors. Hence a difference in results is observed between intrinsic reactivity and overall char burnout, especially since the latter incorporates the pressure of the combustion gas (O_2 or CO_2) into the intrinsic reactivity equation.

In addition to this, the model for the Coal C sample showed a decline in reactivity for both gasification and oxidation reactions across all temperatures and O_2 concentrations used in the study. This was found to be due to the maceral correction factor that was used from petrographic analysis. This indicates the incompatibility of char combustion models and char characterisation models for South African coals, especially those with high inertinite content, or inertinite to vitrinite ratios exceeding 2.8 (e.g., the Coal C sample). See Appendix B2 for the derivation of this ratio from empirical formulae 6.1 and 6.2 quoted above.

7.2.1. Gasification reaction

In oxy-fuel conditions, the gasification reaction rate was found to be lower for all oxygen concentrations by a magnitude of approximately 10 $kg/m^2.s$, indicating that gasification does take place under oxy-fuel conditions, but at a lower rate than

oxidation under the temperature and pressure conditions observed (for all coal samples presented).

7.2.2. Comparison of CO_2 yields

Due to the different char burn out rates reflected in the model, it can be inferred that the CO_2 yields will follow the same pattern (at least qualitatively). The reaction curve for Coal A shows a higher burn rate than Coal B, implying that the CO_2 yield may be higher for this sample. Given the relatively high inertinite content of the Coal C sample compared to the remaining two samples (determined in the petrographic analysis and used in the theoretical models), the char burnout of a Coal C sample is expected to be the lowest thus yielding the least amount of CO_2, per unit carbon, of the three samples analysed.

In final summary, the results conclusively prove that empirical char combustion models do not apply to low grade, inert-rich coals such as those most common in South Africa. Char reactivities differed from coal to coal and that petrographic analyses and tests reflects likely performance in OFC more effectively than proximate, CV and ultimate analyses. Oxy-fuel firing can be applied in SA.

CHAPTER 8

8. RECOMMENDATIONS

Based on the current investigation, the following recommendations are made;

I. As the maceral correction factor that has been developed for Southern hemispheric coals is not applicable for high inertinite coals, further investigations need to be undertaken in this field for the low grade South African coals.

   This is important in the South African context because of the depletion of higher grade SA coals that are often used for export and the subsequent increase in the use of low grade coals and coal blending.

II. It is recommended that combustion tests in air and oxygen conditions be performed to determine carbon conversion in order to confirm this conclusion.

III. Furthermore, it is recommended that TGA can be undertaken for further analyses and verification of the intrinsic rate parameters used here. Finally, oxy-fuel combustion tests can be performed in a pilot scale drop tube furnace (DTF) to further verify the results obtained.

Presentations and Publications

The conference paper that has emanated from this research project is listed below:

Dorcas Molise. Application of Oxy-fuel combustion on South African Coals using Thermogravimetric Analyses. **Oral Presentation**. 20th Southern African Conference on Research in Coal Science and Technology: Latest Research at Universities and R&D Organisations, North-West University, Northwest Province, South Africa. 24 November 2015.

REFERENCES

Air Products and Chemicals, Inc., 2008 (27918). *Air Products*. Online: http://www.airproducts.com/ASUsales (Accessed 10 December 2013).

Alvarez, D., Fernandez Dominguez, I., Borrego, A. G. 2005. *Comparison of pulverised coal combustion performance under O2/CO2 and O2/N2 atmospheres*. Tsukuba: National Institute of Advanced Industrial Science and Technology.

American Society for Testing and Materials. 1998. *Standard Classification of Coals by Rank*. Online: https://law.resource.org/pub/us/cfr/ibr/003/astm.d388.1998.pdf. (Accessed 16 September 2014).

Andersson, K. and Johnson, F. 2006. *Combustion and flame characteristics of oxy-fuel combustion - experimental activities within the ENCAP* project. Trondheim : GHGT

Andersson, K. and Johnsson, F. 2006. *Radiative properties of a 100 kW Oxy-fuel flame experiments and modelling of the Chalmers test facility*. Florida: Coal Technologies Associates

Anglo American. 2012. *Anglo American Opens R4.2 Billion Coal Mine*. Online: http://southafrica.angloamerican.com/our-operations/thermal-coal.aspx. (Accessed 16 April 2014)

Annamalai, K and Ryan, W., 1993. Interactive processes in gasification and combustion –II. Isolated carbon, coal and porpous char particles. *Progress in Energy and Combustion Science 19 (5)*: 383-446

Ballantyne, A., Chou, H., Neoh, K., Orozco, N., Stickler, D. 1984. Cold atmosphere pyrolysis of pulverized coal using 10. 6. um laser heating. *Fuel Chemistry*, *29* (2), 119-128.

Baukal, C. 2005. *Pollution Control: Everything you need to know about NOx*. Online: http://www.johnzink.com/wp-content/uploads/everything-about-nox.pdf. (Accessed September 14, 2014)

Bejarano, P. A., Levendis, Y. A. 2007. Combustion of coal chars in oxygen-enriched atmospheres. *Combustion Science and Technology*, *179*(8), 1569-1587.

Bejarano, P. A., Levendis, Y. A. 2008. Single-coal-particle combustion in O2/N2 and O2/CO2 environments. *Combustion and Flame*, *153*(1-2), 270-287.

Bono, A. 2012. *Coal Geology and Petrology Section, Lecture 13: Coal Rank, Grade and Type., ERTH 3117*. Accessed Online: http://www.slideshare.net/adhlino_bono/coal-mine (Accessed 14 March 2014).

Borrego, A G., Alvarez, D., Fernandez-Dominguez, I., Ballestros, J C., Menedez, R. 2005. *Oxy-combustion of high rank coals*. Spain: Instituto Nacional del Carbón, CSIC.

BP. 2013. *Statistical review of world energy*. Online: https: //www. bp.com /content /dam /bp/pdf / statistical review/statistical_review_of_world_energy_2013.pdf (Accessed 17 March 2014).

Brently,V, R and Thomas, W, A. 1983. Damp Coal Screening-Effect of Screen Size and Coal Surface Moisture on Fines Removal Efficiency. Oak Ridge National Laboratory, Engineering Technology Division, Department of Energy

Brix, J., Petersen, S, M., Grossmann, J, B., Glarborg, P., Jensen, P, A., Jensen A, D. n.d. Coal Char Reactivity: A Thermogravimetric Study on Chars Obtained in O2/N2 and O2/CO2 in an Entrained Flow Reactor Under Suspesion Fired Conditions and in a TGA. Department of Chemical and Biochemical Engineering., Denmark

Buhre, B, J, P., Elliot, L, K., Sheng, R,P., Gupta,T,F, Wall, T,F. 2005. Oxy-fuel combustion technology for coal-fired power generation. *Progress in Energy and Combustion Science*, *31*, 283-307.

Chen, L., Yong, S. Z. Ghoniem, A. F. 2012. Oxy-fuel combustion of pulverised coal: Characterisation, fundamentals, stabilization and CFD modeling. *Combustion Science, 38*, 156-214.

Cohen, B., 2013. *The Future of Coal: Existing Power Stations Considerations for New Stations.*Online: http://stias.ac.za/wp-content/uploads/2013/03/WS-10-Cohen-Future-of-Coal.pdf (Accessed 23 April 2014)

Creamer, T. 2013. *Mining Weekly: First Majuba Coal Train Scheduled for May 2016.* Online: http://www.miningweekly.com/article/first-majuba-coal-train-scheduled-for-may-2016-2013-09-19
(Accessed 15 March 2014).

Department of Energy, 2013. *Integrated Resource Plan*. Online: http://www.doe-irp.co.za (Accessed 23 April 2014)

Dhaneswar, R. S. 2011. *Effect of coal rank during oxy-fuel combustion: role of char-CO2 reaction.* USA: Pennsylvania State University.

Dhaneswar, R. S., Pisupati, S. V. 2012. Oxy-fuel combustion: The effect of coal rank and the role of char-CO2 reaction. *Fuel Processing Technology,102*. 156-165.

Dhaneswar, S. R. 2011. *Effect of coal rank during oxy-fuel combustion: role of char-carbon dioxide reaction.* Pennsylvania: Pennsylvania State University.

Eberhard, A. 2011. *The Future of South African Coal: Market, Investment and Policy Challanges.* Stanford: Spogli Institute

Eisermann, W., Johnson, P., Conger, W. L. 1980. Estimating thermodynamic properties of coal, char, tar and ash. *Fuel Processing Technology 3*, 39-53.

Energy Information Administration. 2013. *South Africa energy data, statistics and analysis-oil, gas, electricity, coal.* Online: http://www.eia.gov/forecasts/ieo/pdf/0484(2013).pdf. (Accessed 17 March 2014).

Eskom Holdings SOC. 2014. *About Electricity,Electricity Technologies,Coal Power*. Online: http://www.eskom.co.za/AboutElectricity/ElectricityTechnologies/Pages/Coal_Power.aspx. (Accessed 15 May 2014).

Falcon, R. 2014. Coal Quality Distribution Geographically and Geologically. Johannesburg : University of the Witwatersrand

Falcon, R. M. 1986. Classification of coals in Southern Africa. *Mineral Deposits of Southern Africa*, 1899-1921.

Falcon, R. M. 1989. Macro-and micro-factors affecting coal-seam quality and distribution in southern Africa with particular reference to the No. 2 seam, Witbank coalfield, South Africa. *Geology*, 681-731.

Falcon, R. M. 2014. Advanced Tests for Coal Combustion. Johannesburg:University of the Witwatersrand

Falcon, R., Ham, A. J. 1988. The characteristics of Southern African coals. *Institute of Mining and Metallurgy 88* (5), 145-161.

Glarborg, P., Jensen, A. D and Johnsson, J. E. 2003. Fuel Nitrogen Conversion in Solid Fuel Fired Systems. *Progress in Energy and Combustion Science 29 (2)*: 89-113

Ham, A.J and Van der Riet, M., 1993, An Assessment of the combustion performance of power plant coal: from the laboratory to the power plant. *VGB Kraftwerkstechnik 73* (4)

Hower, J. C. 2008. Maceral/microlithotype partitioning with particle size of pulverised coal: Examples from power plants burning Central Appalchain and Illinois basic coals. *Coal Geology 73*, 213-218.

Hu, Y. 2011. *Carbon dioxide capture from oxy-fuel combustion power plants.* Stockholm: KTH Royal institute of Technology

Hu, Y., Yan, J., Li, H. 2011. Effects of flue gas recycle on the performance of particles, SOx and NOx removal in oxy-coal power generation system. *Applied Energy*, 841-852.

Hurt, R. H., Calo, J. M. 2001. Semi-global Intrinsic Kinetics for char combustion modelling. *Combustion and Flame 125*, 1138-1149.

IEAGHG. 2010. *Oxyfuel Combustion of Pulverised Coal.* London, UK: IEA Clean Coal Centre. Online: http://www.ieaghg.org/docs/General_Docs/Reports/2010-07.pdf. (Accessed 7 September 2014)

Jeffrey, L. S. 2005. Characterisation of the coal resources of South Africa. *Institute of Mining and Metallurgy*, 95-102.

Kangwanpongpan, T. 2013. *Contribution to CFD Modelling of Lignite Oxy-fuel Combustion with Special Focus on Radiation Properties*. Bangkok: Brandenburg University of Technology

Kee, J. S. 2014. *Coal rank: Coal classification*. Online:http://www.shibang-china.com/coal-project/coal-classification.html. (Accessed 22 February 2014)

Khatami, R., Stivers, C., Joshi, K., Levendis, Y. A., Sarofim, A. F. 2012. Combustion behaviour of single particles from three different coal ranks and from sugar cane bagasse in O2/N2 and O2/CO2 atmospheres. *Combustion and Flame, 159*, 1253-1271.

Kilpinen, P., Kallio, S., Konttinen, J and Barišić, V. 2002. Char-nitrogen oxidation under fluidised bed combustion conditions - single particle studies. *Fuel 81:* 2349-2362

Krugar, T, J., A. 2003. Generic Framework for Continuous Energy Management at Cryogenic Air Separation Plants. South Africa: University of Pretoria.

Li, Q., Zhao, C., Chen, X., Wu, W., Li, Y. 2010. Pyrolysis and combustion characteristics of an Indonesian low-rank coal under O2/N2 and O2/CO2 conditions. *J. Anal. Appl. Pyrolysis, 85,* 521-528.

Li, X. et al., 2010. Pyrolysis and combustion characteristics of an Indonesian low-rank coal under O2/N2 and O2/CO2 conditions. *Energy Fuels, 24,*. 106-164.

Liu, Giu-su., Tate, A, G., Bryant, G, W., Wall, T, F. 2000. Mathematical modeling of coal char reactivity with CO2 at high pressures and temperatures. *Fuel, 79*, 1145-1154.

Liu, H., Zailani, R., Gibbs, B. M. 2005. Comparisons of pulverised coal combustion in air and in mixtures of O2/CO2. *Fuel*, 833-840.

Liu, Y., Gupta, R., Sharma A, Wall, T., Butcher, A., Miller, G., Gottlieb, P., French, D. 2005. Mineral matter-organic matter association characterization by QEMSCAN and applications in coal utilization. *Fuel, 84*, 1259-1267.

Man, C. K., Gibbins, J. R., Cashdollar, K. L. 2007. *Effect of coal type and oxyfuel combustion parameters on pulverised fuel ignition.* Nottingham: Clean Coal Centre

Mining Atlas. 2014. Zibulo mining. Online: http://www.miningatlas.com/operation/Zibulo_Thermal_Coal_Mine.php. (Accessed 12 March 2014)

Mitchell, G. D. 2013. *Coal Utilisation in the Steel Industry: Steelworks*. Online: https://www.steel.org/Making%20Steel/How%20Its%20Made/Processes/Processes%20Info/Coal%20Utilization%20in%20the%20Steel%20Industry.aspx (Accessed 12 January 2014).

Molina, A., Shaddix, C. R. 2005. Effect of O2/CO2-firing on coal particle ignition. Pittsburgh: Pittsburgh Coal.

Molina, A., Shaddix, C. R. 2007. Ignition and devolatilization of pulverised bituminous coal particles during oxygen/carbon dioxide coal combustion. *Combustion Institute, 31*(2), 1905-1912.

Molina, A., Hecht, E. S., Shaddix, C. R. 2009. *Ignition of a group of coal particles in oxyfuel combustion with carbon dioxide recirculation*. Clearwater: Fuel Systems

Murphy, J. J., Shaddix, C. R. 2006. Combustion kinetics of coal chars in oxygen-enriched environments. *Combustion and Flame 144*, 710-729.

Muthu, S. S., Steinberg, M and Fallon, P. n.d. Enhanced Ethylene Production via Flash Methanolysis of Coal. *Recent Results on the Kinetics of Coal Pyrolysis and Hydropyrolysis and their Relationship to Coal Structure.* Process Science Division, Dept. of Applied Science New York 11973. 129-140

Naredi, P. 2009. *Coal combustion in oxygen/carbon dioxide medium for power generation: Numberical Modelling of Char Burnout, NOx and CO Emissions,* USA*:* Pennsylvania State .

Naredi, P., Pisupati, S. V. 2007. *Comparison of char structural and reactivity parameters for air-coal and oxygen/carbon dioxide-coal combustion*. USA: IEA Clean Coal Centre.

Naredi, P., Pisupati, S. V. 2007. *Oxy-fuel combustion: effect of recycled carbon dioxide on pyrolysis behaviour and char reactivity*. USA: Pittsburgh Coal Centre.

Naredi, P., Pisupati, S. V. 2008. Comparison of char burnout and CO emissions from oxy-coal combustion with combustion in air: an experimental and numerical study. *Coal Technology,* 177-187.

Naredi, P., & Pisupati, S. V. 2009. *On the prediction of char burnout from oxy-coal combustion*. Germany: Greenhouse gas R&D

Niksa, S., Liu, G., Hurt, R. H. 2003. Coal conversion submodels for design applications at elevated pressures. Part I. devolatilization and char oxidation", *Progress in Energy and Combustion Science 29*: 425–477.

Niu, S. L., Lu, C. M., Han, K. H., Zhao, J. L. 2009. Thermogravimetric analysis of combustion characteristics and kinetic parameters of pulverised coals in oxy-fuel atmosphere. *Thermal analysis and calorimetry 98*(1), 267-274.

Oboirien, B., North, B., Kleyn, T. 2014. Techno-economic assessments of oxy-fuel technology for South African coal-fired power stations. *Energy 66*, 550-555.

Osborne, D., 2013. The Coal Handbook: Towards Cleaner Production, Coal Production. In: D. Osborne, ed. S.l: Woodhead Pub Limited.

Pallares, J., Arauzo, I., Williams, A. 2007. Integration of CFD codes and advances combustion models for quantitative burnout determination. *Fuel 86*(15), 2283-2290.

Parr, S. W. 1928. *The Classification of Coal*. Urbana: University of Illinois.

Pohlmann, J. G., Osorio, E., Vilela, C. F., Borrego, A. G. 2010. Reactivity of CO2 in O2/N2 and O2/CO2 mixtures for pulverised coal injection (PCI) in blast furnace in relation to char petrographic characteristics. *Coal Geology*, 293-300.

Power Plant CCS. 2014. *Vattenfall Schwarze Pumpe-Project Profile*. Online: http://www.powerplantccs.com/ccs/cap/con/of/vsp_pp.html. (Accessed 13 March 2014).

Pressly, D. 2013. *Business Report.* Online: http://www.iol.co.za/business/news/wcc-can-fill-eskom-coal-supply-gap-for-100-years-1.1608314#.Vgqiyd-qqko. (Accessed 13 March 2014).

Rathnam , R. K., Elliot, L. K., Wall, T. F., Liu, Y., Moghtaderi, B. 2009. Differences in reactivity of pulverised coal in air (O2/N2) and oxy-fuel (O2/CO2) conditions. *Fuel Processing Technology 90*(6), 797-802.

Rathnam, R. K., Elliot, L., Moghtaderi, B., Gupta, R., Wall , T. 2006. *Differences in coal reactivity in air and oxy-fuel conditions and implications for coal burnout*. Florida: Coal Utilization and Fuel Systems. 77-88.

Rathnam, R. K., Wall, T. F., Eriksson, K., Stromberg , L., Moghtaderi, B. 2008. *Reactivity of pulverised coals in simulated air (O2/N2) and oxy-fuel (O2/CO2) atmospheres*. Pittsburgh: Coal Utilization and Fuel Systems. 16.

Rathnam, R. K., Wall, T and Moghtaderi, B. 2013. Reactivity of pulverised coals and their chars in oxyfuek (O2/CO2) and air (O2/N2) conditions. *3rd Oxyfuel Combustion Conference*, Ponferrada, Spain.

Riaza, J., Alvarez, L., Khatami, R., Levendis, Y. A., Gil, M. V., Pis, J. J., et al. (n.d.). *Ignition behaviour of coal and biomass blends under oxy-firing conditions with steam additions.* Boston: Northeastern University.

Ryan, B. 2014. *Mining New Territory: Waterberg Coalfield, Financial Mail.* Online: http://www.financialmail.co.za/coverstory/2014/03/27/mining-new-territory-waterberg-coal-field. (Accessed 16 April 2014).

Sami, M., Annamalai, K., Wooldridge, M., 2001. Co-firing of Coal and Biomass Fuel Blends. *Progress in Energy and Combustion Science 27*, 171-214

Seyler, C. A., 1923. The Classification of Coals. *Fuel 2*, 272.

Smith, A. R., Klosek, J., 2001. A review of air separation technologies and their integration with energy conversion processes. *Fuel processing technology 70*, 115-134.

Smith, I. W., 1982. The Combustion rates of coal chars: a review. *Nineteenth Symposium (International) on Combustion/The Combustion Institute,* 1045-1065

Smoot, L,D and Pratt, D,T., 1979. Pulverized-Coal Combustion and Gasification. Springer Science + Business Media New York, pp 150

Solomon, P. R., Serio, A. A and Suuberg, E. M., 1992. Coal Pyrolysis: Experiements, Kinetic Rates and Mechanisms. *Progress in Energy and Combustion Science 18 (2),* 133-220

Steel Construction. 2010. *Projects: Zibulo* Colliery. *Steel Construction 34,* 28-30.

Tan, Y., Croiset, E., Douglas, M. A., Thambimuthu, K. V. 2006. Combustion characteristics of coal in a mixture of oxygen and recycled flue gas. *Fuel 85*(4), 507-512.

The Southern African Coal Processing Society, 2011. *Coal Preparation in South Africa*. S.l: s.n

Tigges, K. D., Klauke, F., Bergins, C., Busekrus, K., Niesbach, J., Ehmann, M., et al. (n.d.). *Oxyfuel Combustion Retrofits for Existing Power Stations.* USA: Hitatchi Power Europe GmbH.

Tillman, D, A. 1991. 'The combustion of Solid Fuels and Wastes', London, UK, Academic Press, Inc. pp 378

Toftegaard, M. B., Brix, J., Putluru, S. R., Montgomery, M., Hansen, K. G., Hansen, B. B.(2011). *PSO 7171-Oxyfuel combustion for below zero CO2 emisions.* Denmark: Technical University of Denmark.

Toporov, D. 2014. *Combustion of Pulverised Coal in a Mixture of Oxygen and Recycled Flue Gas.* London: Elsevier.

United Nations. 1998. *International Classification of in-Seam Coals*. Geneva: International Classification of in-Seam Coals.

Unsworth, J. F., Fowler, C. S., Heard N. A., Weldon, V. L. and McBrierty, V. J. (1988) "Moisture in coal 1. Differentiation between forms of moisture by NMR. and microwave attenuation techniques." Fuel. Butterworth & Co. 67: 1111- 1119.

Unsworth, J F., Fowler C S. and Jones, L. F. (1989) "Moisture in coal 2. Maceral effects on pore structure." Fuel, Butterworth & Co. 68: 18-12.

Van Alphen, C. 2007. Automated mineralogical analysis of coal and ash products-challenges and requirements. *Minerals Engineering, 20,* 496-505.

Wall, T., Liu, Y., Spero, C., Elliot, L., Khare, S., Rathnam.2009. An overview on oxyfuel coal combustion-state of the art research and technology development. *Chemical Engineering Research and Desig,n 87,* 1003-1016.

Wang, C. S., Berry, G. F., Chang, K. C., Wolsky, A. M. 1988. Combustion of Pulverised Coal Using Waste Carbon Dioxide and Oxygen. *Combustion and Flame, 72,* 301-310.

Wigley, F., Williamson, J., Gibb, W. H. 1997. The distribution of mineral matter in pulverised coal particles in relation to burnout behaviour. *Fuel 76* (13), 1283-1288.

Williams, A., Pourkashanian, M., Jones, J. M. 2000. The combustion of coal and some other solid fuels. *Proceedings of the Combustion Institute 28* (2), 2141-2162.

Yi, B. et al., 2015. Investigating the combustion characteristic temperature of 28 kinds of Chinese coal in oxy-fuel conditions. *Energy Conversion and Management,* 103, 439-447.

APPENDICES

Appendix A-Methods and Standards used for coal characterization and analyses

A.1 Standards accreditation

Table A1: Methods and Standards used for coal characterisation and analyses

Analysis	Method	Revision	Accreditation
Analytical Moisture	Eskom Method Nr 103	2	Accredited
Volatile Matter	Eskom Method Nr 102	1	Accredited
Ash	Eskom Method Nr 101	1	Accredited
Gross CV	Eskom Method Nr 105	1	Accredited

A.2 Proximate Analyses

Each coal sample was pulverised in a mill and prepared according to SABS 0135 Part II-1977. The following analyses were determined for each coal sample: inherent moisture content, volatile matter, ash content, fixed carbon (by difference) and calorific value.

A.2.1 Inherent Moisture (IM) content[5]:

The inherent moisture of the coals was performed using Eskom method number 103 which is adopted from SABS Method 925.

This was determined by gravimetric means whereby the coal was weighed, heated in an air-oven at 105℃ (378.15K) for 90 minutes and then re-weighed. Allowance was

[5] The surface moisture could have also been determined by gravimetric means by heating the coal sample until no further weight loss was recorded in the oven however, this was not done because the surface moisture would be useful in indicating the total moisture, TM (when added to IM), but the results here are only reported in AD, DB and DAF bases which do not require TM when converting between them (the different bases).

made for maximum 110℃ (383.15K). The difference in masses weighed is reported here as mass loss due to inherent moisture evaporation.

A.2.2 Volatile Matter determination:

After the inherent moisture was driven off, the volatile matter was determined using Eskom method number 102 (which is in turn has been adopted from SABS 927).

Here, the coals were first weighed (and should read the same weight as recorded after IM determination above), and then heated for 7 minutes in an isothermal and uncontaminated oven (i.e. no contact with air) at 900℃ ($1173.15K$). Allowance was given for$\pm$10℃ ($\pm 283.15K$). A stopwatch was used to time the devolatilisation to 7 minutes as the crucibles were already heated (in the oven) prior to the experiment being conducted. Thereafter, the coal was weighed again and the difference attributed to loss of volatilises being driven off. This is in accordance with SABS 927.

A.2.3 Ash analysis:

Ash is defined as the products of coal combustion, after the combustion process is complete. It consists of oxidised mineral matter and inorganic complexes. The method to determine this was to heat the pulverised coal sample in 815℃ (1088.15K), allowance was given for$\pm$10℃($\pm 283.15K$) until the coal mass ceased to change and all combustion was complete. This is in accordance with Eskom method number 101 and/or SABS Method 928

A.2.4 Fixed carbon:

Fixed carbon content of the coals was not measured but was calculated according to the mass balance given in Eskom Method number 128 (SABS 928). Since the other parameters are reported in mass percentage, fixed carbon (%) is then calculated by subtracting the sum of IM, VM and Ash from 100.

For verification purposes, all analysis made above were conducted in duplicate crucibles for each coal sample simultaneously with a "standard"[6]. The results are reported on an air-dried basis.

A.3 Ultimate Analyses

3.2.2.1. Carbon, Hydrogen and Nitrogen contents

To determine the Carbon, Hydrogen and Nitrogen contents of the coal samples, the LECO CHN-1000 Carbon, Hydrogen and Nitrogen elemental analyser was used.

As prescribed in Eskom method no 137 (rev 1) and LECO CHN-1000 method manual, the following instructions were followed:

The sample was first ground to -212 microns according to the SABS 0135 (part 2 1997) procedure. The coal sample was then weighed and placed into the sample holder. When 'analyse' was selected on the LECO instrument, the sample was then transferred into the combustion chamber where the furnace temperature and oxygen flow rate were set to allow for spontaneous combustion to take place. During combustion, elemental carbon, hydrogen and nitrogen in coal were converted into CO_2, H_2O and NOx respectively. These gases were then passed through the infrared cell to back-calculate the carbon and hydrogen content from which they were derived. For Nitrogen, a thermal conductivity cell was used.

3.2.2.2. Oxygen content

The oxygen content was determined by difference i.e. Oxygen is the difference between 100 and the sum of the remaining elements: Carbon, Hydrogen, Nitrogen and Sulphur.

3.2.2.3. Total sulphur content

The sample was first ground to -212 microns according to the SABS 0135 (part 2 1997) procedure.

[6] A standard "is a reference coal sample whose proximate analyses are already known (for determining accuracy).

The following method was used as referenced in LECO S632 and Eskom method nr. 104 (rev 2):

Coal was placed in the combustion system which is typically regulated at 1350 ^{0} C with pure oxygen environment. The combination of furnace temperature and air flow caused the sample to combust. The oxidative reduction process takes place where sulphur forms SO_2. Sulphur (as SO_2) was then released into carrier flow as sample gases which flowed through the Anhydrone tube to remove moisture and dust. The sulphur IR (infrared) cells measured the concentration of sulphur dioxide gas. The instrument converts that value using an equation present in the software, which takes place into account the sample weight, calibration and known moisture value. Answers are reported as percentage in the results section.

A.4 Net Calorific Value

Refer to AC-350 Automatic calorimeter instruction manual version and SABS method 929.

The coal sample was burned in oxygen in a bomb calorimeter and associated computer program. Once combustion had taken place, the program then calculated, using the mass and energy expelled during the combustion process, the calorific value of the coal sample.

A LECO instrument was used, from Eskom's Research and Testing laboratories: LECO AC600.

A.5 Ash Elementals by the X-Ray Fluorescence (XRF) Spectrometer method

The apparatus that was used is the Philips PW 1404 x-ray fluorescence spectrometer at Eskom Research, Testing and Development laboratory. The glass ash bead was used, which was first radiated with primary x-rays. Secondary x-rays were then

produced by the elements present in the ash that was produced from the individual coal samples. These (secondary x-rays) are typically determined by the spectrometer and submitted to the computer for data reduction. More details on ash sample preparation and reagents used may be found on Eskom's method manual (method number 121 rev 2) or Philips operation manual: Software for XRF X44 from which the Eskom method of analyses was derived.

A.6 Ash Fusion Temperature

This method was adapted from the LECO AF600 ash fusion determinator instruction manual and Eskom method manual 125 (rev 1).

The sample was first ground to -212 microns according to the SABS 0135 (part 2 1997) procedure and weighed. The ash was then prepared by following the method described above (adopted from Eskom method no. 101) and ground to <75 micron meshed size sieve.

The ash was then placed in the instrument; LECO AF600 ash fusion determinator which had been automated and programmed by video imaging to capture the initial deformations, softening, hemisphere and flow temperatures of ash.

Appendix B- Conventional analyses results: from Proximate and Ultimate Analyses

B1 Results from Proximate and Ultimate Analysis

Table B1: Proximate analyses results

Coal	**Coal A**	**Coal B**	**Coal C**
Inherent Moisture Content (%)	1.4	2.1	2.1
Volatile Matter Content (%)	25.0	23.0	22.7
Ash (%)	32.3	32.8	37.5
Fixed Carbon (%) (by difference)	41.3	42.1	37.7
Gross Calorific Value (MJ/kg)	19.82	21.12	17.37

Table B2: Ultimate analyses results

Coal/Chemical composition (%)	**Coal A**	**Coal B**	**Coal C**
Carbon	50.60	50.70	45.54
Hydrogen	3.06	2.68	2.59
Nitrogen	1.11	1.19	1.07
Total Sulphur	0.93	0.75	0.60
Carbonate	2.58	2.60	2.31
Oxygen (by difference)	8.02	7.18	8.29

Table B3: Fuel ratio, O/C and H/C ratios from Proximate and Ultimate Analyses

	Coal A	**Coal B**	**Coal C**
Fuel ratio	1.652	1.830435	1.660793
O/C	0.158498	0.141617	0.182038
H/C	0.060474	0.05286	0.056873

B1.1 Ash Analyses by X-ray Flourescence (XRF)

Table B4: X-ray fluorescence analyses results

Coal/Mineral Oxides (%)	**Coal A**	**Coal B**	**Coal C**
SiO_2	58.74	53.46	55.24
TiO_2	1.37	1.65	1.59
Al_2O_3	26.94	29.91	30.26
Fe_2O_3	4.79	3.04	3.29
MgO	1.09	1.69	1.07
CaO	3.49	5.44	4.70
Na_2O	0.28	0.43	0.36
K_2O	0.88	0.84	0.73
P_2O_5	0.47	0.59	0.41
SO_3	2.59	2.57	2.57
MnO (Calculated)	0.02	0.01	0.01

B1.2 Ash Fusion Temperatures (AFTs)

Table B5: AFT Results

Coal/Temperatures (℃)	**Coal A**	**Coal B**	**Coal C**
Deformation Temperature	1460	1460	1500
Softening Temperature	1470	1470	1500
Hemisphere Temperature	1480	1480	1500
Flow Temperature	1490	1490	1500

Appendix C- Specialised Analyses Results: QUEMSCAN, TGA and Optical Petrography

C1 Results from QEMSCAN analyses

The results obtained from QEMSCAN are tabulated below.

Table C1: Mineral matter content of coals as determined by QEMSCAN SEM

Renormalise to 100	Coal A +106um	Coal A -212um	Coal C -212 um	Coal C +106um	Coal C -106um	Coal B -212um	Coal B-106um
Liptinite	0.00	0.00	0.00	0.00	0.00	0.00	0.00
Vitrinite	14.09	5.97	6.04	10.36	2.41	9.44	3.40
RSF	6.92	3.75	1.36	4.22	1.35	5.48	1.86
SFusinite	1.25	1.91	1.74	1.70	1.51	1.56	1.05
Fusinite(S)	6.35	9.12	3.77	4.40	6.25	7.12	3.42
Fusinite	15.18	29.38	36.83	30.04	31.62	30.48	15.86
Fusinite/Scl(Hi C)	2.97	4.20	1.07	3.88	3.41	1.10	3.42
Albite	0.01	0.02	0.02	0.04	0.06	0.34	1.01
Ferrosilite	0.02	0.03	0.10	0.07	0.06	0.05	0.11
Kaolinite	28.24	16.97	29.53	28.19	23.89	12.36	22.92
Quartz	14.35	14.26	12.44	9.47	15.13	16.25	17.79
Alunite/Gibbsite	0.07	0.04	0.26	0.74	0.26	0.03	0.11
Glauconite/Chlorite/Biotite	0.01	0.00	0.02	0.04	0.13	0.60	3.55
Smectite Clay	0.49	0.19	0.12	0.11	0.13	0.10	0.24
Muscovite	0.15	0.12	0.33	0.92	0.80	0.44	1.70
Illite	0.75	0.48	0.60	1.37	1.06	1.80	5.16
Microcline	0.68	0.44	0.12	0.30	0.93	3.29	7.33
Pyrite	1.95	6.01	1.43	0.33	1.87	4.33	5.48
Gypsum	0.00	0.01	0.00	0.00	0.10	0.00	0.02
Calcite	1.24	3.16	2.29	1.15	3.90	3.89	3.15
Dolomite	1.73	0.91	0.45	0.96	2.09	0.37	0.36
Apatite	0.17	0.28	0.21	0.30	0.16	0.10	0.05
Siderite	3.17	2.43	0.95	0.89	2.35	0.65	1.51
Ilmenite/Ti Magnetite	0.00	0.01	0.00	0.00	0.00	0.00	0.06
Rutile	0.05	0.07	0.14	0.18	0.23	0.10	0.21
Zircon	0.09	0.10	0.07	0.22	0.10	0.08	0.06
Others	0.07	0.14	0.07	0.11	0.19	0.05	0.16
Total	100.00	100.00	100.00	100.00	100.00	100.00	100.00
Mineral Matter Mass	53.24	45.67	49.18	45.39	53.44	44.82	70.98
Mineral Volatiles	7.79	8.46	6.61	5.72	8.22	6.51	9.45
QS Ash (Calculated)	45.45	37.21	42.56	39.67	45.22	38.32	61.52
Chem Ash(Meas)	0.00	0.00	0.00	0.00	0.00	0.00	0.00

C1 Calculation for mass weighted ash percent for the three coals

The results above were mass weighted to account for the differences in coal samples weighed per size fraction as indicated in the table below.

$$\boldsymbol{Mass\ weighted\ avg}\ (\%) = \frac{\boldsymbol{sample\ mass}\ (\boldsymbol{g})}{\boldsymbol{total\ mass}\ (\boldsymbol{g})} \times \boldsymbol{ash\ content}\ (\%) \qquad \text{Equation 1}$$

Table C2: Weighted average ash % of the three different size fractions

Sample Mass (g)	+106microns	-106mircons	-212	Total mass (g)
Coal A	0.21	0.175	0.18	0.565
Coal B	0.21	0.187	0.2	0.597
Coal C	0.19	0.17	0.22	0.58
Ash (%)	+106microns	-106mircons	-212	
Coal A	45.45	40.12	37.21	
Coal B	41.06	61.52	57.085	
Coal C	39.67	45.22	43.185	
Mass weighted avg ash (%)	+106microns	-106mircons	-212	Total ash (%)
Coal A	16.89292035	12.42654867	11.85451	41.1739823
Coal B	14.44321608	19.27008375	19.12395	52.83725293
Coal C	12.99534483	13.25413793	16.38052	42.63

C2 Optical Petrographic Analyses

Results are displayed here and used in the theoretical model. Discussion of these results is provided in section 5.7.

Table C3: Petrographic analyses results

Maceral Group	**Maceral (vol %)**	**Coal A**	-	**Coal B**	-	**Coal C**	-
Vitrinite	Tellinite	0.8	1	1	1.4	0.6	0.7
	Collotelinite	32.5	43.5	35.4	51.3	10.9	13
	Vitrodetrinite	6.7	8.9	7.9	11.4	3.8	4.6
	Collodetrinite	1.2	1.6	0	0	0	0
	corpogelinite	0	0	0	0	0	0
	Gelinite	0.4	0.5	0.2	0.3	0	0
	pseudovitrinite	1.2	1.6	1	1.4	0	0
Inertinite	Fusinite	1.8	2.4	2.6	3.7	0.8	0.9
	Reactive semifusinite	1	1.3	1.4	2	2.3	2.7

	Inert semifusinite	12.9	17.3	8.6	12.5	21.2	25.4
	micrinite	0	0			1.3	1.6
	Macrinite	0.2	0.3			0	0
	Secretinite	1.4	1.8			3.2	3.9
	Funginite	0	0			0	0
	Inertrodetrinite R	1.2	1.6			1.3	1.6
	Inertrodetrinite I	9.8	13.1			33.4	40
Liptinite	Sporinite	3.7	5			4.4	5.3
	cutinite	0.2	0.3			0	0
	resinite	0	0			0.2	0.2
	alginite	0	0			0	0
	liptodetrinite	0	0			0	0
	subernite	0	0			0	0
	exsudatinite	0	0			0	0
Mineral Matter	Silicate (clay/qz)	19.6				13.2	
	sulfide	2				0.6	
	carbonate	3.3				2.5	
	other	0.2				0.4	
Maceral Group Totals (vol%)	Vitrinite	42.8	57.1			15.3	18.3
	Inertinite	28.3	37.8			63.5	76.1
	Liptinite	3.9	5.3			4.6	5.5
	Mineral Matter	25.1	0			16.7	0
	Total Inertinite	28.3	37.8			63.5	76.1
	Total Reactive Macerals	48.9	65.3			23.5	28.1

For the reflectance of vitrinite analyses were conducted under oil immersion under magnification of x500.

Table C4: Vitrinite reflectance of the three coals under investigation

Vitrnite reflectance (RoV%)	-	**Coal A**	**Coal B**	**Coal C**
	Rrandom	0.65	0.66	0.54
	st. dev	0.054	0.038	0.044
	max	0.77	0.74	0.64
	min	0.54	0.57	0.46
	Rank category	Med rank C	Med Rank C	Med rank D

Limitations of coal properties to be used with empirical formula for determining the maceral correction factor

$$\boldsymbol{F_{mac} = 1.68Vit - 0.6In}$$ Equation 2

For $q_{cmb} > 0, F_{mac}\ must\ be > 0$. (According to equation 5.1)

Therefore;

$$F_{mac} = 1.68Vit - 0.6In > 0$$

$$1.68Vit > 0.6In$$

$$0.6In < 1.68Vit$$

$$In < \frac{1.68}{0.6}Vit$$

i.e.: Inertinite to Vitrinite content must not exceed 2.8

Table C5: Inertinite to Vitrinite ratios (volume %) from petrographic analyses

Coal	Coal A	Coal B	Coal C
Total Vitrinite	57.1	65.8	18.3
Total Inertinite	37.8	31.8	76.1
Inertinite/Vitrinite	0.661996	0.483283	4.15847

C3 TGA Results combustion in air

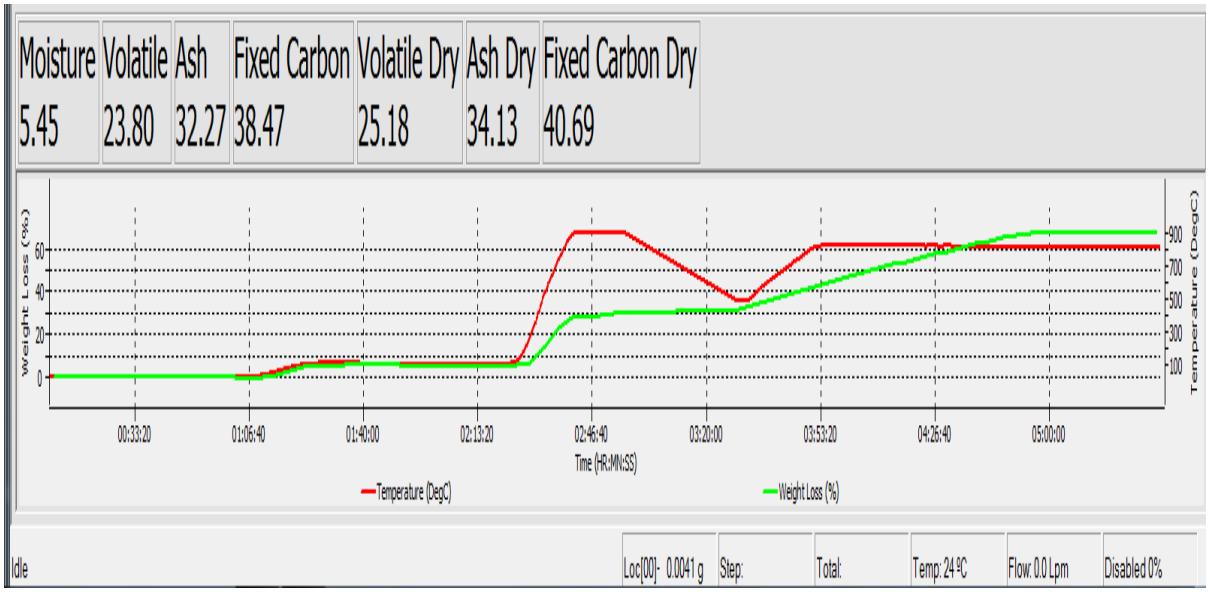

Figure C1: Coal C -212μm (sample I)

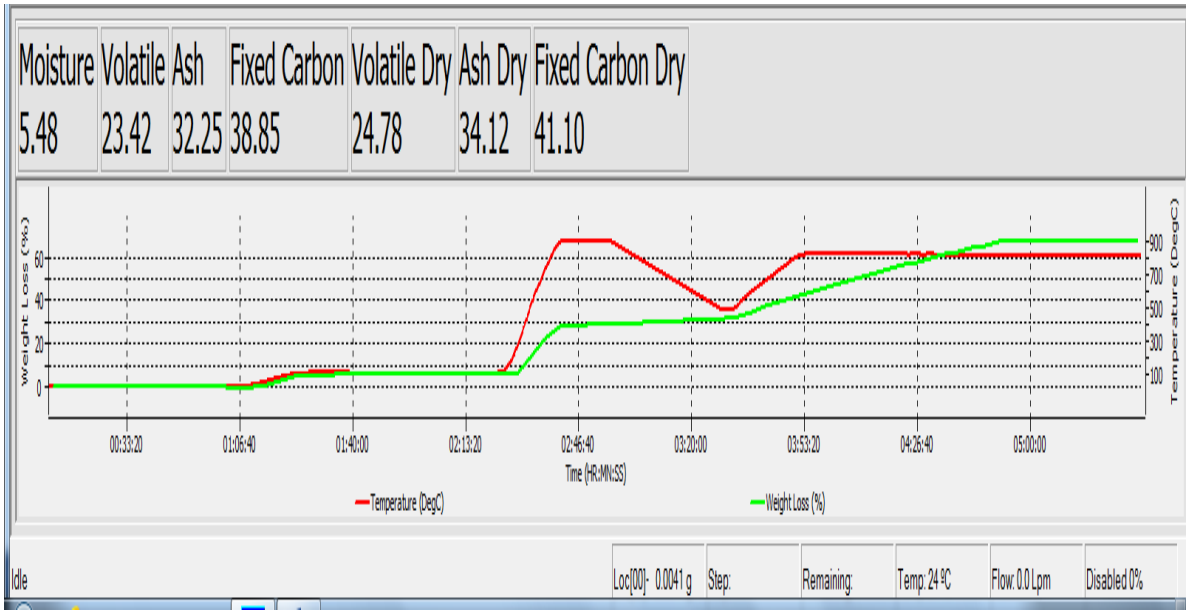

Figure C2: Coal C -212μm (sample II)

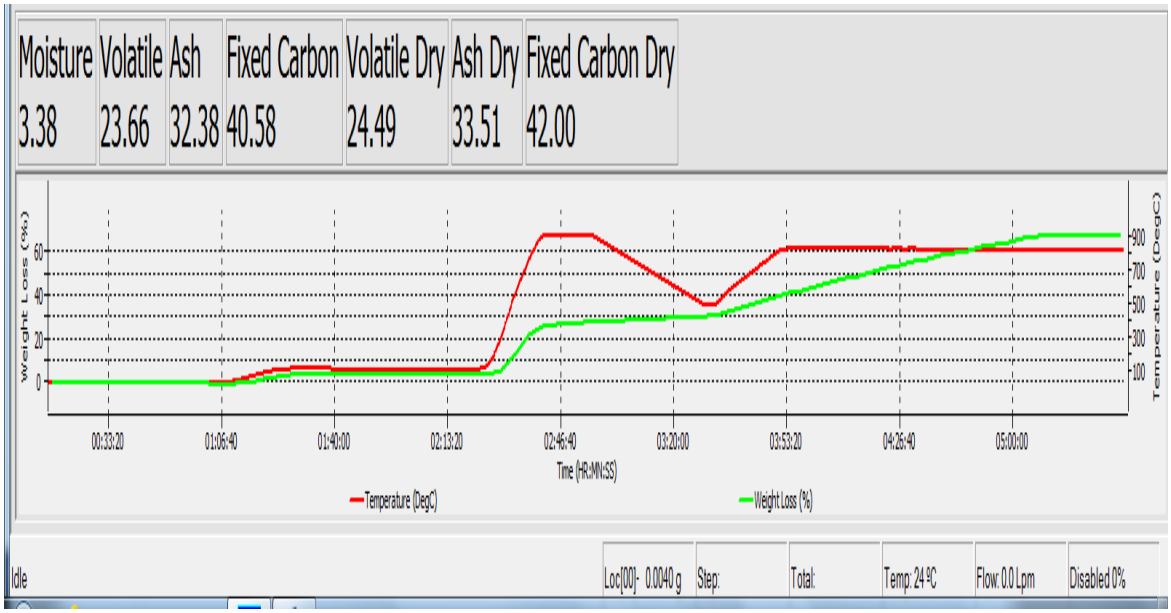

Figure C3: Coal C +106μm (sample I)

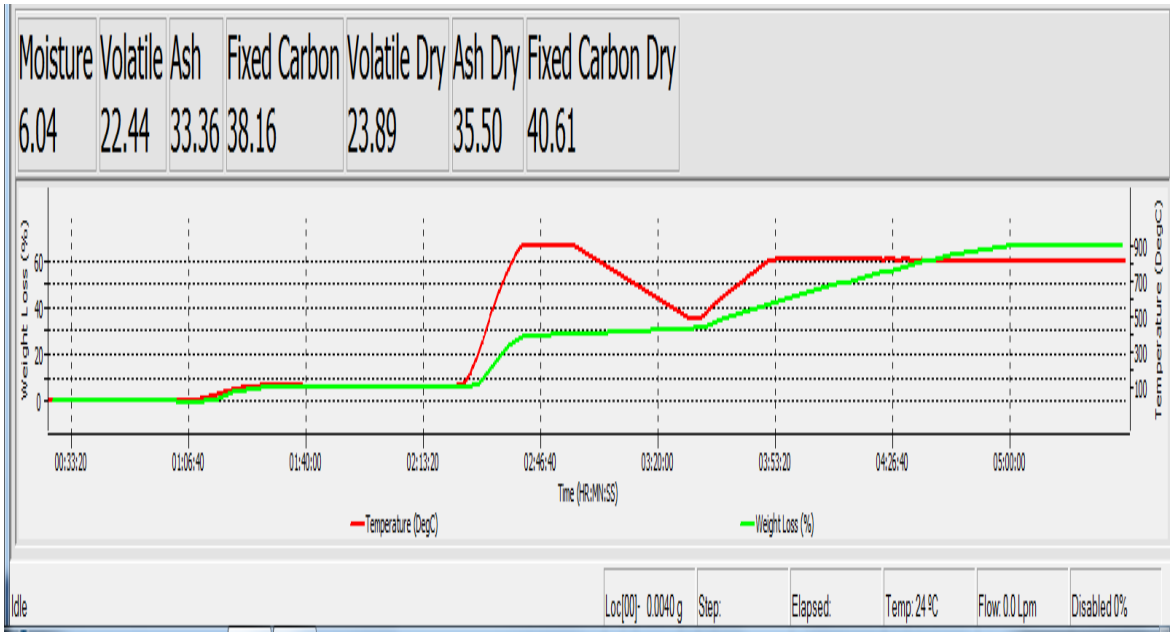

Figure C4: Coal C +106μm (sample II)

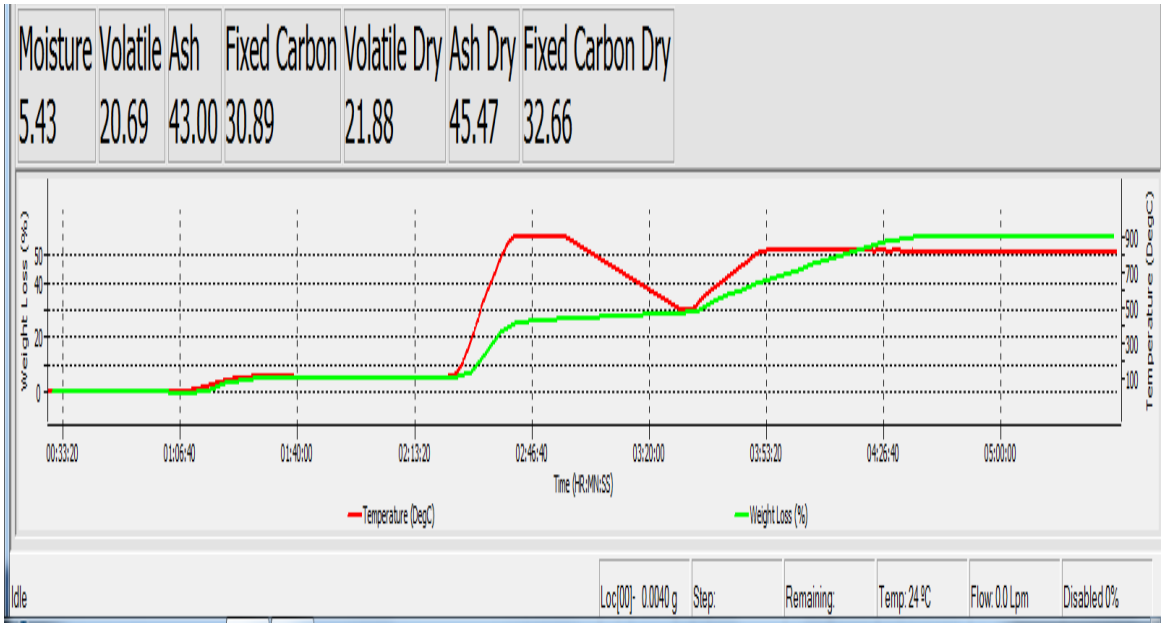

Figure C5: Coal C -106μm (sample I)

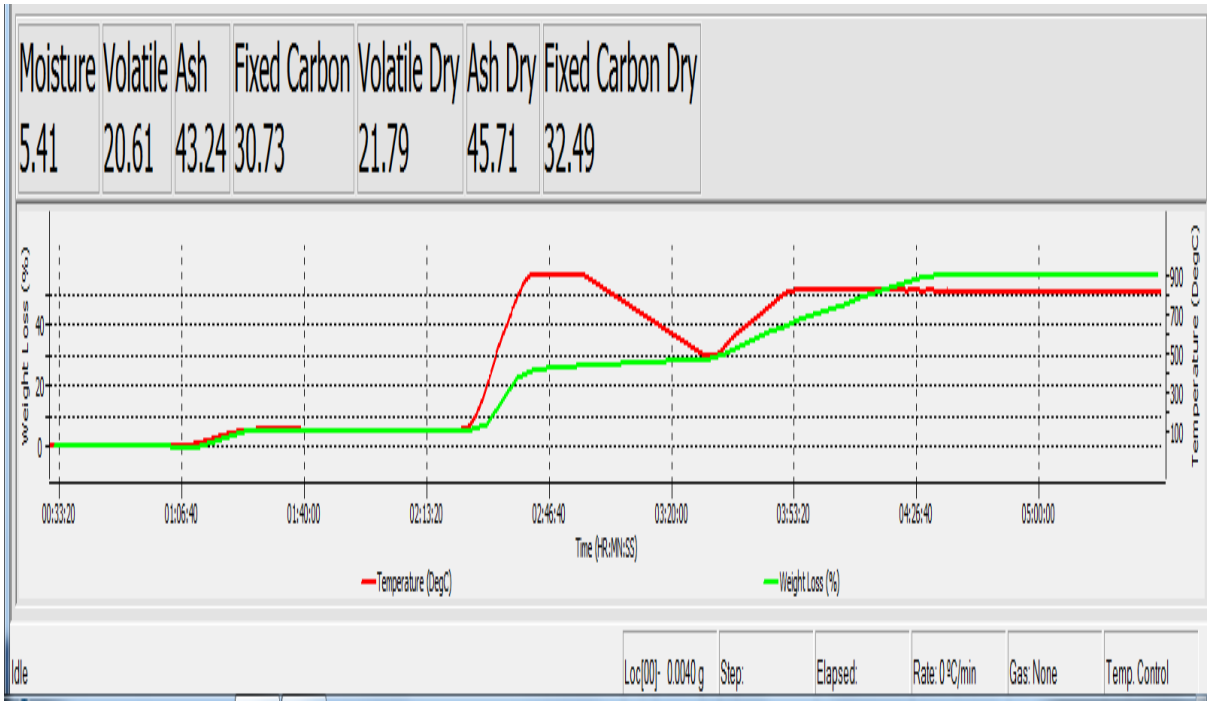

Figure C6: Coal C -106μm (sample II)

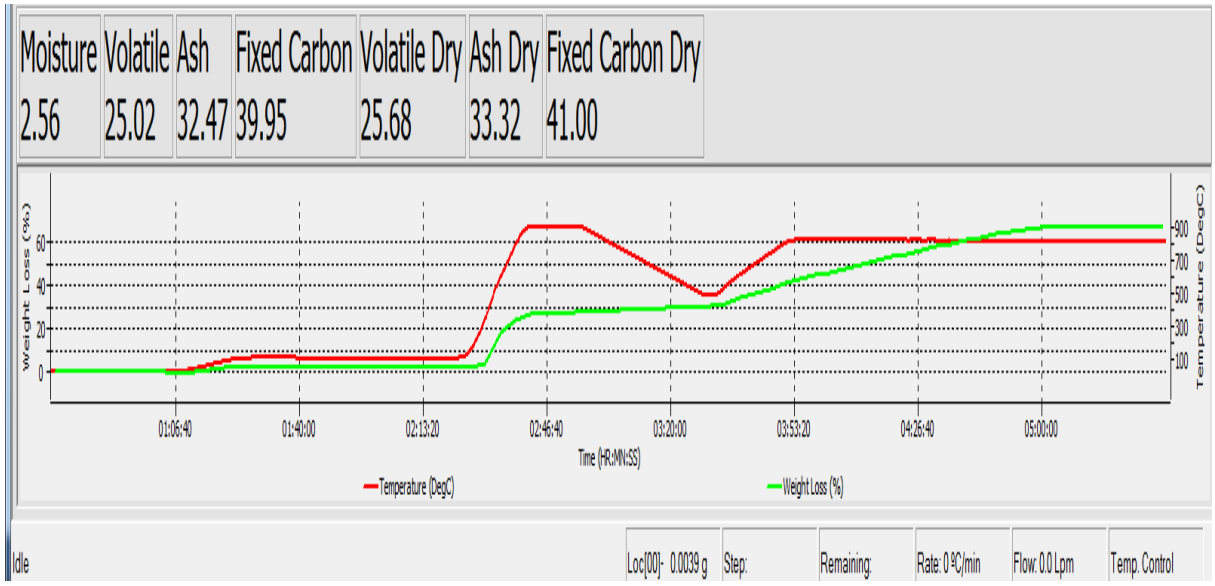

Figure C7: Coal A -212μm (sample I)

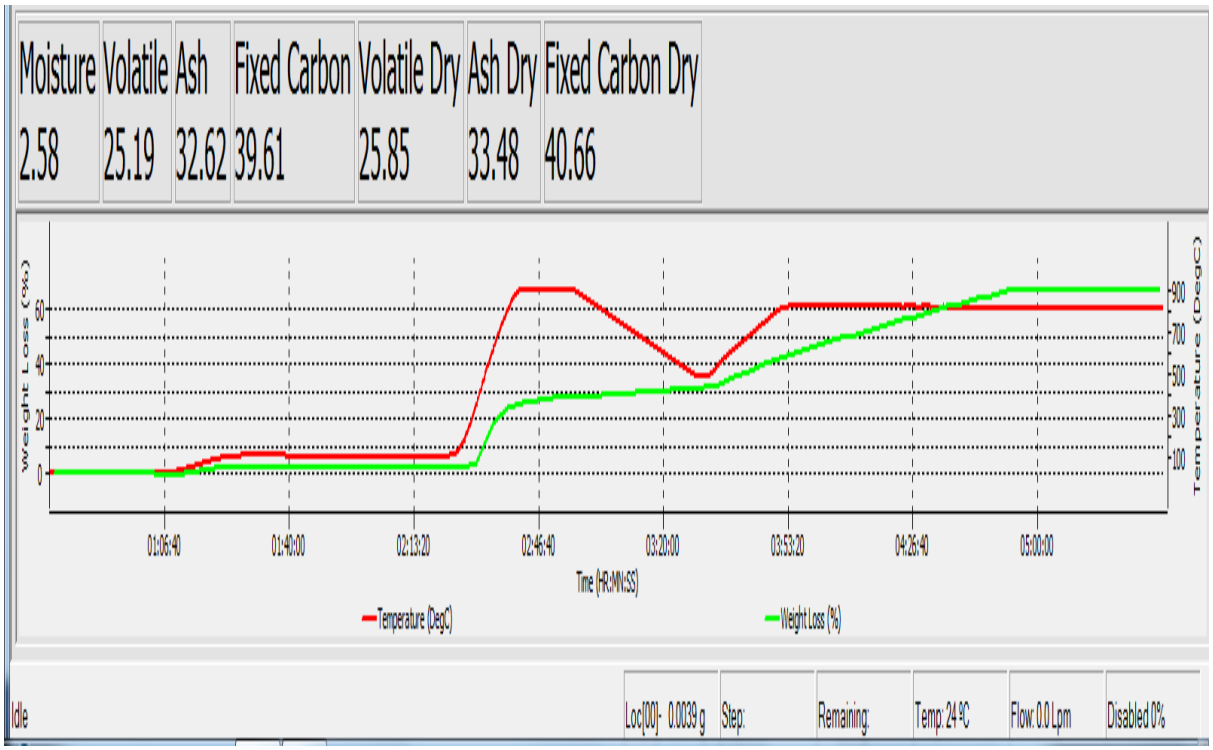

Figure C8: Coal A -212μm (sample II)

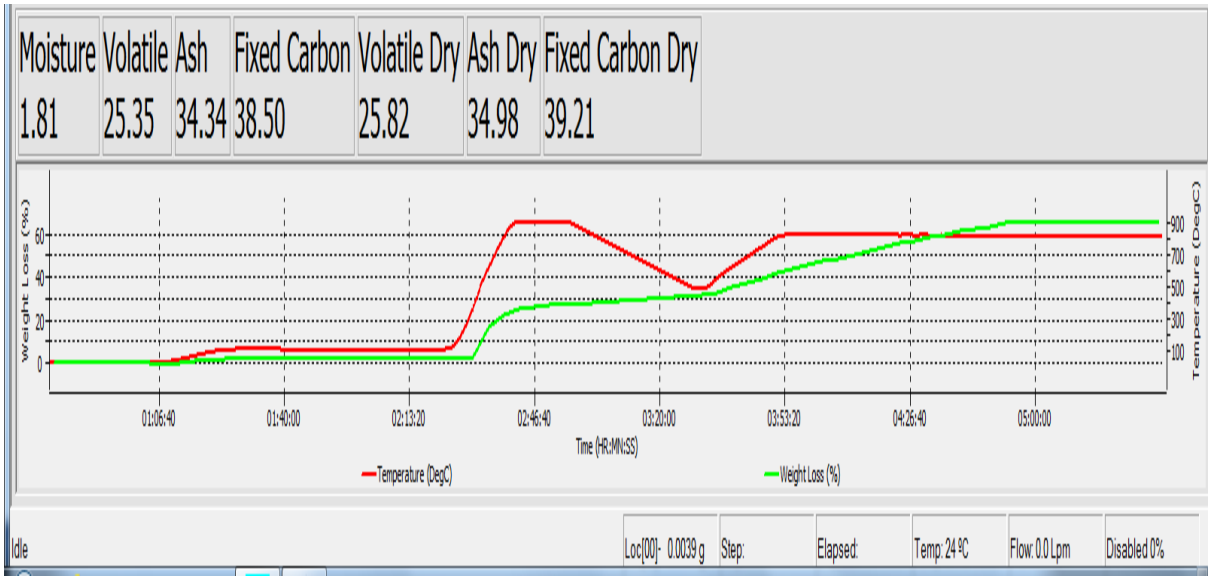

Figure C9: Coal A +106μm (sample II)

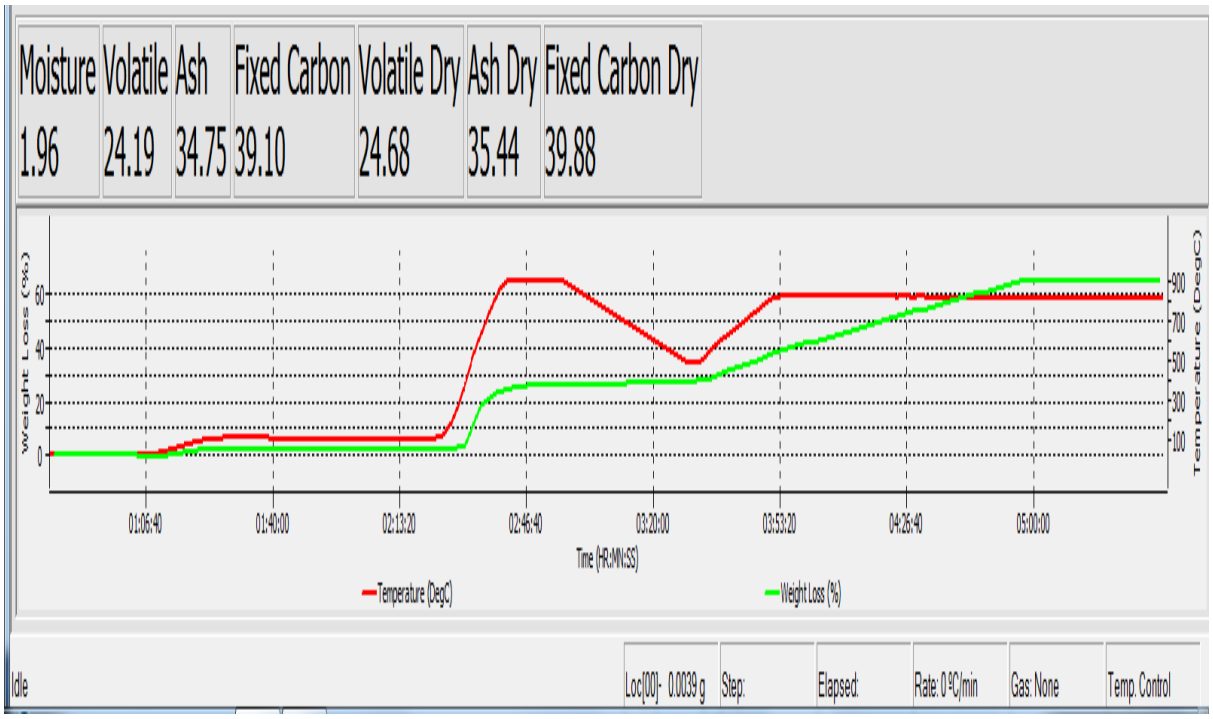

Figure C10: Coal A +106μm (sample II)

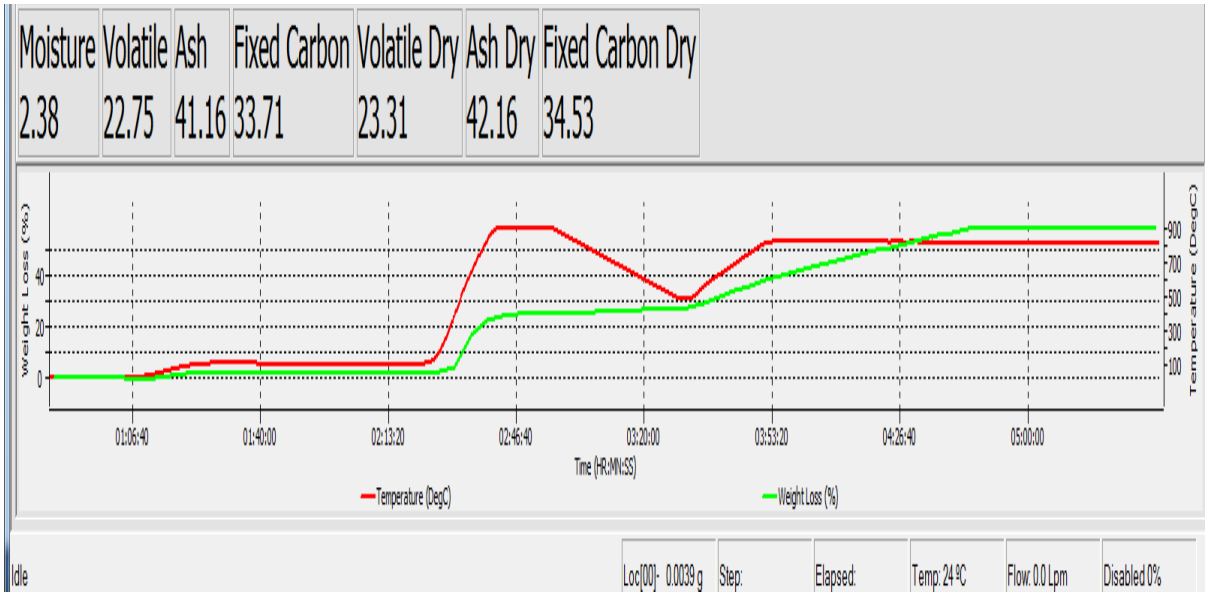

Figure C11: Coal A -106μm (sample I)

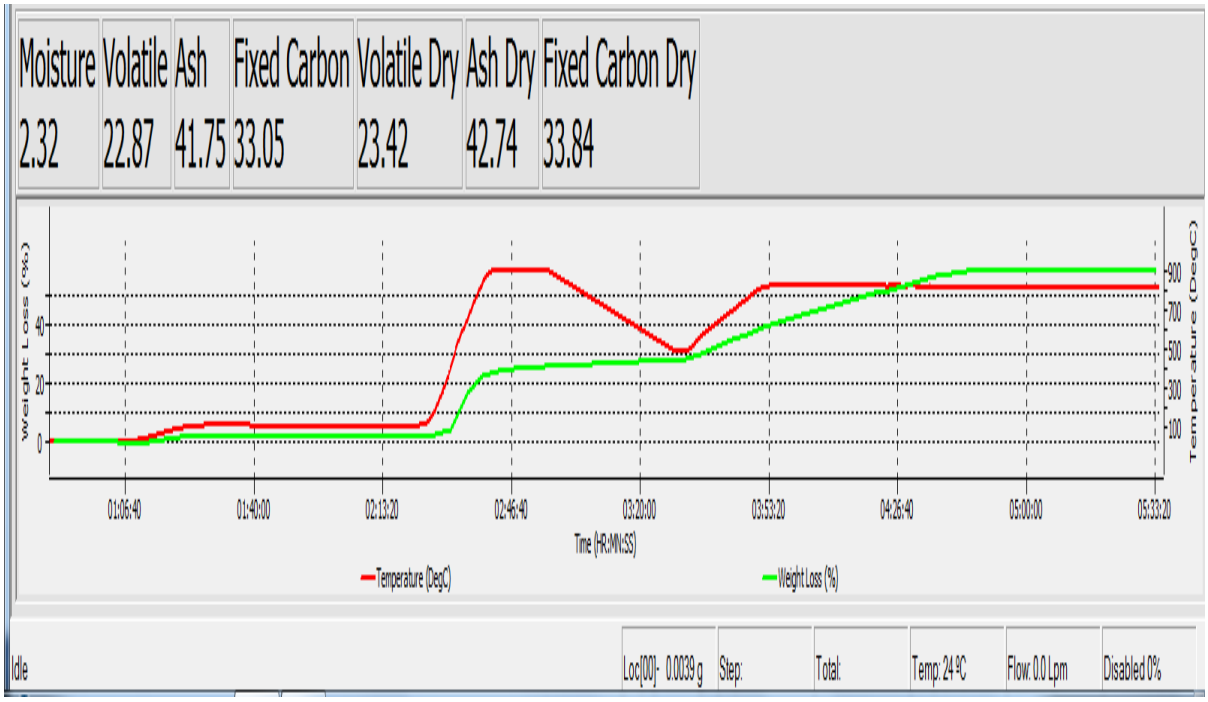

Figure C12: Coal A -106μm (sample II)

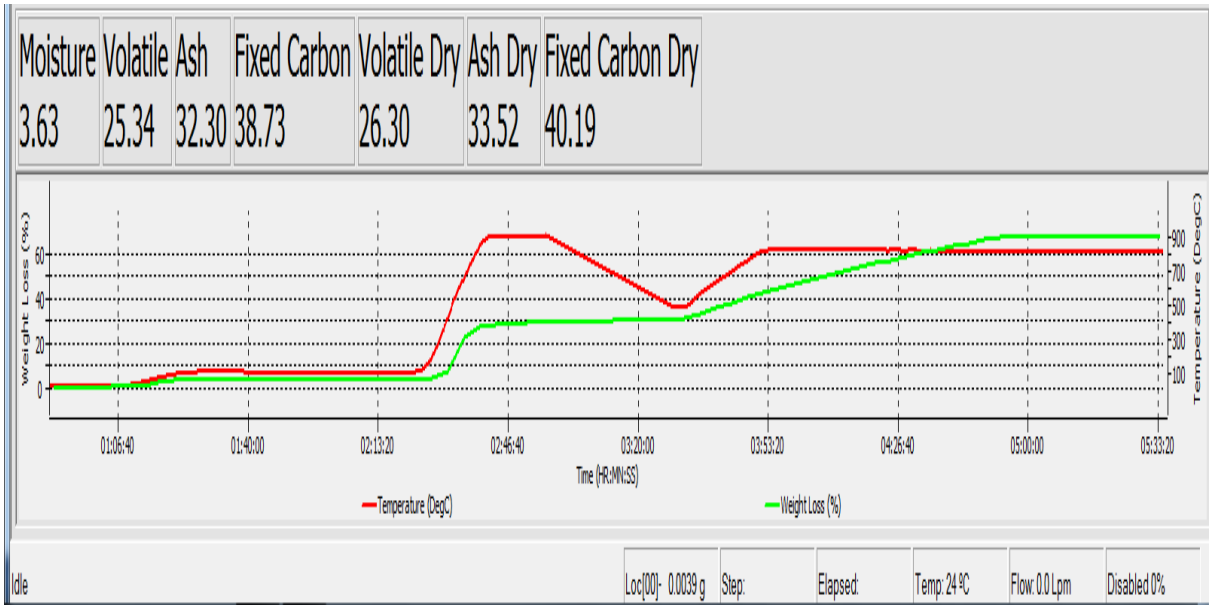

Figure C13: Coal B -212μm (sample I)

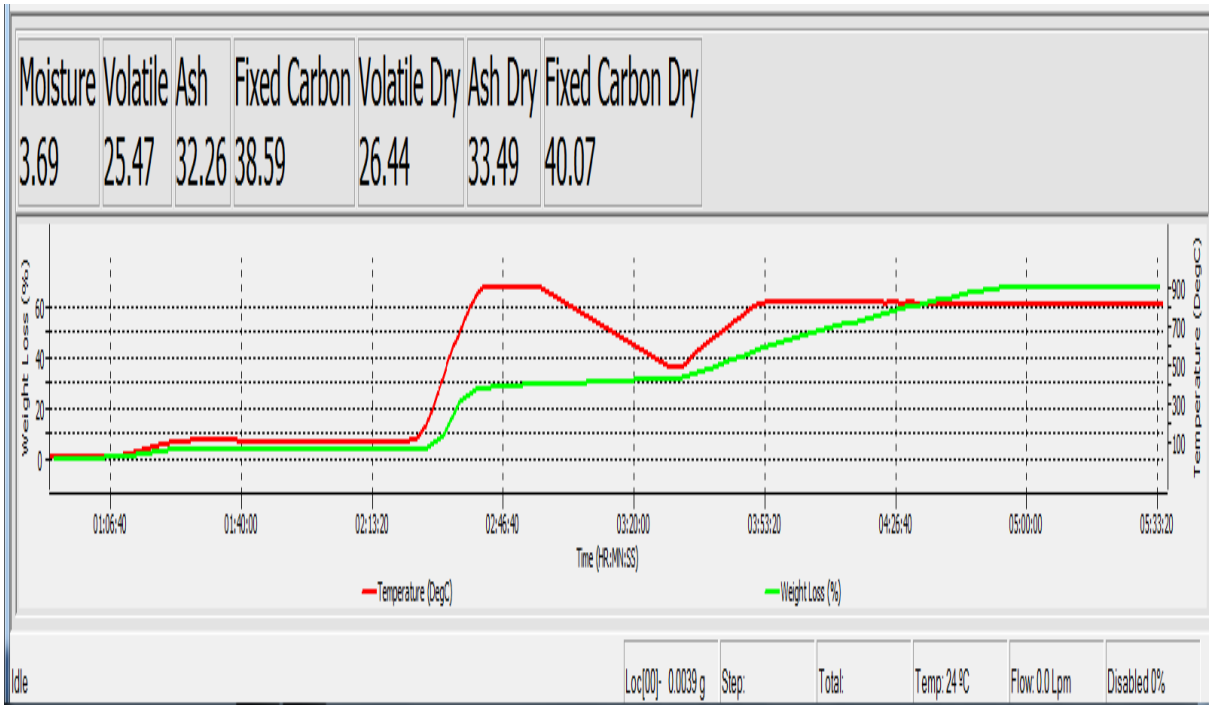

Figure C14: Coal B -212μm (sample II)

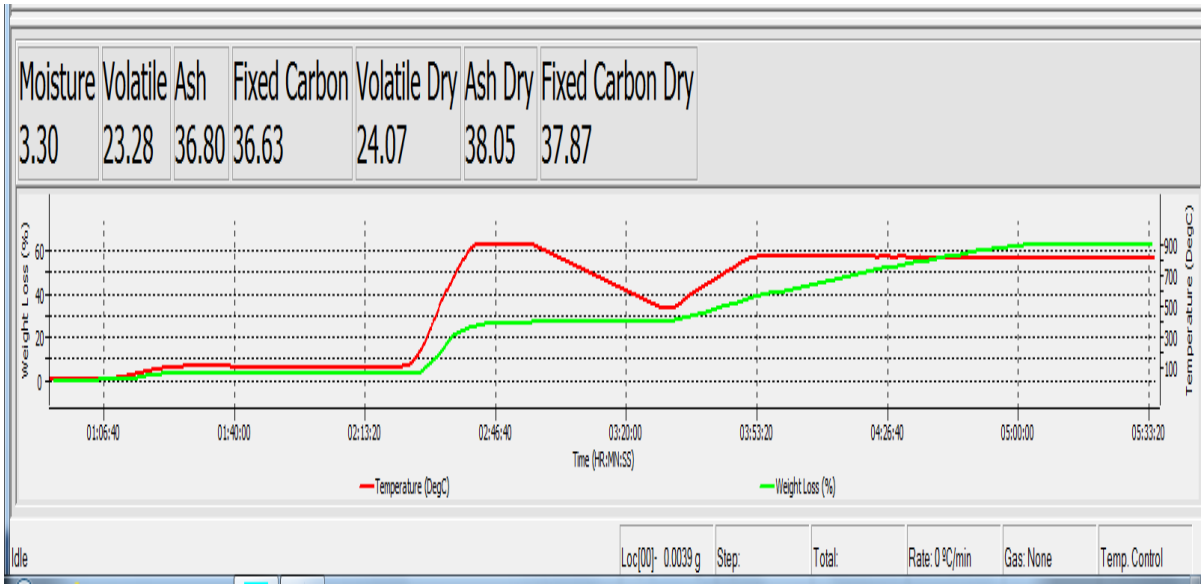

Figure C15: Coal B +106μm (sample I)

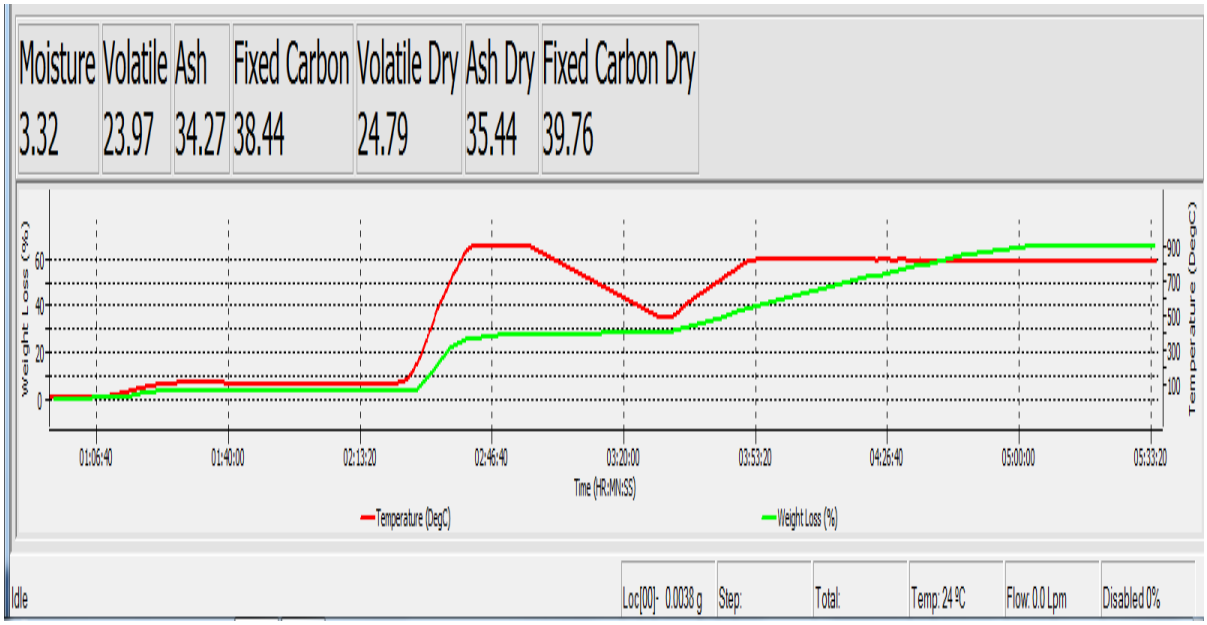

Figure C16: Coal B +106μm (sample II)

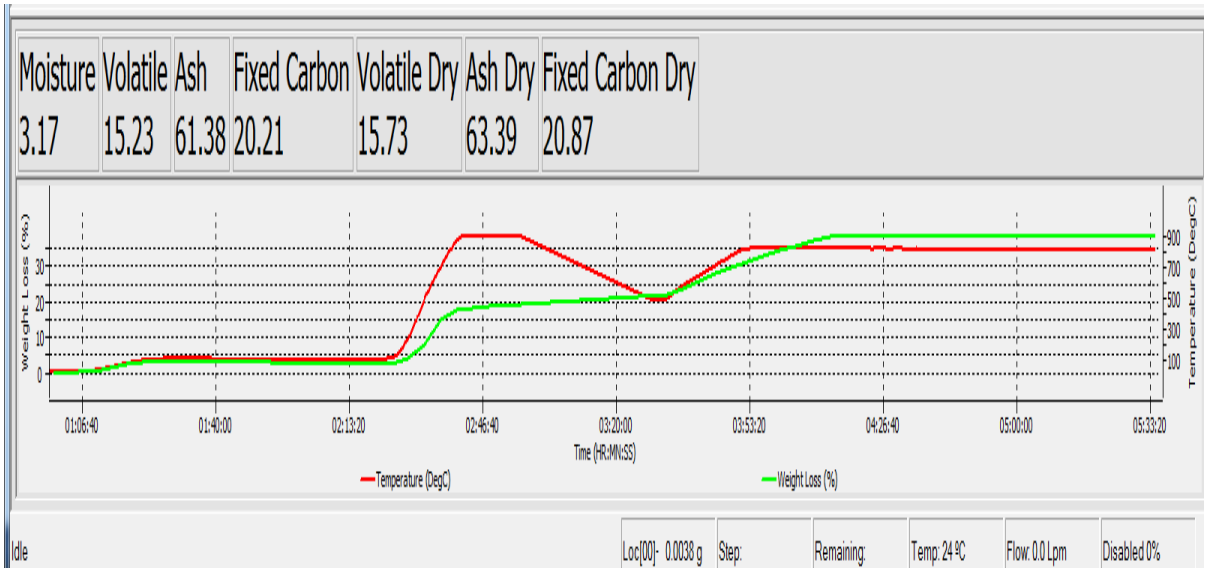

Figure C17: Coal B -106μm (sample I)

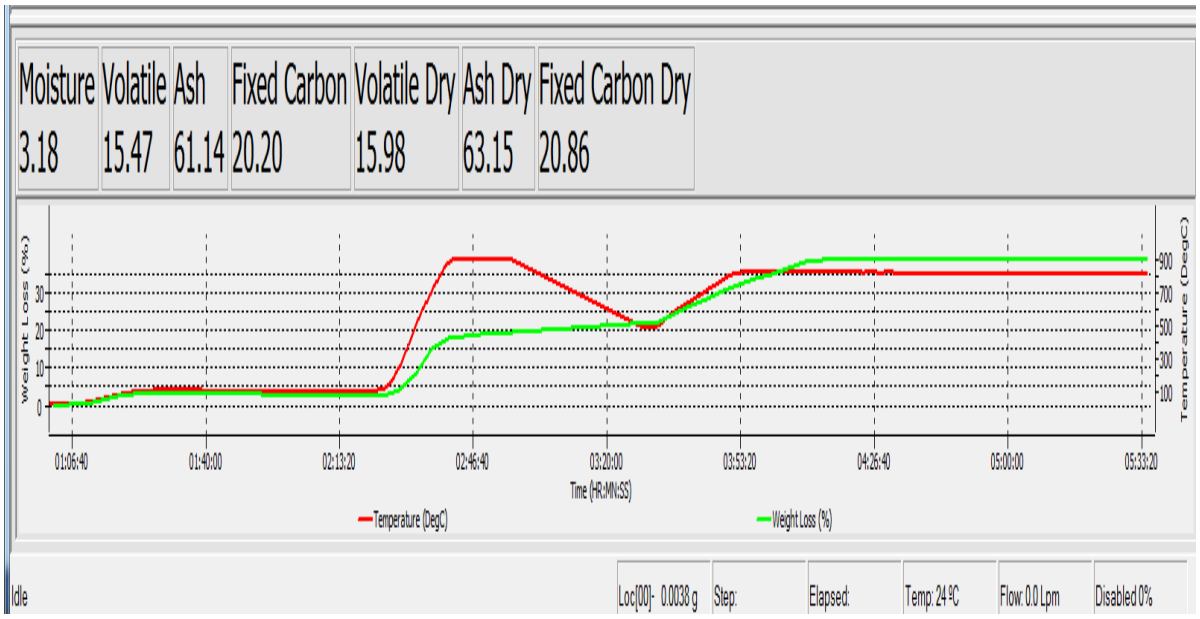

Figure C18: Coal B -106μm (sample II)

Appendix D: Theoretical model data used in Microsoft Excel

D1: Input Data

Table D1: Coal A Theoretical char burnout model input data

Constants	**Oxidation**		**Gasification**	
	A (kg/m2.s.Pa)	E (kJ/mol)	A (kg/m2.s.Pa)	E (kJ/mol)
HV-B	0.3	97.1	289.119	306.1
Reaction order, n	0.5	0.3	0.8	
R (kJ/kmol K)	8.314			
Sample mass, mp (mg)	4.5			
Vit	82.8			
In	13.2			
Maceral correction factor, Fmac	131.184			
Pg, partial pressure	O_2	0.21	CO_2	0.79
		0.3		0.7
		0.4		0.6
		0.5		0.5

Table D2: Coal B Theoretical char burnout model input data

Constants	**Oxidation**		**Gasification**	
	A (kg/m2.s.Pa)	E (kJ/mol)	A (kg/m2.s.Pa)	E (kJ/mol)
HV-B	0.3	97.1	289.119	306.1
Reaction order, n	0.5	0.3	0.8	
R (kJ/kmol K)	8.314			
Sample mass, mp (mg)	4.5			
Vit	65.8			
In	31.9			
Maceral correction factor, Fmac	91.404			
Pg, partial pressure	O_2	0.21	CO_2	0.79
		0.3		0.7
		0.4		0.6
		0.5		0.5

Table D3: Coal C Theoretical char burnout model input data

Constants	**Oxidation**		**Gasification**	
	A (kg/m2.s.Pa)	E (kJ/mol)	A (kg/m2.s.Pa)	E (kJ/mol)
HV-B	0.3	97.1	289.119	306.1
Reaction order, n	0.5	0.3	0.8	
R (kJ/kmol K)	8.314			
Sample mass, mp (mg)	4.5			
Vit	15.3			
In	63.5			
Maceral correction factor, Fmac	-12.396			
Pg, partial pressure	O_2	0.21	CO_2	0.79
		0.3		0.7
		0.4		0.6
		0.5		0.5

D2: Results from Theoretical Model Calculations

Table D4: Coal A Theoretical Model Calculations on Microsoft Excel

Temperature	Oxidation									Gasification								
	Effectiveness factor, η				Intrinsic Reactivity	21%O2	30%O2	40%O2	50%O2	Effectiveness factor, η				Intrinsic Reactivity	79% CO2	70% CO2	60% CO2	50% CO2
T (K)	**η at 21%CO2**	η at 30%CO2	η at 40%CO2	η at 50%CO2	Rs (kg/m2.s.Pa)	**R (kg/m2.s)**	**R (kg/m2.s)**	**R (kg/m2.s)**	**R (kg/m2.s)**	**η at 79%CO2**	η at 70%CO2	η at 60%CO2	η at 50%CO2	Rs (kg/m2.s.Pa)	**R (kg/m2.s)**	**R (kg/m2.s)**	**R (kg/m2.s)**	**R (kg/m2.s)**
800	1.8E-02	1.8E-02	1.8E-02	1.8E-02	1.4E-07	9.2E-07	8.1E-07	9.3E-07	1.0E-06	1.0E+00	1.0E+00	1.0E+00	1.0E+00	3.0E-18	1.5E-15	1.3E-15	1.2E-15	1.0E-15
1000	4.0E-03	4.0E-03	4.0E-03	4.0E-03	2.5E-06	3.8E-06	3.3E-06	3.8E-06	4.3E-06	1.0E+00	1.0E+00	1.0E+00	1.0E+00	3.0E-14	1.4E-11	1.3E-11	1.2E-11	1.0E-11
1100	2.3E-03	2.3E-03	2.3E-03	2.3E-03	7.3E-06	6.3E-06	5.5E-06	6.3E-06	7.1E-06	9.9E-01	9.9E-01	9.9E-01	9.8E-01	8.4E-13	4.1E-10	3.7E-10	3.3E-10	2.8E-10
1200	1.5E-03	1.5E-03	1.5E-03	1.5E-03	1.8E-05	9.6E-06	8.4E-06	9.7E-06	1.1E-05	8.5E-01	8.5E-01	8.2E-01	7.9E-01	1.4E-11	5.7E-09	5.2E-09	4.4E-09	3.7E-09
1400	7.0E-04	7.0E-04	7.0E-04	7.0E-04	7.1E-05	1.8E-05	1.6E-05	1.9E-05	2.1E-05	1.8E-01	1.8E-01	1.6E-01	1.5E-01	1.1E-09	9.7E-08	8.8E-08	6.8E-08	5.4E-08
1473	5.6E-04	5.6E-04	5.6E-04	5.6E-04	1.1E-04	2.2E-05	2.0E-05	2.3E-05	2.5E-05	9.6E-02	9.6E-02	8.4E-02	7.7E-02	4.0E-09	1.9E-07	1.7E-07	1.3E-07	1.1E-07
1600	4.0E-04	4.0E-04	4.0E-04	4.0E-04	2.0E-04	3.0E-05	2.6E-05	3.0E-05	3.4E-05	3.6E-02	3.6E-02	3.1E-02	2.8E-02	2.9E-08	5.1E-07	4.6E-07	3.6E-07	2.8E-07
1800	2.6E-04	2.6E-04	2.6E-04	2.6E-04	4.6E-04	4.4E-05	3.8E-05	4.4E-05	4.9E-05	9.7E-03	9.7E-03	8.5E-03	7.7E-03	3.8E-07	1.8E-06	1.6E-06	1.3E-06	9.9E-07
1873	2.3E-04	2.3E-04	2.3E-04	2.3E-04	5.9E-04	4.9E-05	4.3E-05	5.0E-05	5.6E-05	6.5E-03	6.5E-03	5.6E-03	5.1E-03	8.4E-07	2.7E-06	2.4E-06	1.9E-06	1.5E-06
2000	1.8E-04	1.8E-04	1.8E-04	1.8E-04	8.7E-04	5.9E-05	5.2E-05	6.0E-05	6.7E-05	3.4E-03	3.4E-03	3.0E-03	2.7E-03	2.9E-06	4.9E-06	4.4E-06	3.4E-06	2.7E-06

Table D5: Coal B Theoretical Model Calculations on Microsoft Excel

Temperature	Oxidation									Gasification								
	Effectiveness factor, η				Intrinsic Reactivity	21%O2	30%O2	40%O2	50%O2	Effectiveness factor, η				Intrinsic Reactivity	79% CO2	70% CO2	60% CO2	50% CO2
T (K)	**η at 21%CO2**	η at 30%CO2	η at 40%CO2	η at 50%CO2	Rs (kg/m2.s.Pa)	**R (kg/m2.s)**	**R (kg/m2.s)**	**R (kg/m2.s)**	**R (kg/m2.s)**	**η at 79%CO2**	η at 70%CO2	η at 60%CO2	η at 50%CO2	Rs (kg/m2.s.Pa)	**R (kg/m2.s)**	**R (kg/m2.s)**	**R (kg/m2.s)**	**R (kg/m2.s)**
800	1.8E-02	1.8E-02	1.8E-02	1.8E-02	1.4E-07	2.9E-07	3.9E-07	4.9E-07	5.9E-07	1.0E+00	1.0E+00	1.0E+00	1.0E+00	3.0E-18	1.0E-15	9.2E-16	8.1E-16	7.0E-16
1000	4.0E-03	4.0E-03	4.0E-03	4.0E-03	2.5E-06	1.2E-06	1.6E-06	2.0E-06	2.4E-06	1.0E+00	1.0E+00	1.0E+00	1.0E+00	3.0E-14	1.0E-11	9.2E-12	8.1E-12	7.0E-12
1100	2.3E-03	2.3E-03	2.3E-03	2.3E-03	7.3E-06	2.0E-06	2.7E-06	3.4E-06	4.0E-06	9.9E-01	9.9E-01	9.9E-01	9.8E-01	8.4E-13	2.8E-10	2.6E-10	2.3E-10	2.0E-10
1200	1.5E-03	1.5E-03	1.5E-03	1.5E-03	1.8E-05	3.1E-06	4.1E-06	5.1E-06	6.1E-06	8.5E-01	8.5E-01	8.2E-01	7.9E-01	1.4E-11	4.0E-09	3.6E-09	3.1E-09	2.6E-09
1400	7.0E-04	7.0E-04	7.0E-04	7.0E-04	7.1E-05	5.9E-06	7.8E-06	9.9E-06	1.2E-05	1.8E-01	1.8E-01	1.6E-01	1.5E-01	1.1E-09	6.7E-08	6.1E-08	4.8E-08	3.8E-08
1473	5.6E-04	5.6E-04	5.6E-04	5.6E-04	1.1E-04	7.1E-06	9.5E-06	1.2E-05	1.4E-05	9.6E-02	9.6E-02	8.4E-02	7.7E-02	4.0E-09	1.3E-07	1.2E-07	9.3E-08	7.3E-08
1600	4.0E-04	4.0E-04	4.0E-04	4.0E-04	2.0E-04	9.6E-06	1.3E-05	1.6E-05	1.9E-05	3.6E-02	3.6E-02	3.1E-02	2.8E-02	2.9E-08	3.6E-07	3.2E-07	2.5E-07	2.0E-07
1800	2.6E-04	2.6E-04	2.6E-04	2.6E-04	4.6E-04	1.4E-05	1.9E-05	2.3E-05	2.8E-05	9.7E-03	9.7E-03	8.5E-03	7.7E-03	3.8E-07	1.3E-06	1.1E-06	8.8E-07	6.9E-07
1873	2.3E-04	2.3E-04	2.3E-04	2.3E-04	5.9E-04	1.6E-05	2.1E-05	2.6E-05	3.1E-05	6.5E-03	6.5E-03	5.6E-03	5.1E-03	8.4E-07	1.9E-06	1.7E-06	1.3E-06	1.0E-06
2000	1.8E-04	1.8E-04	1.8E-04	1.8E-04	8.7E-04	1.9E-05	2.5E-05	3.2E-05	3.8E-05	3.4E-03	3.4E-03	3.0E-03	2.7E-03	2.9E-06	3.4E-06	3.1E-06	2.4E-06	1.9E-06

Table D6: Coal C Theoretical Model Calculations on Microsoft Excel

Temperature	Oxidation									Gasification								
	Effectiveness factor, η				Intrinsic Reactivity	21%O2	30%O2	40%O2	50%O2	Effectiveness factor, η				Intrinsic Reactivity	79% CO2	70% CO2	60% CO2	50% CO2
T (K)	**η at 21%CO2**	η at 30%CO2	η at 40%CO2	η at 50%CO2	Rs (kg/m2.s.Pa)	**R (kg/m2.s)**	**R (kg/m2.s)**	**R (kg/m2.s)**	**R (kg/m2.s)**	**η at 79%CO2**	η at 70%CO2	η at 60%CO2	η at 50%CO2	Rs (kg/m2.s.Pa)	**R (kg/m2.s)**	**R (kg/m2.s)**	**R (kg/m2.s)**	**R (kg/m2.s)**
800	1.8E-02	1.8E-02	1.8E-02	1.8E-02	1.7E-06	-5.1E-07	-6.7E-07	-8.5E-07	-1.0E-06	1.0E+00	1.0E+00	1.0E+00	1.0E+00	9.3E-10	-4.3E-08	-3.9E-08	-3.4E-08	-3.0E-08
1000	4.0E-03	4.0E-03	4.0E-03	4.0E-03	2.8E-05	-1.8E-06	-2.4E-06	-3.0E-06	-3.6E-06	1.0E+00	1.0E+00	1.0E+00	1.0E+00	2.1E-08	-9.5E-07	-8.6E-07	-7.6E-07	-6.6E-07
1100	2.3E-03	2.3E-03	2.3E-03	2.3E-03	7.7E-05	-2.8E-06	-3.8E-06	-4.8E-06	-5.7E-06	9.9E-01	9.9E-01	9.9E-01	9.8E-01	6.4E-08	-2.9E-06	-2.6E-06	-2.3E-06	-2.0E-06
1200	1.5E-03	1.5E-03	1.5E-03	1.5E-03	1.8E-04	-4.2E-06	-5.5E-06	-7.0E-06	-8.3E-06	8.5E-01	8.5E-01	8.2E-01	7.9E-01	1.6E-07	-6.4E-06	-5.8E-06	-4.9E-06	-4.1E-06
1400	7.0E-04	7.0E-04	7.0E-04	7.0E-04	6.7E-04	-7.5E-06	-1.0E-05	-1.3E-05	-1.5E-05	1.8E-01	1.8E-01	1.6E-01	1.5E-01	7.1E-07	-5.9E-06	-5.4E-06	-4.2E-06	-3.3E-06
1473	5.6E-04	5.6E-04	5.6E-04	5.6E-04	1.0E-03	-8.9E-06	-1.2E-05	-1.5E-05	-1.8E-05	9.6E-02	9.6E-02	8.4E-02	7.7E-02	1.1E-06	-4.9E-06	-4.4E-06	-3.4E-06	-2.7E-06
1600	4.0E-04	4.0E-04	4.0E-04	4.0E-04	1.8E-03	-1.2E-05	-1.5E-05	-1.9E-05	-2.3E-05	3.6E-02	3.6E-02	3.1E-02	2.8E-02	2.2E-06	-3.5E-06	-3.2E-06	-2.5E-06	-2.0E-06
1800	2.6E-04	2.6E-04	2.6E-04	2.6E-04	3.9E-03	-1.6E-05	-2.2E-05	-2.7E-05	-3.3E-05	9.7E-03	9.7E-03	8.5E-03	7.7E-03	5.1E-06	-2.3E-06	-2.1E-06	-1.6E-06	-1.3E-06
1873	2.3E-04	2.3E-04	2.3E-04	2.3E-04	5.0E-03	-1.8E-05	-2.4E-05	-3.0E-05	-3.6E-05	6.5E-03	6.5E-03	5.6E-03	5.1E-03	6.7E-06	-2.0E-06	-1.8E-06	-1.4E-06	-1.1E-06
2000	1.8E-04	1.8E-04	1.8E-04	1.8E-04	7.3E-03	-2.1E-05	-2.8E-05	-3.6E-05	-4.3E-05	3.4E-03	3.4E-03	3.0E-03	2.7E-03	1.0E-05	-1.6E-06	-1.5E-06	-1.1E-06	-8.8E-07